Dissertation

submitted to the
Combined Faculties of the Natural Sciences and Mathematics
of the Ruperto-Carola-University of Heidelberg, Germany
for the degree of

Doctor of Natural Sciences

Put forward by

M.Sc. Carolina Bergfors

born in Skellefteå, Sweden

Oral examination: November 30, 2011

Formation of stars, substellar objects and exoplanets:

Observations of multiplicity

Referees: Prof. Dr. Thomas Henning
Prof. Dr. Ralf Klessen

Abstract

Many nearby stars are part of a binary or multiple system. Details about their history are preserved in their multiplicity characteristics, and observations of binary/ multiple star systems provide a way to measure fundamental physical properties of the stars as well as clues to their formation and evolution. Moreover, planet formation and dynamics may also be affected by the presence of a second star, or by giant planets in the same system.

In this thesis, high resolution imaging of low-mass stars, planet host stars and a multiple planet system is presented. The results of observations and analyses include the discovery of several previously unknown companion stars and multiplicity statistics for M dwarfs in the largest M dwarf multiplicity survey to date. We also present near-infrared characterization of four close M dwarf systems, previously unknown companion candidates to exoplanet host stars, and investigate how a close companion may affect planet formation. New astrometric data is presented for three of the directly imaged planets in the HR 8799 system, and an analysis of a possible orbital configuration of planet HR 8799 d.

Zusammenfassung

Viele Sterne in der Sonnenumgebung sind Teil eines Doppel- oder Mehrfachsystems. Die Eigenschaften dieser Systeme spiegeln deren Entstehungsgeschichte wider. Beobachtungen der Doppel- und Mehrfachsysteme ermöglichen die Messung grundlegender physikalischer, stellarer Eigenschaften, und bieten Hinweise auf die Entstehung und Entwicklung der Sterne. Weiterhin könnten Planetenentstehung und -dynamik durch das Vorhandensein eines zweiten Sterns oder weiterer Gasplaneten im selben System beeinflusst werden.

In der vorliegenden Doktorarbeit werden hochaufgelöste Bilder massearmer Sterne, Sterne mit Exoplaneten und eines Systems mit mehreren Exoplaneten vorgestellt. Die Ergebnisse der Beobachtungen und Analysen umfassen die Entdeckung mehrerer vorher unbekannter stellarer Begleiter, und bilden so die Grundlage der größten und umfassensten bisher durchgeführten Untersuchung der Doppelsterneigenschaften der M-Sterne. Für vier enge Mehrfachsysteme unter den M-Sternen wurde eine detailliertere Spektralklassifizierung auf der Basis von Infratrotrspektren durchgeführt. Aufbauend auf der Suche nach stellaren Begleitern zu Sternen mit Exoplaneten wird untersucht inwieweit ein stellarer Begleiter die Planetenentstehung beeinflussen könnte. Weiterhin werden neue astrometrische Daten für drei der direkt beobachteten Planeten der HR 8799-Systems präsentiert, und eine Analyse der erlaubten Bahnparameter des Planeten HR 8799d durchgeführt.

CONTENTS

CHAPTER 1

INTRODUCTION

The multiplicity properties of stars hold keys to their formation and early evolution. Of the stars in our immediate neighbourhood, almost 50% are part of binary or multiple systems [1]. Binary/multiple stars can provide us with much information, including fundamental physical parameters such as mass from their orbital motion, and clues to their formation and early evolution are preserved in their multiplicity characteristics. Observing these properties, and recognizing how they depend on environment and mass, is therefore of utmost importance for understanding star formation in general.

The multiplicity of stars also affects planet formation. The formation of planets in disks surrounding young stars may be a natural outcome of the star formation. Many exoplanets have been discovered in binary or multiple star systems, but in what way their formation and evolution is affected by the presence of another star is debated. Will the presence of a close stellar companion inhibit or stimulate the formation of planets? And will the system be dynamically stable?

Further clues to what rules the formation of planets may be found in systems containing several planets. The orbital properties of the planets constrain their formation and dynamical history, as may comparison of properties of planets within the same system.

In this thesis, observations of binary/multiple stars and one multiple planet system are presented. From their observed properties, we look for clues to the formation and evolution of low-mass stars, substellar objects and exoplanets.

Chapter 2 provides a short overview of how observations of multiplicity relate to theoretical predictions of the formation of binary/multiple low-mass stars, of brown dwarfs and exoplanets. It ends with a brief introduction to the Lucky Imaging technique, which was used in two surveys for binary stars presented in this thesis.

In Chapter 3, the multiplicity of M dwarfs is investigated in what is the largest survey of its kind to date. We observed a large number of M dwarfs in order to investigate how multiplicity properties change in the mass region between solar-type stars and brown dwarfs, which show very different multiplicity characteristics. We also wanted to find nearby, young, close binaries suitable for further spectroscopic char-

[1] RECONS (REsarch Consortium On Nearby Stars) census of all known objects within 10 pc, 14 Sep 2011, `http://www.chara.gsu.edu/RECONS/census.posted.htm`

acterization and dynamical mass measurements. Near-infrared spectra of four such close, mid- to late-M type binaries or close couples in triple systems are presented in Chapter 4. These systems are characterized by spectral types and signs of activity.

In Chapter 5, a survey for binary companions to the hosts of transiting exoplanets is presented. Most Sun-like stars are part of binary or multiple systems, and so far most exoplanet searches have focused on solar type stars. However, faint stars at close angular separations to the planet host stars are often missed in seeing-limited surveys. Here, we discover candidate binary companions to host stars of transiting exoplanets using high angular resolution observations, and look for correlations between binary separation and planet properties in order to derive clues to planet formation in binary/multiple star systems.

The final research chapter investigates the orbits of giant planets in the HR 8799 system. Properties related to the formation and dynamical evolution of planets can be inferred from comparison with companions in the same system. Observations of the so far only directly imaged multiple exoplanet system HR 8799 are presented in Chapter 6. We present astrometric observations, and perform an orbital analysis of the planet HR 8799 d.

The last chapter summarizes the results of the research presented in this thesis, and provides an outlook towards related future work.

Chapter 3 and 6 have been published in Astronomy and Astrophysics (Bergfors et al., 2010a, 2011).

CHAPTER 2

BINARY STARS, SUBSTELLAR OBJECTS AND EXOPLANETS: AN OVERVIEW

2.1 Formation of low-mass stars in binary/multiple systems

Observations of young stars show that a large fraction of low-mass stars are born in multiple systems (see e.g., Goodwin et al., 2007; Duchêne et al., 2007). Multiplicity observed in different star forming regions, young associations and among field dwarfs of different masses are important for finding out how stars form and interact dynamically, and how star formation depends of the environment. For low-mass T Tauri stars ($0.1 - 0.5\,M_{\odot}$) as well as for field stars, the multiplicity fraction and distributions of mass-ratio and separation are dependent on the mass of the primary star (see e.g., Duchêne et al., 2007, for a review on the multiplicity of young stars).

In addition to reproducing the Initial Mass Function (IMF), models of star formation need also to account for properties such as multiplicity, clustering and mass segregation in star-forming regions (Bonnell et al., 2007). It has been argued by, e.g., Clarke (2007) that multiplicity characteristics provide the strongest observational constraints on theoretical models of star forming clusters, since the range of properties that need to be reproduced (e.g., binary/multiple frequency, distributions of mass-ratio and separation) is unlikely to emerge from the simulations by accident. Observations of stellar and brown dwarf multiplicity show trends of these properties with mass. Figure 2.1 show the distributions of mass-ratio ($q = M_{Sec}/M_{Prim}$) and separation for solar-type stars, early- to mid-type M dwarfs, and very-low-mass stars ($M < 0.1M_{\odot}$) and brown dwarfs.

Many theories for the formation, and disruption, of binary and multiple stellar systems exist. Some scenarios predict different outcomes in multiplicity properties, and thus observations of multiplicity can be used for testing theoretical predictions. Most binary/multiple systems are in general believed to form by fragmentation, either of collapsing molecular cloud cores or later on in circumstellar disks. Theories of binary star formation have been reviewed by e.g., Goodwin et al. (2007); Tohline (2002); Bodenheimer et al. (2000), and here I provide a short summary which includes the

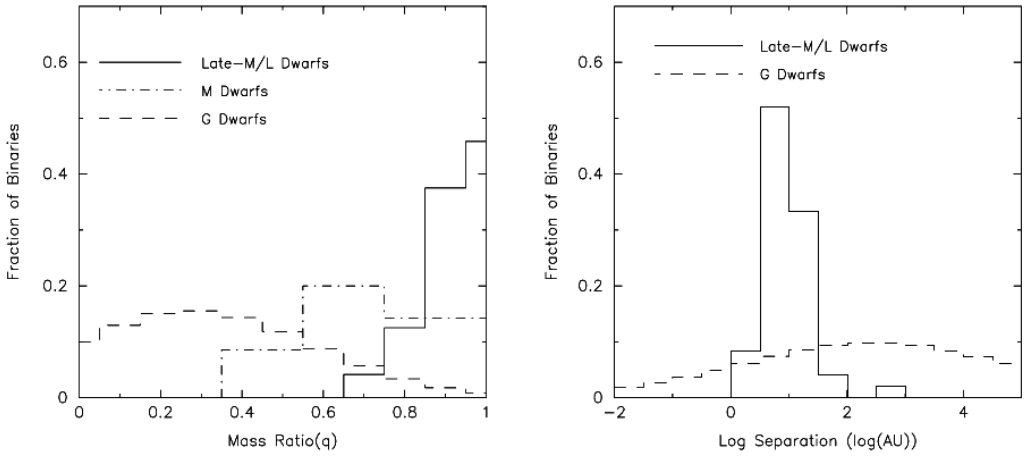

Figure 2.1: Distributions mass-ratio and semi-major axis for solar-type stars, early to mid-type M dwarfs, and VLM objects. Figure from Allen (2007).

predictions for multiplicity, if any.

2.1.1 Fragmentation of prestellar cores

A "typical" prestellar core is described as one of the denser structures within molecular clouds that have radius r $\sim$ 0.1 pc, density n $\gtrsim 10^4\,\mathrm{cm}^{-3}$ and velocity dispersion of $\sigma \sim 0.5\,\mathrm{km\,s}^{-1}$ (Goodwin et al., 2007). The first phase after a prestellar core becomes gravitational unstable and the collapse begins is an isothermal phase in which the gas is thin and the energy can escape. While the density increases in this phase, the temperature is thus constant at $\sim$ 10 K. The second stage sets in when the density reaches $\sim 10^{10}\,\mathrm{cm}^{-3}$ and the opacity increases to the point that the energy from contraction can no longer escape freely. The gas is now adiabatic, and the temperature rises. A hydrostatic core has now formed in the center. Continued accretion onto this so-called first core increases the density and temperature. At a temperature of around 2000 K (n $\sim 10^{16}\,\mathrm{cm}^{-3}$) H_2 dissociates, causing a second collapse at the end of which a protostar emerges (Goodwin et al., 2007; Chabrier et al., 2007; Machida, 2011).

If the necessary angular momentum is provided, by bulk rotation or by turbulence, the prestellar cores can fragment to produce multiple star systems. Fragmentation mechanisms are discussed in the review by Goodwin et al. (2007). The fragmentation of cores is expected to produce binaries or multiple systems with maximum separations of a few hundred AU, but systems closer than $\sim 20 - 30$ AU appear difficult to form. It is possible that a second phase of fragmentation occurs on smaller scales, or that some hardening mechanism is responsible for closer binaries (Goodwin et al., 2007).

2.1.2 Disk fragmentation

Binaries can also form at later stages of star formation, from the fragmentation into one or more components of a circumstellar disk that forms around the protostar. Gravitational instabilities in a massive disk can be induced by close encounters with other stars or disks, or without external interactions. One of the requirements is that the disk is massive enough ($\sim 0.1\,M_{\odot}$), which means that binary formation via disk fragmentation can only occur around solar-type or more massive stars.

Smoothed particle hydrodynamic (SPH) simulations by Stamatellos et al. (2007); Stamatellos & Whitworth (2009) show that massive, extended disks can form around solar-type stars, which fragment rapidly (within a few thousand years) and form very-low-mass stars, brown dwarfs and planetary-mass objects. The model is successful in explaining several observed properties of very-low-mass stars and brown dwarfs, such as the brown dwarf desert (paucity of brown dwarfs at close separations to solar-type stars), the large disks observed around brown dwarfs, and their low binary fraction. They also find that almost all binaries are close ($a < 2\,\mathrm{AU}$), and more than half of the binaries have mass ratios $q > 0.7$. This scenario may complement formation by turbulent fragmentation at close binary separations for very-low-mass objects (see Sect. 2.2.1).

2.1.3 Capture

The formation via dynamical encounters is not likely to be responsible for most binaries. The main problem with the formation of binaries from capture of another star is dynamical, since kinetic energy must be carried away from the system in order to form a binary. The excess orbital energy may be carried away by a third star in a three-body encounter (Goodman & Hut, 1993). Alternatively, in encounters between only two stars it could be absorbed by tidal dissipation in protostellar disks, if present. Formation by capture naturally predicts that the multiplicity fraction should increase with age. Observations show that young stars have high multiplicity, and they are therefore likely to form directly as binaries instead of at later stages. Formation of binaries from dynamical capture might occur to some extent in very densely populated regions, but is not a likely formation scenario for most binaries in typical star-forming regions, and even less so for higher order multiple systems.

2.1.4 Fission

In the classical fission-scenario, a rotating protostellar core or protostar flattens and deforms into a triaxial bar-shape, which may evolve into a pear-shaped or dumbbell-shaped configuration from which the two binary components detach and produce a close binary system. It has been shown by several hydrodynamical simulations and stability analyses that formation of binaries via this process is not likely to occur, and the classical fission theory has been largely abandoned (see Bodenheimer et al., 2000, and references therein).

2.2 Formation of very-low-mass stars and substellar objects

Observations of multiplicity also provide powerful constraints to theoretical models of the formation of very-low-mass stars and substellar objects [1] (see e.g., Burgasser et al., 2007, for a review of the multiplicity properties of very-low-mass stars and brown dwarfs). If very-low-mass (VLM) star and brown dwarf formation is just a scaled-down version of star formation, then trends with mass of properties such as the multiplicity fraction and the distributions of mass-ratio and separations, which are seen for stars, should be continued into the substellar mass region. However, it has been suggested that VLM stars and brown dwarfs cannot simply form like stars via the processes mentioned in the previous section. Thies & Kroupa (2007) found that the different multiplicity properties of stars on the one hand, and VLM stars and brown dwarfs on the other, cause a discontinuity in the IMF close to the boundary between low-mass stars and brown dwarfs when the mass function is corrected for unresolved binarity. In favour of a different formation is the existence of the brown dwarf desert for solar type stars, and the lower binary fraction of VLM stars and brown dwarfs. Another strong indication is that the separation distributions, and thus the binding energies, are significantly different for brown dwarfs compared to stars.

2.2.1 Turbulent fragmentation

In classical star formation, the minimum mass for fragmentation in a molecular cloud is the Jeans mass M_J, which is proportional to the temperature and inversely proportional to the density. This is usually assumed as the stellar minimum mass. The problem with forming brown dwarfs is that in order for the proto-brown dwarf cores to reach the Jeans mass and become gravitationally unstable and collapse, exceptionally cold and dense environments are required. Padoan & Nordlund (2004) suggested that brown dwarfs can be formed when supersonic turbulence produces density variations in the molecular cloud. The turbulent shocks create regions in which the density is high enough for very low-mass cores to collapse and produce brown dwarfs. In this formation scenario, brown dwarfs thus form like stars, but in a scaled-down version.

2.2.2 Brown dwarf ejection

One example of a non-starlike process to form substellar objects is to remove the stellar embryos from their birth site before they become too massive. Brown dwarfs thus begin to form as any other protostars from fragmenting protostellar cores or in a fragmenting disk (see Sect. 2.1.1 and 2.1.2), but the lowest mass protostars are ejected via dynamical N-body interactions before the hydrostatic cores can accrete enough of the surrounding material and reach the hydrogen burning mass limit (Reipurth & Clarke, 2001).

[1] How to define substellar mass objects is heavily debated (see, e.g., Boss et al., 2003). We adhere to the definition of a substellar object as an object that is not massive enough to sustain hydrogen fusion, i.e., brown dwarfs and free-floating planetary-mass objects formed by the same processes (sub-brown dwarfs). In a similar fashion as the substellar definition, one may follow the working exoplanet definition by IAU of a planet as an object that orbits a star and has a mass below the deuterium burning limit.

Hydrodynamical simulations by e.g. Bate et al. (2002); Bate (2009) have demonstrated that brown dwarfs may be formed from either the collapse of a turbulent molecular cloud into subsequently dynamically ejected stellar embryos, or formed by fragmentation of circumstellar disks from gravitational instabilities. Analytical N-body calculations of the dynamical decay of accreting triple systems by Umbreit et al. (2005) also found that brown dwarfs are readily formed by ejection.

In terms of multiplicity, the predictions of Reipurth & Clarke (2001) include the brown dwarf desert (since brown dwarfs are ejected, or continue to accrete mass and become a star), and the paucity of wide brown dwarf binaries (since wide couples would be disrupted from the ejection). In the to date largest hydrodynamical simulation of star cluster formation, Bate (2009) found that the simulation produced many observed properties of stellar and substellar multiplicity, such as the decreasing multiplicity fraction with decreasing mass, and the trends that are observed in the distributions of mass-ratio and separations. However, other properties such as the formation of too many brown dwarfs compared to stars, and too few low mass-ratio systems for solar-type stars were less well reproduced in these simulations.

2.2.3 Photoevaporation

Another way to prevent that hydrogen burning mass is reached is photoevaporation of prestellar cores by a nearby massive O or B star (Whitworth & Zinnecker, 2004). Massive prestellar cores that would in the absence of the eroding radiation form stars of low to intermediate mass instead lose the outer layers and turn out as free-floating brown dwarfs. Since this could only happen in the vicinity of very massive stars, it can not be the primary process for forming brown dwarfs, but could occur in high-mass star-forming regions.

2.3 Multiplicity and planet formation

2.3.1 The formation of giant planets

Circumstellar disks in which planets form are the result of the conservation of angular momentum in a collapsing cloud core, and the formation of planets is thus very strongly linked to the formation of stars. The first exoplanet discovered around a solar-type star, 51 Peg in 1995 (Mayor & Queloz, 1995), was only the first of many massive planets in very close orbits around their host stars that have since been called Hot Jupiters. The new class of planets so different from the ones we knew before clearly showed that our solar system may not at all be representative for all planetary systems. The first discoveries of exoplanets belonging to a member of a binary/multiple stellar system came less than two years later: the exoplanet host star 16 Cyg B is the secondary star in a triple system (Cochran et al., 1997), and the planets υ And b, τ Boo b, and 55 Cnc b all belong to the primary stars in binary systems (Butler et al., 1997). Today we know of around 50 systems where the planets belong to one component of a binary/multiple star (an S-type orbit), and seven planet candidates that orbit both components of a close binary (P-type orbit). Observations of the overall frequency of planets in binary/multiple systems provide not only a census of the occurrence of

planets, since many stars are part of a binary/multiple system, but correlations between properties of the stellar system and the planets provide constraints on theories of planet formation and evolution.

There are two widely supported models for planet formation: core-accretion and gravitational instability. In the core-accretion scenario (e.g., Pollack et al., 1996; Lissauer & Stevenson, 2007), the planets start from coalescing dust particles and gradually grow from collisions of larger and larger clumps to eventually becoming planetesimals and planets. Giant planets form as rocky/icy cores of 10 – 15 Earth masses and subsequent runaway accretion of a gaseous envelope. Because of the long timescales involved to form giant planets in the core accretion scenario, planet migration and disk evolution is usually assumed in order for the planet to accrete enough mass before the gas disk dissipates (e.g., Alibert et al., 2005). The efficiency of planetesimal formation from core accretion depends very strongly on metallicity. High metallicity leads to fast planet core formation, leaving lots of time to accrete gas (e.g., Johansen et al., 2009).

While core accretion is commonly favoured as the model of formation for most planets, partly because of the observed correlations between high metallicity and the occurrence of exoplanets, some observed systems seem to be more readily explained by gravitational instability formation. In the gravitational instability model (Boss, 1997, 2006; Durisen et al., 2007), giant planets are formed by gravitational collapse and fragmentation of large scale spiral structures in the protoplanetary disks on relatively short timescales ($\lesssim$ 10 000 years). For planet formation to occur, the surface density of the disk needs to be large enough to be gravitationally unstable, and in order to fragment the cooling must also be efficient (Toomre, 1964; Gammie, 2001; Rice et al., 2003). Therefore, planet formation via gravitational instability is only efficient at large separations. For instance, directly imaged exoplanets such as Fomalhaut b and at least the outer planets in the HR 8799 system studied in Chapter 6 in this thesis are considered good candidates for having formed by gravitational instability (Dodson-Robinson et al., 2009; Nero & Bjorkman, 2009; Marois et al., 2010).

2.3.2 The influence of a second star

How a second, closely separated star in the system affects planet formation is debated. Artymowicz & Lubow (1994) found analytically and numerically that a typical disk is truncated at a radius $r_t \sim 1/3\, a_{bin}$ in a binary system with mass-ratio q = 0.5 and eccentricity $e_{bin} = 0.3$. By truncating the disk, material that might have formed planets is reduced. Nelson (2000) found numerically that a stellar companion influences giant planet formation negatively in either formation mechanism in an equal mass close binary system with semi-major axis $a \sim 50$ AU. The temperatures become so high during the periodic heating that condensation of solid material is reduced, required for core accretion, and it hinders the onset of gravitational instability since spiral structures decay to quickly. On the other hand, Boss (2006) found that a stellar companion stimulates the formation via gravitational collapse, and Mayer et al. (2005) concluded that if formed by gravitational instability, the influence of a close stellar companion will affect planet formation negatively, but planets formed by core accretion should be common. Figure 2.2 shows observations and simulations by Mayama et al. (2010) of interacting circumstellar disks in the multiple system SR24.

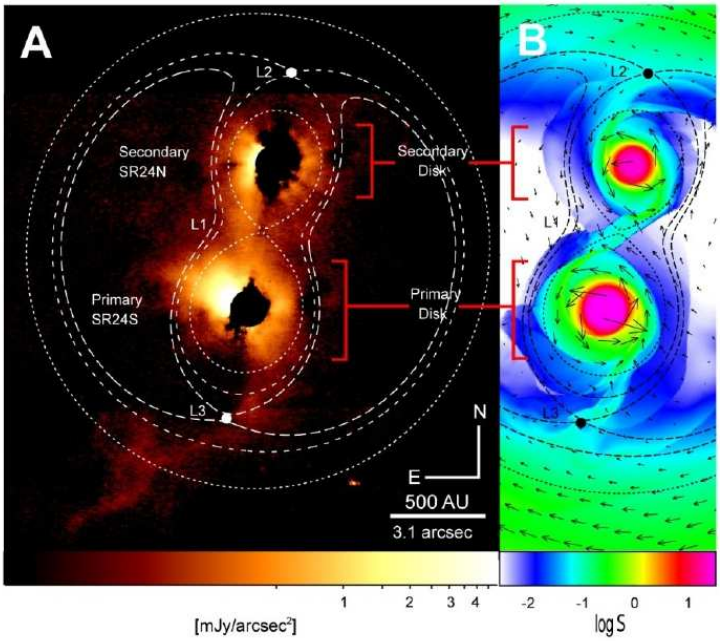

Figure 2.2: Multiple system with interacting circumstellar disks. (A): coronagraphic H-band image of the SR24 multiple system, (B): 2D numerical simulation of the accretion (Mayama et al., 2010).

A stellar companion may also affect later stages in planet formation. In numerical simulations of a planet embedded in a protoplanetary disk by Kley (2000), the secondary star does not only truncate the disk, but the migration rate and mass growth of the planet is also affected. A secondary star in a highly inclined orbit ($i > 39.2^o$) may interact secularly via the Kozai mechanism, i.e., an exchange of angular momentum between the planet and the secondary star that induces periodic oscillations in eccentricity and inclination (Kozai (1962); also Holman et al. (1997); Takeda & Rasio (2005)). The long-term stability of planets in binary systems have been investigated by e.g., Holman & Wiegert (1999); Pilat-Lohinger & Dvorak (2002). Eggenberger et al. (2004) summarizes how a secondary star influences the formation and evolution of planets, and how it can be observed.

2.4 Multiple planets systems

A large fraction of exoplanets have been found in multiple planet systems, and it appears to be a very common outcome of planet formation (see e.g. review by Udry & Santos, 2007). About 1/3 of transiting planet candidates discovered in the first four months of the Kepler mission are part of multiple planet systems (Latham et al., 2011). Only one multi-planet system has been directly observed so far, the HR 8799 system, which contains at least four giant planets at large orbital separations from the star.

For directly imaged systems of multiple planets, long-term astrometric observations

can provide accurate masses from dynamical studies without relying on untested evolutionary models. E.g., Dupuy et al. (2009) found that evolutionary and atmospheric models are largely inconsistent, and tend to underestimate luminosities when compared to a binary brown dwarf system with precise dynamically determined masses. For multiple planet systems, it can also in general be assumed that the planets in the system formed at the same approximate time and from the same original protoplanetary disk. Differences between the planets in, e.g., atmospheric composition can therefore tell us something about the structure (temperature, chemical composition) of the disk, and from astrometric observations orbital period, eccentricity, resonant configurations, etc., may tell us about their formation (gravitational instability vs. core accretion) and dynamical evolution (e.g., disk migration, see Papaloizou et al. (2007) and references therein; planet-planet scattering, Rasio & Ford (1996); Chatterjee et al. (2008); Veras et al. (2009); Scharf & Menou (2009)).

2.5 The Lucky Imaging technique

For resolving the close binaries in the surveys described in this thesis, high angular resolution observations are needed to overcome the blurring effects of the turbulent atmosphere. In the near-infrared, adaptive optics is commonly implemented on large (8-10 m) telescopes, detecting and correcting for wavefront distortions in real time using a system of wavefront sensor and deformable mirror. Lucky Imaging is another high angular resolution imaging technique, with which almost diffraction-limited resolution can be achieved with 2–4 m class telescopes at optical wavelengths.

Lucky Imaging is a passive technique, the principle of which is to reduce the effects of seeing by selecting and combining only the best few percent of many, very short integrations. The probability that the distortion of the wavefront is minimal for a very short exposure time is dependent on the diameter of the telescope and observatory seeing conditions, (i.e., proportional to the exponential of the squared ratio of the aperture D and the Fried parameter r_0, Fried, 1978). This corresponds to usual optimal performance in the wavelength range of 700-1100 nm for medium-sized 2-4 m telescopes. For best results, the integrations should be shorter than the atmospheric coherence time so as to effectively "freeze" the atmosphere, i.e., $\sim$ 10 ms. Of a total $\sim$ 10 000 frames, the least distorted are selected and combined to yield the "lucky" result. Figure 2.3 illustrates the efficiency of Lucky Imaging with the AstraLux Sur instrument. The target is a triple M dwarf system in which the close secondary and tertiary components are separated by $\rho_{\rm BC} \approx 0.15''$.

The Lucky Imaging technique has the advantage of providing similar performance as adaptive optics in terms of spatial resolution, but with medium-sized telescopes and at shorter wavelengths. The very short instrumental time overheads also means that many targets can be observed in short time. The technique has been very successful for stellar multiplicity surveys of, e.g., very-low-mass stars (Law et al., 2005, 2006, 2008), and massive stars (Maíz Apellániz, 2010). The technique has also been combined with adaptive optics, e.g., at the Palomar 5 m telescope Law et al. (2009), and at the 4 m William Herschel Telescope (WHT), where the combination was used for high-contrast imaging of the close brown dwarf binary GJ569Bab (Femenía et al., 2011). MPIA has built two Lucky Imaging instruments, AstraLux Norte for observing the northern sky with the 2.2 m telescope at the Calar Alto observatory in Spain, and

Figure 2.3: Lucky Imaging with AstraLux Sur. From left to right: (1) Sum of 50 000 images with 25 ms integration time in SDSS z'-band. (2) All 50 000 images, shifted on the brightest pixel in each image and added together. The resolution is seeing limited. (3) Best 50% of the images combined, selected by Strehl ratio. The seeing halo is dramatically reduced. (4) Best 10% combined. (5) Best 1% combined. The resolution is almost diffraction limited and the closely separated secondary and tertiary star are clearly resolved. Taken from Hippler et al. (2009).

AstraLux Sur for southern sky observations with the NTT at La Silla, Chile (Hormuth et al., 2008; Hippler et al., 2009).

CHAPTER 3

LUCKY IMAGING SURVEY FOR SOUTHERN M DWARF BINARIES

Abstract:

While M dwarfs are the most abundant stars in the Milky Way, there is still large uncertainty about their basic physical properties (mass, luminosity, radius, etc.) as well as their formation environment. Precise knowledge of multiplicity characteristics and how they change in this transitional mass region, between Sun-like stars on the one side and very low mass stars and brown dwarfs on the other, provide constraints on low mass star and brown dwarf formation.

In the largest M dwarf binary survey to date, we search for companions to active, and thus preferentially young, M dwarfs in the solar neighbourhood. We study their binary/multiple properties, such as the multiplicity frequency and distributions of mass-ratio and separation, and identify short period visual binaries, for which orbital parameters and hence dynamical mass estimates can be derived in the near future. The observations are carried out in the SDSS i' and z' band using the Lucky Imaging camera AstraLux Sur at the ESO 3.5 m New Technology Telescope. Lucky Imaging is a very efficient way of observing a large sample of stars at an angular resolution close to the diffraction limit.

In the first part of the survey, we observed 124 M dwarfs of integrated spectral types M0-M6 and identified 34 new and 17 previously known companions to 44 stars. We derived relative astrometry and component photometry for these binary and multiple systems. More than half of the binaries have separations smaller than 1″ and would have been missed in a simply seeing-limited survey. Correcting our sample for selection effects yields a multiplicity fraction of 32±6% for 108 M dwarfs within 52 pc and with angular separations of 0.1″ – 6.0″, corresponding to projected separations of 3-180 AU at median distance 30 pc. Compared to early-type M dwarfs ($M \gtrsim 0.3 M_{\odot}$), later-type (and hence lower mass) M dwarf binaries appear to have closer separations, and more similar masses.

From Bergfors et al., 2010, A&A 520, A54

3.1 Introduction

M dwarfs form a link between solar-type stars and brown dwarfs, two mass regions that exhibit very different multiplicity characteristics. Because properties such as binary fraction, period distribution, and mass-ratio distribution provide important constraints on models of star formation and dynamical evolution (Goodwin et al., 2007; Burgasser et al., 2007), precise knowledge of multiplicity characteristics and how they change within this transitional mass region is important to understanding the formation of low-mass stars and brown dwarfs. Repeated astrometric observations of binary systems can also provide dynamical mass estimates, which are crucial to the empirical calibration of the mass-luminosity relation and evolutionary models. While being well known for solar-type stars, these relations are not very well constrained for lower mass stars. Theoretical models have been shown to under predict the masses of M dwarfs ($M \lesssim 0.5 M_{\odot}$) by 5-20%, and are particularly inconsistent for masses below $0.3 M_{\odot}$ (e.g., Hillenbrand & White, 2004).

It is generally agreed upon that the binary fraction $f_{\rm bin} = N_{\rm binaries}/N_{\rm total}$ decreases with decreasing stellar mass (see, e.g., review by Burgasser et al., 2007). While the binary fraction of Sun-like stars is ≈57% (Duquennoy & Mayor, 1991) over the full range of orbital separations, the fraction of multiple stars decreases to ≈26-42% for M0-M6 dwarfs (Delfosse et al., 2004; Reid & Gizis, 1997; Fischer & Marcy, 1992). For very low mass stars ($M < 0.1 M_{\odot}$) and brown dwarfs, the binary frequency is only 10-30% (e.g., Bouy et al., 2003; Reid et al., 2008; Joergens, 2008; Goldman et al., 2008). These previous surveys of M dwarfs are limited to relatively small individual sample sizes, the largest until now being that of Delfosse et al. (2004), which consisted of 100 stars.

Whether the observed multiplicity characteristics are smooth functions of mass - implying that very low mass stars (VLMSs) and brown dwarfs (BDs) form like more massive stars - or if another process is primarily responsible for the formation of VLMSs and BDs, is debated. The multiplicity distributions of VLMSs and BDs show some important differences from those of Sun-like stars. The semi-major axis distribution of VLMSs and BDs is narrow and peaks at small separations (3-10 AU, e.g., Burgasser et al., 2007), in strong contrast to the separation distribution of solar-type binaries, which is wide and peaks at around 30 AU (Duquennoy & Mayor, 1991). The mass-ratio distribution also differs for VLMSs and BDs from that of Sun-like stars, showing a clear preference for equal mass binaries (e.g., Burgasser et al., 2007) as opposed to the flat distribution of the more massive stars (Duquennoy & Mayor, 1991). For M dwarfs, the mass range in-between, Fischer & Marcy (1992) found a relatively flat mass-ratio distribution, while Reid & Gizis (1997) found a preference for almost equal mass systems. The differences in binary characteristics have been argued by, e.g., Thies & Kroupa (2007) to support the existence of two populations, 'star-like' and 'BD-like', which are formed by different processes.

The AstraLux M dwarf survey (Hormuth et al., 2009) investigates the multiplicity characteristics of low-mass stars using high-resolution Lucky Imaging performed by the two AstraLux instruments, AstraLux Norte at the Calar Alto 2.2 m telescope (Hormuth et al., 2008) and AstraLux Sur at NTT at La Silla (Hippler et al., 2009). The full survey will include ~800 stars in the range of spectral types M0-M6 within 52 pc from the Sun, selected from the Riaz et al. (2006) catalogue of young, nearby late-type

stars. The choice of observing young stars is motivated by the higher sensitivity to substellar companions, which at young ages are still warm and hence brighter and easier to detect than around older stars. A 0.072 $M_{\odot}$ brown dwarf is 3.2 magnitudes brighter in I-band at the age of 0.5 Gyr than at an age of 5 Gyr (Baraffe et al., 2003). Thus, by surveying young M dwarfs we can also detect brown dwarf companions with masses close to the stellar/substellar boundary. The large sample will allow a detailed statistical analysis of multiplicity characteristics, in the mass region between Sun-like stars and brown dwarfs where these properties change drastically. Follow-up observations of close, nearby multiple systems will also enable dynamical masses to be determined, allowing calibration of the mass-luminosity relation for stars less massive than $0.5 M_{\odot}$. We present here the first southern sky sample, consisting of 124 M dwarfs.

3.2 Observations and data reduction

3.2.1 Observations

The first subsample of the 124 nearby M dwarfs presented here (see Table A.1) was observed with the AstraLux Sur high resolution camera mounted at the Nasmyth B focus of the ESO 3.5 m New Technology Telescope (NTT) at La Silla on November 12-16, 2008. The targets were selected from the Riaz et al. (2006) catalogue of ≈ 1000 nearby active M dwarfs. All of our targets have spectral types M0-M6 and lie within 52 pc of the Sun. We do not have direct age estimates for more than a few individual stars (see Appendix B), although the Riaz et al. (2006) sample was compiled by correlating 2MASS with ROSAT data, and the sample as a whole, based on its typically strong coronal emission and low tangential velocity (< 40 km s^{-1}), is very likely young.

AstraLux Sur (Hippler et al., 2009) is a high-speed electron multiplying camera for Lucky Imaging observations at the NTT. The instrument is an almost identical copy of the common user AstraLux Norte camera at the Calar Alto 2.2 m telescope (Hormuth et al., 2008). The Lucky Imaging principle is to minimize atmospheric seeing effects by taking many (∼ 10 000) very short exposures (∼ 10 ms) of the target, thereby effectively "freezing" the atmosphere in each image. Only the least distorted few percent of the frames, selected on the basis of Strehl ratio, are then combined to achieve almost diffraction-limited resolution. The Drizzle algorithm (Fruchter & Hook, 2002) shifts and adds the slightly undersampled raw images by centering on the brightest pixel, thereby generating an oversampled output image with a pixel scale of ≈ 15.37 mas (Hormuth et al., 2008).

On each night of observations, the M dwarf targets were observed in either the SDSS i' or z' filter. Each star was observed in full-frame mode (FoV 15.74″, integration time 29.45 ms) and in some cases, if the flux was high enough, in subframe mode (FoV 7.87″, integration time 15.29 ms), allowing for shorter integration times and hence less distortion by atmospheric turbulence. Twilight sky-flats were obtained whenever the weather conditions were suitable, otherwise we used dome flats. Astrometric reference stars in 47 Tuc and Trapezium (see Köhler et al., 2008) were observed several times each night, allowing us to determine the plate scale and detector orientation. We assume atmospheric refraction to cause a negligible amount of field distortion (∼1 mas) since separations between the binaries are small. The IRAF *geomap* procedure was

used to determine the plate scale of the drizzled images to be 15.373 mas/px with a mean scaling uncertainty of 0.002 mas/px, and a rotation angle of $1.71^{o} \pm 0.3^{o}$.

3.2.2 Photometry and astrometry of the candidate binaries/multiples

Binary separations, position angles, and magnitude differences in SDSS i' and z' filters were obtained for each binary/multiple system by fitting model PSFs from a set of reference stars (see Bouy et al., 2003). We used single stars from our observed sample with symmetric PSFs as references. The astrometric and photometric values presented are weighted averages of several measurements. The weighting is based on the residuals of the PSF fits. In our analysis, we primarily used the highest quality 10% selection of 10 000 integrations with 30 ms exposure time each, yielding a total integration time of 30 s per target and filter. In a few rare cases, we used the 1% selection to achieve a slightly higher astrometric accuracy.

Since the Lucky Imaging produces a stellar PSF with an almost diffraction-limited core and a seeing halo, high-pass filtering was implemented before fitting the model PSF when the stellar companion was much fainter than the primary star and close enough to reside within the halo. For the astrometric parameters (binary separation and position angle), we used only the z'-band images since they are affected by less atmospheric refraction than the i'-band frames. For the wide binaries (separation $\rho > 2''$), the PSFs of the companions do not overlap and we used the IRAF aperture photometry task *phot* for the astrometry and photometry. This approach produces results with approximately the same uncertainty as the PSF fitting procedure. A combination of the two procedures was employed in a few cases for the triple systems. The dominant errors in the determined position angles arise from the uncertainty in field rotation (see Sect. 3.2.1) and is therefore assumed to be 0.3^{o} for all systems. The average error in separation is 4 mas.

If the two stars are close and of similar magnitude, the Lucky Imaging drizzle combination sometimes centres on the secondary star instead of the primary, leading to the appearance of a fake third stellar component in the image. In that case, a ghost stellar image appears at the same separation from the primary but at a 180^{o} angle from the real secondary. To recover the flux ratio of the two "real" binary components from the fake triple, we measured the flux of the three components and used the "de-tripling" equation of Law (2006) given by

$$F_{\mathrm{R}} = \frac{2I_{13}}{I_{12}I_{13} + \sqrt{I_{12}^2 I_{13}^2 - 4I_{12}I_{13}}} \tag{3.1}$$

where F_{R} is the true binary flux ratio, $I_{12} = F_1/F_2$ and $I_{13} = F_1/F_3$.

Table A.1 lists the complete sample of observed stars with integrated spectral type, distance, J magnitude, and $\log[L_x/L_{bol}]$ from Riaz et al. (2006), the filter(s) in which the star was observed and corresponding epoch. Table A.2 lists the astrometric and photometric properties derived for the binary/multiple systems in our sample. Component A is the primary star, which is defined as the brightest of the components in z'-band. Figure 3.1 shows all observed multiple systems with separations closer than $1''$, and Fig. 3.2 shows the wider systems with separations of between $1''$ and $5.5''$.

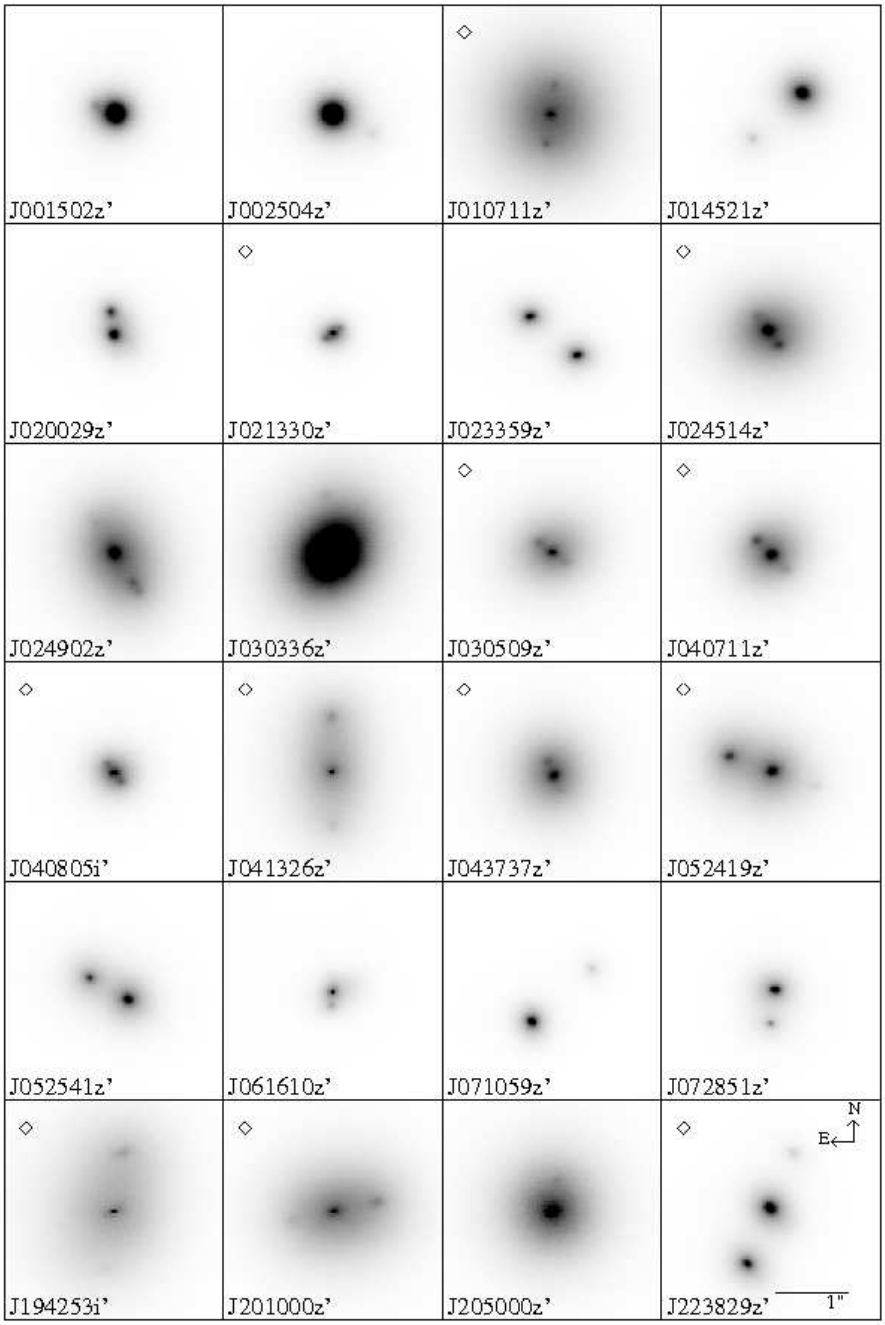

Figure 3.1: AstraLux Sur images of the systems closer than 1″. The last character in the ID refers to the filter in which the star is imaged (SDSS i' or z'). The images are shown in a logarithmic intensity scale. The scale and orientation is the same for all images and is shown in the bottom right image. The only physical triple system in the figure is J024902. What appears as a third star at 180° angle from the true secondary in some images is an effect of the Lucky Imaging drizzle combination described in Sect. 3.2.2. Images affected by this effect are marked with a diamond in the upper left corner.

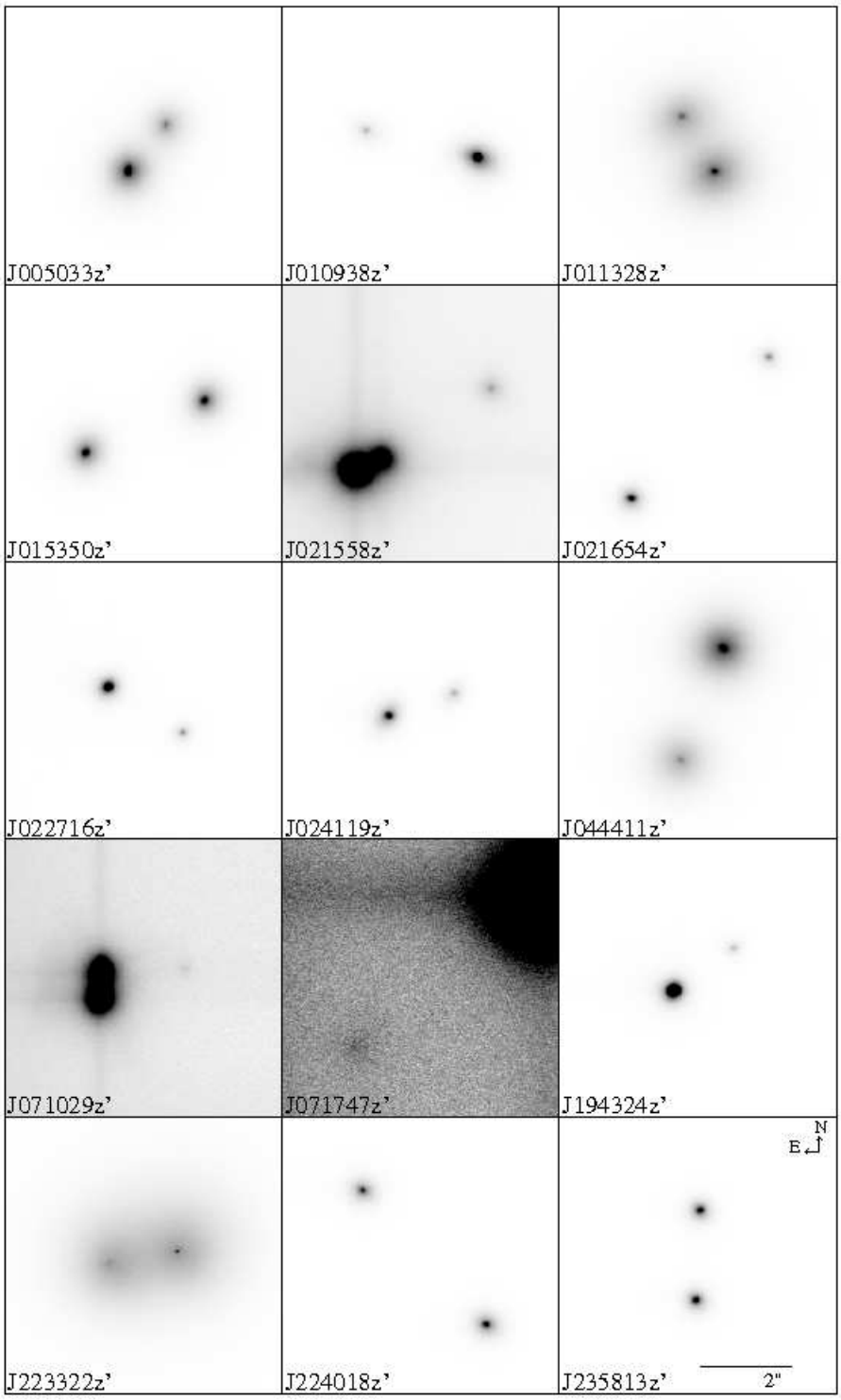

Figure 3.2: AstraLux Sur images of the systems with separations between 1″ and 5.5″. The last character in the ID refers to the filter in which the star is imaged (SDSS *i*′ or *z*′).The scale and orientation is the same for all images and is shown in the bottom right image. The images are shown in a logarithmic intensity scale, except for J021558*z*′, J071029*z*′, and J071747*z*′, which are shown on a logarithmic square root scale.

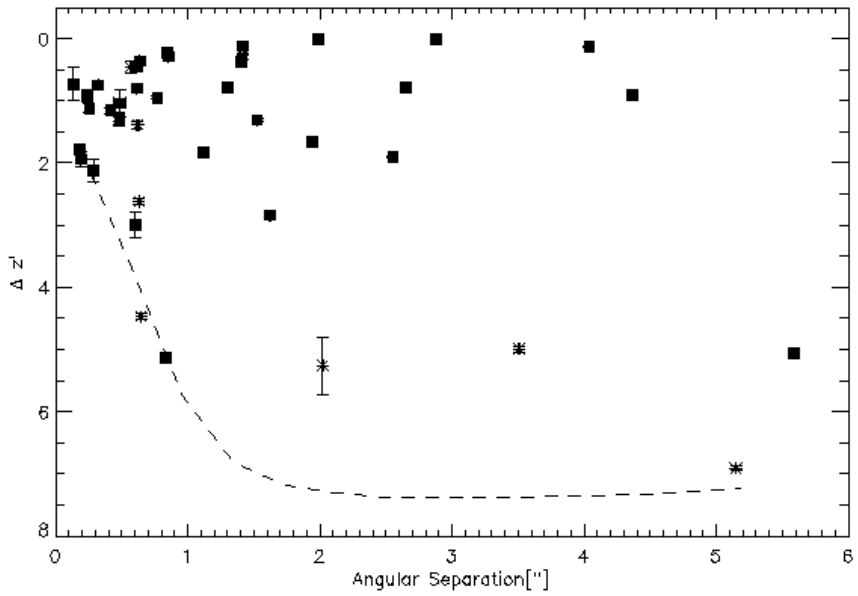

Figure 3.3: Observed z'-band magnitude difference $\Delta z'$ as a function of angular separation. Squares denote binary systems and asterisks components in triple/quadruple systems. Only systems selected from the criteria in Sect. 3.3.2 are included. The dashed line corresponds to the typical 5σ detection limit in these observations.

Brightness differences achieved are typically 3.5 magnitudes for angular separations $\sim 0.5''$ and ≥ 6 magnitudes at $\sim 1''$ (Fig. 3.3).

3.3 Results

3.3.1 Stellar ages and spectral types

The observed sample is, as a whole, assumed to be young ($\lesssim 600$ Myr), based on its typically strong coronal emission and low tangential velocity (Riaz et al., 2006). As the velocity dispersion of stars steadily increases with time (e.g., Seabroke & Gilmore, 2007), the low tangential velocities of smaller than 40 km s^{-1} of the stars in the Riaz et al. (2006) sample combined with activity indicators provide evidence of their youth. Holmberg et al. (2009), e.g., calibrated the age-velocity relation (AVR) for FG stars. By scaling their 3D AVR of FG stars to the tangential (2D) velocity dispersion of our sample of M dwarfs, we derive an upper age limit of $\approx$1 Gyr.

The spectral types of the individual components in the multiple systems were estimated to a precision of ± 1 subclasses following the method of Daemgen et al. (2007).

We assumed that the flux ratios of the individual components obtained from the PSF fitting are linearly related to the integrated spectral types provided by Riaz et al. (2006). This relation was combined with the Kraus & Hillenbrand (2007) magnitude - spectral type relations, using linear interpolation to derive individual spectral types in 0.5 subclasses. Table A.3 summarizes the separate component spectral types. The spectral types were determined from observations in both filters i' and z' when available, which are in most cases consistent and otherwise noted in the Appendix B. For some stars, we derived primary star spectral types that are 0.5 subclasses earlier than the integrated spectral types. The primary spectral type range for the multiple systems is thus K7.5-M5.5 (see Table A.3). Only the systems where the primary star has a spectral type M0 or later are used in the statistical analysis.

The Kraus & Hillenbrand (2007) relations can be used for spectral types no later than L0. However, we estimate that five of the companions are of later spectral type. Four of these objects were only observed in z' filter (see Appendix B). For these five companions, we do not determine the spectral types in any more detail than "later than L0" until we can assign more precise spectral types using future spectroscopic observations. The multiple systems containing these faint objects are excluded from the following mass ratio analysis, because of their unknown spectral types (and hence unknown masses).

3.3.2 Binary/multiplicity fraction

In our sample of 124 observed M dwarfs in the integrated spectral type range M0-M6, we find 51 companions belonging to 44 stars in the angular separation range 0.1″-9.5″ and z'-band magnitude difference $0 < \Delta z' < 6.9$. The observed number of single:binary:triple:quadruple stars is 80:38:5:1. However, the survey is most likely insensitive to companions fainter than $\Delta z' > 2$ in the angular separation range 0.1″-0.5″, and is incomplete for separations greater than 6″ because of the small FoV. Figure 3.3 shows the z'-band magnitude difference achieved as a function of the component angular separation and the typical 5σ detection limit. Figure 3.4 depicts the number of binaries per angular separation. The distribution is strongly peaked at close separations, with more than half of the companions being within 1″ to the primary star, suggesting that the vast majority of the observed binaries are indeed physical companions and not the product of background star contamination. While most companions were discovered in this survey (34 stars, see Table A.2), some of the binaries in our sample were already known to be co-moving pairs and some are confirmed here by second epoch observations (17 companions, see Table A.2 and Appendix).

For the following statistical analysis (multiplicity fraction, mass ratio distribution, and separation distribution), we exclude stars/systems

- that lie farther than 52 pc from the Sun (J06061342-0337082);
- components of the binary/multiple systems with separations greater than 6″ from the primary star (the components J06583980-2021526C, J08224744-5726530C, and the systems J21103147-2710578 and J22171899-0848122);
- binary/multiple systems for which we derive primary spectral type earlier than M0 (J01452133-3957204, J04071148-2918342, J04373746-0229282), or which

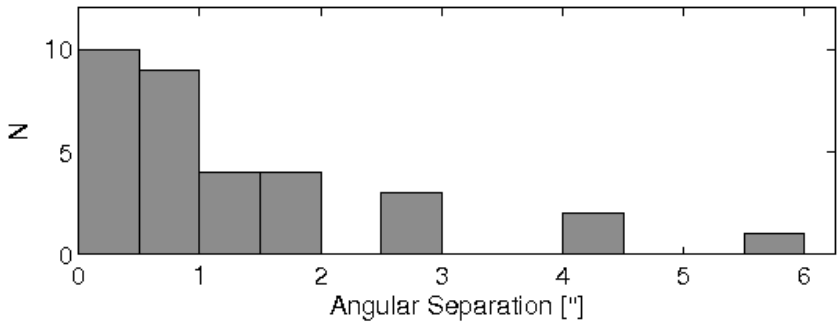

Figure 3.4: Binary separation in arcsec for all observed binary systems with separation $\rho < 6.0''$. The triple and quadruple systems are not included. Note that more than half of the binaries are closer than 1″, indicating that the vast majority of the binaries in the sample are physical companions and not background stars.

Table 3.1: Number of systems used in multiplicity and mass-ratio analysis.

Fraction	Single	Binary	Triple	Quadruple
$f_{\rm Mult}$	70	34	4	0
q	...	33	3	0

are part of a wider known system containing a primary star of spectral type earlier than M0 (J04373746-0229282, J07174710-2558554);

- 'single' stars that are not really single but part of a wide, known system partly outside our field of view.

This ensures that

- all the single stars in our sample are indeed single, to the best of our knowledge;
- the binary/multiple statistics is limited to stars/systems with primary spectral type M0-M6, for stars that lie within 52 pc of the Sun and have separations in the range $0.1'' \leq \rho \leq 6.0''$ (see Table A.1).

The observed multiplicity frequency $f_{\rm obs} = N_{\rm Multiple}/N_{\rm Total}$ is, after this selection, 35 ± 6% (Poisson errors), where $N_{\rm Multiple}$ is the number of binary or multiple systems (38) and $N_{\rm Total}$ is the number of observed systems (108). Figure 3.5 shows the observed multiplicity fraction for each primary spectral type. The multiple systems included in the following analysis can be found in Table A.2, and the number of single:binary:triple:quadruple systems in Table 3.1.

To compute the actual multiplicity frequency, we need to consider two effects: (i) at small separations, we detect more equal brightness binaries than systems with large component brightness differences, and (ii) a brightness-limited sample is biased in favour of (previously unresolved) binaries or multiple systems compared to single stars.

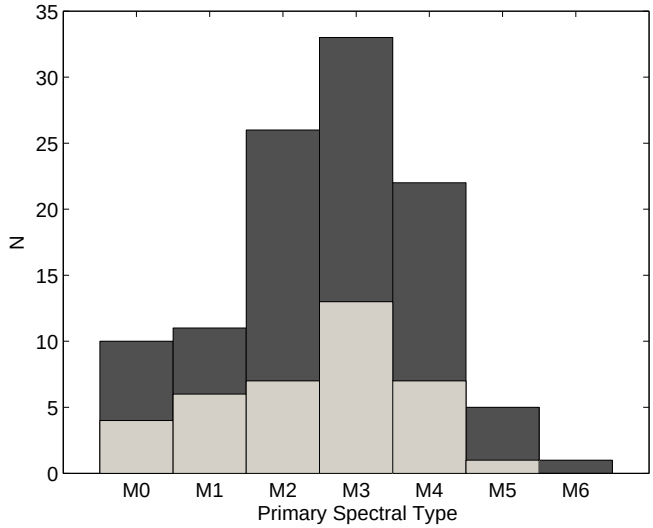

Figure 3.5: Multiplicity fraction for each spectral type. The dark grey bins show all observed stars of each spectral type after selection criteria described in Sect. 3.3.2 have been imposed on the observed sample. The light grey bins represent the number of multiple systems in the survey.

Assuming that the flux ratio distribution is independent of the separation in the observed range (which can be transformed into a flat mass ratio distribution), we estimate the number of multiple systems of close separations that we miss using the following method. We divide the number of binaries in Fig. 3.3 of observed $\Delta z'$ as a function of angular separation ρ into four different regions of interest. Assuming that our sample is complete to $\Delta z' < 5.5$ between angular separation 0.5″-3″ and complete to $\Delta z' < 2.5$ for closer separations, the ratio of companions in the region $\rho = 0.5'' - 3''$, $\Delta z' = 2.5 - 5.5$ and $\rho = 0.5'' - 3''$, $\Delta z' = 0 - 2.5$ is the same as the ratio of companions in $\rho = 0.1'' - 0.5''$, $\Delta z' = 2.5 - 5.5$ and $\rho = 0.1'' - 0.5''$, $\Delta z' = 0 - 2.5$. This would result in the survey missing two binary companions in the close separation - high flux ratio region, hence the total multiple fraction should be increased to $37 \pm 6\%$.

We compute the multiplicity fraction for a volume-limited sample, f', following the method and Eq. (4) of Burgasser et al. (2003)

$$f' = \frac{f'_{\rm obs}}{f'_{\rm obs} + \alpha(1 - f'_{\rm obs})} \tag{3.2}$$

where $f'_{\rm obs} = 0.37$ is the fraction of observed binaries after sensitivity correction. Burgasser et al. (2003) consider α values in the range 2.8, corresponding to only equal brightness systems, to 1.9, which corresponds to a flat flux ratio distribution. The distribution of z'-band brightness ratios (see Table A.2) in our sample is more peaked towards unequal systems (on a linear brightness ratio scale), resulting in $\alpha = 1.73$. According to Eq. (4) of Burgasser et al. (2003), this then yields a multiplicity fraction for a volume-limited sample of $f' = 25 \pm 6\%$.

However, the Riaz et al. (2006) sample is based on a correlation of M dwarf candidates selected from the 400 million sources in the 2MASS point source catalogue (PSC, angular resolution $\sim 2''$, Cutri et al., 2003) with the 150 000 sources in the ROSAT All Sky Survey (RASS, angular resolution $\sim 30''$ Voges et al., 1999), thus the brightness limit is imposed by the X-ray luminosity of the sources. Hence, we need to correct for the excess of multiple systems as two or more stellar components emit more X-rays than the corresponding primary component would do if it were single. We can do this straightforwardly by simply examining all our a posteriori known multiple systems and determining which ones would not have been included in the sample if the primary had been single. X-ray counts and errors are available from ROSAT (Voges et al., 1999) for each of the 44 multiple systems (except for one system, J20500010-1154092, which is counted as a non-detection here). Given that the components in any given system should be coeval, it is assumed that the X-ray brightness depends only on the stellar luminosity. According to Riaz et al. (2006), L_X/L_{bol} is roughly constant as function of spectral type, hence to a reasonable approximation the X-ray count rate can be assumed to be directly proportional to the brightness fraction in z'-band in linear units. Thus, we use the known $\Delta z'$ for each system in combination with the unresolved X-ray count rate to estimate the rate for the primary component alone. If the new value results in $S/N < 3.3$, the multiple system in question is counted as having been positively selected for and is excluded for the purpose of calculating the multiple fraction for a volume-limited sample, where $S/N = 3.3$ is the relevant criterion for detection according to the tables of Voges et al. (1999). In total, 7 systems are identified as contaminants in this way. Hence, applying corrections for the X-ray flux limit as described above, it follows that the multiplicity fraction f is given by $f = (38 - 7)/(108 - 7) * 1.053 = 32 \pm 6\%$.

While both multiplicity fractions f and f' agree within the uncertainties, in the following we assume a multiplicity fraction $f = 32 \pm 6\%$, as the brightness limit is primarily imposed by the X-ray luminosity. We note that some overabundance of short-period binaries (P<20 days) might be present in the X-ray selected sample, but this cannot be quantified until future radial velocity observations have been performed. We also note that this fraction might still include a small contamination by non-physical ("optical") binaries, as second-epoch observations for some of the systems are still pending, although we reiterate that the fraction of binaries that are merely optical must be very small (see Fig. 3.4).

3.3.3 Mass ratio distribution

The individual component photometric spectral types from Sect. 3.3.1 are transformed to approximate masses using the mass estimates of Kraus & Hillenbrand (2007) for young (~ 500 Myr) stars. We interpolate linearly to obtain masses for subclasses of 0.5 and calculate the mass-ratios, $q = M_2/M_1$. The binaries where the secondary star is suspected to be an L dwarf are not included in the mass-ratio distribution because of the high uncertainties in mass. We also exclude components at separations greater than $6''$ from the primary star and systems where the primary star is of spectral type earlier than M0 (see Tables A.2 and A.3). Since we also wish to include the triple systems in the multiplicity statistics, and all of our triple systems consist of one close pair and one wider component, we follow Reid & Gizis (1997) and calculate the triple mass-ratio as if the system consists of two separate binary systems, one close pair $q_{close} = M_B/M_A$

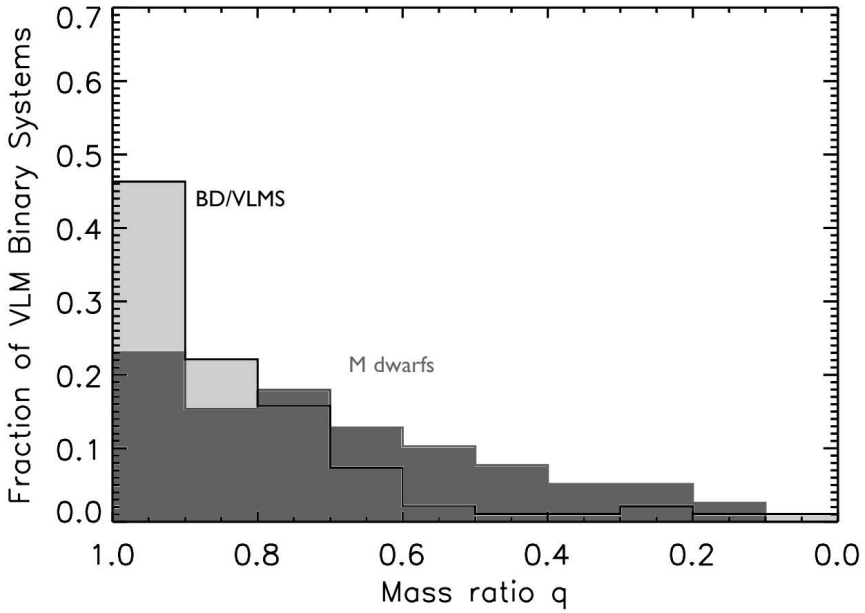

Figure 3.6: Mass-ratio distribution. The dark grey distribution shows the mass-ratios of the AstraLux M dwarf binaries. The light grey distribution shows all known VLM binaries ($M < 0.2M_{\odot}$) from the Very Low Mass Binaries Archive at `http://www.vlmbinaries.org` for comparison. Triple systems are included as two binaries as described in Sect. 3.3.3. Systems where one component is a suspected L dwarf, where the primary star is of spectral type earlier than M0, and companions with greater separation than 6″ from the primary are not included.

and one wider system with the combined mass of the close system as the higher mass component, e.g., $q_{\rm wide} = M_{\rm C}/(M_{\rm A} + M_{\rm B})$. The quadruple system J06583980-2021526 contains one close pair of spectral types M4+M4 and two more distant suspected L dwarfs, (one of which is also outside the 6″ limit). This system is, therefore, treated as a regular binary system, ignoring the two fainter components.

The mass-ratio distribution has been seen to vary from a flat distribution among solar-type stars to peak at almost equal mass systems for VLMSs and brown dwarfs (see e.g., Allen, 2007, and references therein). Figure 3.6 shows the mass-ratio distribution for our M0-M5.5 binaries compared to the distribution for all known VLMS and brown dwarf binaries compiled from the Very Low Mass Binaries Archive[1] (total system mass $< 0.2M_{\odot}$). We applied small updates to the July 28, 2009 version of the archive. Almost equal mass binaries are preferred for VLMSs/brown dwarfs, but the M dwarf distribution is much flatter. While our sensitivity limit makes our survey incomplete at the low mass-ratio end of the distribution, equal mass systems should easily be seen. The lack of a peak near $q \sim 1$ is therefore a real property of the M dwarf binary systems in the separation range $0.1''-6.0''$. We note that the mass-ratio distribution for

[1] `http://www.vlmbinaries.org`

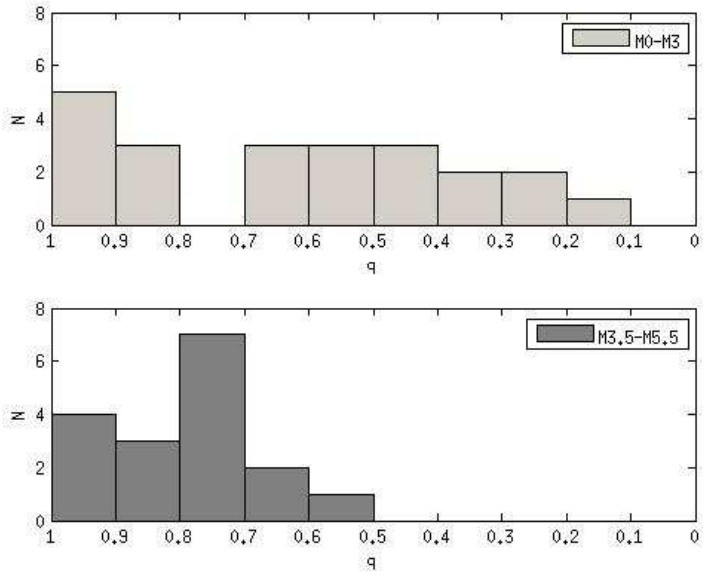

Figure 3.7: Mass-ratio distribution divided into early-M type primaries (M0-M3) and late-M type (M3.5-M5.5). Triple systems are included as described in Sect. 3.3.3. Systems where one component is a suspected L dwarf and components at separations greater than 6″ are not included.

VLMSs and BDs might be flatter in the case of very young systems (Burgasser et al., 2007). The samples are however very small, even if we account for more recently discovered systems, and we are therefore unable to address the age effects. No correlation between mass-ratio and component separation is seen in our sample.

When we divide our sample into early M dwarfs of primary spectral type M0-M3 ($M \gtrsim 0.3M_{\odot}$) and late M dwarfs of spectral type M3.5-M5.5 ($M \lesssim 0.3M_{\odot}$), we see some indication of a peak in the distribution around $q \gtrsim 0.7 - 0.8$ for the late type M dwarfs that is not present in the very flat $f(q)$ distribution of the early type M dwarfs (see Fig. 3.7). Assuming that our survey is not complete for mass-ratios $q < 0.4$, a Kolmogorov-Smirnov (K-S) test shows that the probability that the 'early-M' and the 'late-M' mass-ratios are drawn from the same distribution is 10%. This might indicate that the shape of the mass ratio distribution is a function of mass, which approaches the $q \sim 1$ peak for the lower mass stars. However, this division into seemingly different populations should be assumed with caution. For mid- to late-M dwarfs, the mass - spectral type relation becomes very steep. Thus, a large brightness difference corresponds to only a very small change in mass for lower mass objects. Hence, a detection limit of $\Delta z' \lesssim 1.5$ magnitudes, which we assume to be valid for all stars in the sample, corresponds to a mass-ratio completeness $q \gtrsim 0.4$ for early-type M dwarfs, while the same detection limits correspond to completeness only for $q \gtrsim 0.6$ for an M3.5 primary star and $q \gtrsim 0.8$ for an M5 primary. While the missing $q \sim 1$ peak is an unbiased feature, the sensitivity to lower q values is strongly dependent on spectral type. With more observations from the full AstraLux M dwarf survey, we will be able to investigate these distributions in greater detail.

3.3.4 Distribution of separations

From the parallax distances, if available, and otherwise the spectroscopic distances provided by Riaz et al. (2006), we calculate the projected separation in astronomical units. The uncertainty in spectroscopic distance according to Riaz et al. (2006) is 37%. Figure 3.8 shows the distribution of projected separation of all binaries and triples in our M dwarf sample compared to that of all known VLMS/BD binaries from the Very Low Mass Binaries Archive.

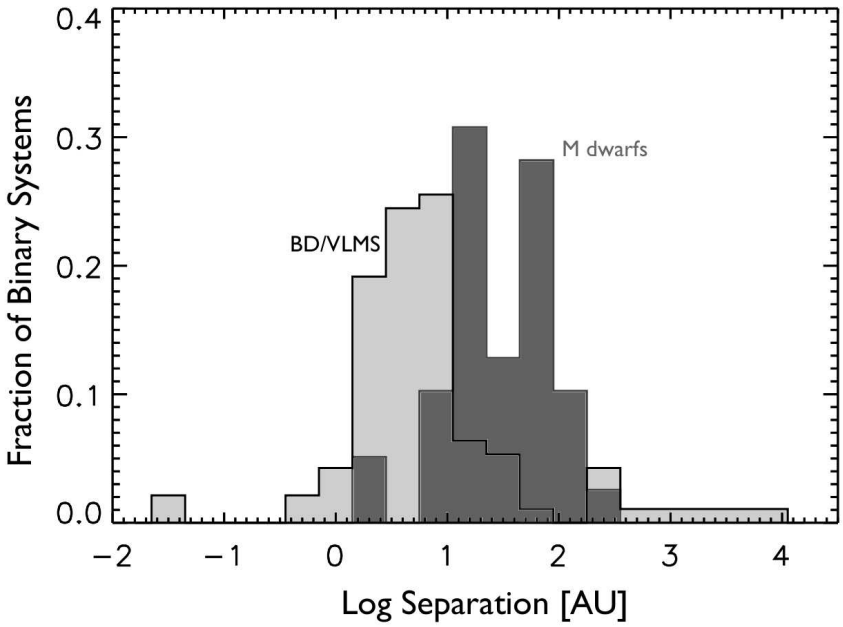

Figure 3.8: Projected separation distributions. The darker grey shows the M dwarf binaries/triples in our sample and the light grey shows VLMS/BD binaries from the Very Low Mass Binaries Archive.

As for the mass-ratio distribution, we divide the observed systems into two groups, containing approximately equal number of systems, to see if the separation distribution is the same for 'early M' and 'late M' type binaries divided at $M \approx 0.3 M_{\odot}$. Figure 3.9 shows the respective mean semi-major axis distributions, where the projected separation has been multiplied with 1.26 to account for random orbital elements (Fischer & Marcy, 1992). We performed a K-S test, which yielded a 9% probability that the distributions are alike. We note that the distributions may peak at close systems in the 'late M' subsample, however more data is necessary to determine whether this is a real property or not.

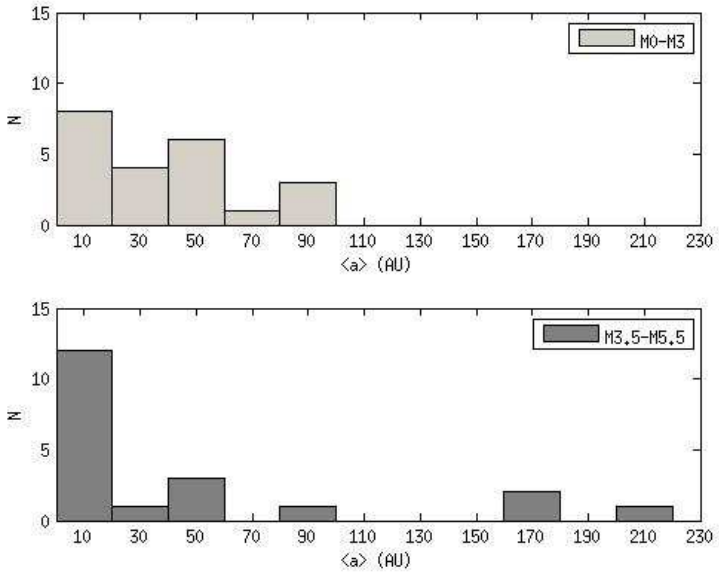

Figure 3.9: Distribution of mean semi-major axis for 'early M' and 'late M' primary spectral types. The binaries are divided into two groups: 'early type M', consisting of the binaries with a primary spectral type M0-M3, and 'late type M' for primary spectral types M3.5-M5.5. All separations are measured from the primary stars.

3.4 Discussion

M dwarfs comprise a transitional region within which the multiplicity properties change from being similar to those of solar-type stars to the very different characteristics of very low mass stars and brown dwarfs. Smaller surveys of different mass ranges have provided some insight into the transitional behaviour. We observed 124 nearby M dwarfs from the Riaz et al. (2006) catalogue. Forty-four of our targets were observed to have potential binary/multiple companions within 0.1″ – 9.5″ of the primary star. Most of these companions were previously unknown.

We have estimated the multiplicity fraction for M0-M6 young ($\lesssim$ 600 Myr) dwarfs with angular separations 0.1″ – 6″, corresponding to projected separation 3-180 A.U. at median distance 30 pc, in this largest sample to date to be 32 ± 6%. While differences in the binary fraction have been found in various nearby star-forming regions (Leinert et al., 1993; Ghez et al., 1993; Brandner & Köhler, 1998; Köhler et al., 2006), observations of the 90 Myr old α Persei and the 600 Myr old Praesepe clusters suggest that the companion star fraction does not significantly decline over an age range from 90 Myr to 5 Gyr (Patience et al., 2002). We therefore did not expect there to be a strong evolution in binary properties from ages $\sim$ 100 Myr to a few Gyr. Our derived $f_{\rm Mult}$ is consistent with previous surveys in the same mass and separation range for field dwarfs (e.g., the multiplicity fraction of the Fischer & Marcy (1992) sample for M0-M4 systems with linear separation 2.6 AU< a <300 AU is $f_{\rm bin}$ = 28 ± 9%, according to Close et al., 2003) and young M dwarfs (23% for < 300 Myr M0-M5 binaries with separations 1.6-300 AU, Daemgen et al., 2007). This is a higher $f_{\rm Mult}$ than found in

high resolution imaging surveys of later type M field dwarfs (e.g., Law et al. (2008) 13.6% for M4.5-M6; Close et al. (2003) 15% for M8-L0.5; Siegler et al. (2005) 9% for M6-M7.5).

Previous large investigations inferred different behaviours for the mass ratio distribution of M dwarfs. For instance, Fischer & Marcy (1992) found that the mass ratio distribution for M0-M6 dwarfs is relatively flat for the full orbital separation range, while Reid & Gizis (1997) found a strong peak for $q \gtrsim 0.8$. However, Delfosse et al. (2004) showed in their large survey that the distribution of mass-ratio is relatively flat for orbital periods P>50 days, while shorter period binaries tend to have equal masses.

When considering only systems in the survey of Reid & Gizis (1997) with M dwarf primaries (M0.5-M5.5) and mean semi-major axis 3.7 AU< a <227 AU, the same region probed in this survey, we find that the distribution is flat (although the sample is very small with only 16 companions). We therefore expect our distribution to be flat as well, in accordance with those of other surveys. We have found that the mass-ratio distribution of all binaries in the primary spectral type range M0-M5.5 is flatter than the distribution for VLMSs and BDs and does not exhibit the prominent peak at $q \sim 1$ detected for the VLMS/BD sample. This is consistent with the results of Reid & Gizis (1997) over the same range of linear separations, and a real feature for M dwarfs in the observed separation range not affected by observational incompleteness. To investigate the transitional properties, we divided our sample into two groups of 'early M' and 'late M' primary stars and found that the 'early M' distribution is relatively flat, while there might be a preference for more similar mass binaries in the 'late M' group. Future analysis of the full AstraLux M dwarf survey will allow us to investigate this possible trend in more detail.

Thies & Kroupa (2007) argued that the differences in binary characteristics of stars and brown dwarfs point to different but related formation processes for these two populations. In their survey of M4.5-M6 binaries, Law et al. (2008) found a bimodal separation distribution where the later type M dwarfs peak at close separations as seen for brown dwarfs, but some of the earlier systems have projected separations greater than 10 AU. This is indicative of a change in the separation distributions at spectral type ~M5, consistent with the Thies & Kroupa (2007) predictions of two separate but overlapping populations. For later type M dwarfs, Siegler et al. (2005) find no binaries with separations $a > 10$ AU in their high-resolution imaging survey of M6-M7.5 field dwarfs covering separations 3-300 AU, and Close et al. (2003) find no binaries wider than 16 AU for the M8-L0.5 dwarfs in the same separation range. We divide our separation distribution into 'early M' and 'late M' groups at $M \sim 0.3 M_{\odot}$. Even though our sample contains somewhat more massive stars than that of Law et al. (2008), the distribution of 'early M' multiples is flatter than the 'late M' distribution in which more than half of the companions reside within 20 AU of the primary star. While our results are still subject to relatively large statistical uncertainties, we note that they may indicate that a bimodal distribution also exist for larger separations and higher masses than the sample of Law et al. (2008). This will be investigated further in the larger sample of the complete survey.

These results show that Lucky Imaging with AstraLux Sur is very efficient at detecting binary stars with small angular separations. Several of our newly discovered companions presented here have been found to be close to the diffraction limit ($\sim 0.1''$).

Future follow-up observations with AstraLux Sur will allow us to determine orbital motions and hence dynamical masses for the closest nearby systems.

CHAPTER 4

NEAR-INFRARED SPECTRA OF FOUR M DWARF BINARIES

Abstract:

The AstraLux M dwarf survey is the largest survey for binary/multiple M dwarfs in the solar neighbourhood to date. Within the first part of the survey, a large number of previously unknown binary/multiple systems were discovered. Some of these are close and nearby systems suitable for further spectroscopic characterization to provide properties such as effective temperature and surface gravity, and ongoing monitoring of their orbits may in the future provide dynamical masses and thus calibration of largely unknown basic properties of these stars, such as the mass-luminosity relation.

We obtained near-infrared J, H+K spectra with the integral field spectrograph SINFONI at VLT of four close, nearby companions in M dwarf binary/triple systems that were discovered or observed within the AstraLux M dwarf survey. The spectral types were determined to within ±1 subclass from comparison with SpeX spectra of stars with known spectral types. The near-infrared spectral types agree within errors with previously derived spectral types from ($i' - z'$) photometry. We find no signs of low surface gravity, and conclude that the nature of the targets is likely to be stellar rather than substellar. Both components B and C of the triple system 2M J22171899-0848122 (GJ 852B) show Brackett γ emission, indicating activity variations.

4.1 Introduction

The spectral class of M dwarfs comprises both low-mass stars and young brown dwarfs, and is thus together with L dwarfs unique in the sense that whether an object of a certain spectral type is stellar or substellar is not only depending on its mass, but also on its age. They are the most common stars in our neighbourhood, yet fundamental physical characteristics such as mass, radius, effective temperature, luminosity, and relations between these properties, are not as well constrained as for Sun-like stars, especially for mid- to late M type stars.

Binary/multiple M dwarfs can provide valuable insight into the structure, formation and evolution of very-low-mass stars and brown dwarfs, through their multiplicity characteristics as well as their physical and orbital properties (e.g., Stassun et al., 2006; Burgasser et al., 2007; Goodwin et al., 2007; Janson et al., 2007). In order to identify a large statistical sample of such binaries, we have performed the AstraLux M dwarf survey, for which first results were presented in Bergfors et al. (2010a). For the survey we chose M dwarf targets mainly from the catalogue compiled by Riaz et al. (2006), which is a collection of supposedly young and nearby, late-type stars (K and M), based on the stars' chromospheric activity and low tangential velocity. By choosing young targets, we would also be sensitive to substellar companions, since these are brighter at young ages before gradually cooling off (see, e.g., Burrows et al., 1997).

In this Chapter, we present near infrared spectra of stars in four close, nearby mid-to-late M dwarf binary or multiple systems observed within that survey. We derive their spectral types and compare to previously derived spectral types from SDSS $(i' - z')$-colours.

4.2 Observations and data reduction

4.2.1 Target selection and observations

Four close, mid-to-late M dwarf binaries or close pairs in hierarchial triple systems were selected from the target list of the AstraLux M dwarf survey as good candidates for follow-up near-infrared spectroscopy and characterization. The binary/multiple character of three of the targets (J02490228-1029220(BC), J04080543-2731349, J06161032-1320422) were discovered within the AstraLux M dwarf survey – a high-resolution Lucky Imaging survey of a large sample of young, nearby M dwarfs (Bergfors et al., 2010a). The fourth target (here called J221718(BC), in which the unresolved binary BC is also known as 2M J22171870-0848186 or GJ 852 B) was discovered to be a close binary in a triple system with J22171899-0848122 by Beuzit et al. (2004), and had also been observed with AstraLux. The target selection for SINFONI observations was based on the following criteria: The targets had been observed in at least two epochs and were confirmed common proper motion binaries, they all had a projected separation of $a < 8$ AU and photometric spectral types M 3.5 or later derived from photometric AstraLux observations in SDSS i'– and z'–band. All stars observed in the first part of the AstraLux M dwarf survey are closer than 52 pc to the Sun (Bergfors et al., 2010a). The spectroscopic distance derived by Riaz et al. (2006) to the primary star of the J221718 system, GJ 852 A, is only 10 pc.

Table 4.1: Observational details.

2MASS ID	Comp.[a]	Obs. Date	AM J	AM H+K	N × DIT J	N × DIT H+K	Telluric Std
J02490228-1029220	B,C	2010-12-01	1.123	1.078	72 × 5	72 × 2	HIP 3820 (B8 V)
J04080543-2731349	A,B	2011-01-09	1.023	1.006	72 × 5	72 × 2	HIP 14898 (B3 V)
J06161032-1320422	A,B	2010-12-01	1.061	1.023	72 × 15	72 × 2	HIP 25931 (B9 V)
J22171899-0848122	B,C	2010-10-21	1.058	1.044	72 × 2	72 × 2	HD 216009 (A0 V)

2MASS ID, Components ID (see Bergfors et al. (2010a) for component definitions), Observing date, Airmass, Number of integrations and integration times in seconds, and telluric standard star.

The targets were observed in service mode with the near-infrared (1.1–2.45 μm) adaptive optics fed integral field spectrograph SINFONI (Spectrograph for INtegral Field Observations in the Near Infrared, Eisenhauer et al., 2003; Bonnet et al., 2004) at the VLT Unit Telescope 4 (Yepun). We used the J (λ = 1.1 – 1.4 μm) and H+K (λ = 1.45 – 2.45 μm) gratings, with a spectral resolution of R≈2000 and 1500 respectively, and the target itself as a natural guide star (NGS). The plate scales of 0.025″ px^{-1} used for J024902(BC)(binary separation ρ = 0.145″), J040805(AB)(ρ = 0.181″) and J061610(AB)(ρ = 0.194″) corresponds to a field-of-view (FoV) of 0.8 × 0.8″. For the wider couple, J22171899-0848122(BC)(ρ = 0.97″), a plate scale of 0.1″ px^{-1} was used, corresponding to a FoV of 8 × 8″. For each observation a telluric standard star of spectral type B3 V – A0 V was observed at similar airmass. Table 4.1 lists the observational details: which components were observed (J221718(BC) and J024902(BC) are part of triple systems with a wider companion), the date of observation, airmass, integration times and number of integrations, and the telluric standard.

4.2.2 Data reduction

J and H+K band data cubes were built from a set of raw data and associated calibration frames using the SINFONI data reduction pipeline version 2.2.5 (see, e.g., Abuter et al., 2006). Some of the raw frames were affected by stripes on slitlet #25 (so called *odd even effect* [1]) and by a bunch of dark horizontal lines. These electronic artefacts were properly removed using custom scripts (Bonnefoy et al. 2011a, A&A, submitted) before providing the frames to the pipeline. The data reduction was checked by eye and a set of quality control parameters were compared to reference values[2].

Binaries are successfully resolved by MACAO. However, their limited angular separation make them cross-contaminating each other. We used a custom spectral extraction tool to deblend the flux of the components, and consequently their spectra, slice per slice in each of the data cubes. The tool is a modified version of the algorithm presented in Bonnefoy et al. (2009). It first estimates the positions of the sources inside the field of view, which usually drift due to the atmospheric refraction[3]. We then applied on each slice a modified version of the Dumas et al. (2001) CLEAN algorithm to retrieve the individual flux of the sources. The algorithm requires the PSF at the

[1] http://www.eso.org/observing/dfo/quality/SINFONI/qc/dark_QC1.html

[2] http://www.eso.org/observing/dfo/quality/SINFONI/qc/qc1.html

[3] The refraction can be corrected by the data reduction pipeline. However, we still noticed some residual drift once this correction was applied.

time of the observation and for each cube wavelength. To provide that, we considered two different approaches. We first used a scaled version of the telluric standard star data cubes observed immediately after our targets (hereafter *PSFstd*). Alternatively, we built the PSF by duplicating the profile (hereafter *PSFdup*) of the brightest binary component (or of the component farthest from the field of view edges). We re-estimated the position of the sources, and re-built the PSF in case *PSFdup* was chosen, applying a second layer of CLEAN. For each input cube, an extracted cube for each binary component, and a residual map that enable to monitor the efficiency of the extraction process was produced. *PSFdup* provides a more accurate extraction. On the contrary, the PSF shape built following *PSFstd* is less appropriate, but the resulting spectra have higher S/N. Therefore, we used the *PSFstd* method for all the data, expect for the H+K band cube of J221718(C).

Custom IDL scripts were used for extracting the spectra from the reduced data cubes. 2-D Gaussians were fitted to the telluric standards and science targets at each wavelength in the cube to find the centroid positions and FWHM. The frames were shifted and added and scaled by 1/FWHM to obtain the total flux at each wavelength. For each set of observations, the spectrum of the telluric standard was divided with a Kurucz model spectrum[4] of Vega smoothed to the observed spectral resolution of our observations (R∼2000/1500). The science spectrum was then divided by the resulting spectral response, containing only remaining instrumental and atmospheric features, to obtain the final spectrum.

4.3 Spectral types, H_2O-index, and chromospheric activity

Spectral types were determined for each component by comparing the spectral shapes and features in the H- and K-bands to SpeX spectra of M type stars obtained from the IRTF spectral Library (Cushing et al., 2005; Rayner et al., 2009) smoothed to the observed spectral resolution (R∼ 1500). The spectra were normalized at J=1.226 μm, H=1.65 μm and K=2.20 μm, except for 2M J040805(AB), 2M J061610(AB) and 2M J024902(B), which were normalized differently because of the low signal-to-noise ratio (S/N) in K-band (see Section 4.3.1 on the individual stars). Over all, the S/N of the spectra was medium to low, and we do not use the J-band spectra for the spectral analysis except for 2M J221718(BC). The derived near-infrared spectral types are assumed to be correct to within ±1 subtype, and are in general accordance with the spectral types previously derived from photometry in $i'-$ and $z'-$band (Bergfors et al., 2010a). Table 4.2 lists the photometric and spectroscopic spectral types. Figures 4.1, 4.2, 4.3 and 4.4 show our near-infrared spectra compared to SpeX spectra of stars with known spectral types.

For additional characterization, we calculated the H_2O spectral index $\langle F_{\lambda=1.550-1.560}\rangle / \langle F_{\lambda=1.492-1.502}\rangle$ derived by Allers et al. (2007). A young brown dwarf can be distinguished from an older field dwarf of the same spectral type by surface gravity dependent features in the near-infrared, e.g., the triangular shape of the H-band spectrum that is caused by strong H_2O absorption in the atmosphere of the low

[4] http://kurucz.harvard.edu/stars.html

Table 4.2: Photometric and spectroscopic spectral types.

ID[a]	$(i' - z')$ Sp.T.[a]	SpeX Sp.T.[b]
2M J024902(B)	M3.5 (2.5–4.5)	M4.0 (3.0–5.0)
2M J024902(C)	M3.5 (2.5–4.5)	M4.5 (3.5–4.5)
2M J040805(A)	M3.5 (2.5–4.5)	M3.5 (2.5–4.5)
2M J040805(B)	M4.5 (3.5–5.5)	M3.5 (2.5–4.5)
2M J061610(A)	M3.5 (2.5–4.5)	M3.0 (2.0–4.0)
2M J061610(B)	M5.0 (4.0–6.0)	M6.5 (5.5–7.5)
2M J221718(B)	M4.5 (3.5–5.5)	M4.0 (3.0–5.0)
2M J221718(C)	M8.5 (7.5–9.5)	M8.0 (7.0–8.0)

[a]Spectral types and component definitions from Bergfors et al. (2010a).

[b]Spectral types derived in this paper from visual comparison with M dwarf spectra from the IRTF SpeX library (Cushing et al., 2005; Rayner et al., 2009).

surface gravity young brown dwarf, H_2O and H_2O + CO absorption in K-band, and the strength of Na I absorption in J-band (see, e.g., Allers et al., 2007, and references therein). In Fig. 4.5 we plot the H_2O spectral index calculated for our stars. We also plot in the same figure the H_2O-index calculated from the SpeX spectra from the IRTF spectral library, which we use to determine spectral types for comparison, and overplot the Allers et al. (2007) H_2O-index – spectral type relation,

$$\frac{\langle F_{\lambda=1.550-1.560}\rangle}{\langle F_{\lambda=1.492-1.502}\rangle} = 0.77 + 0.040(\mathrm{SpT}) \tag{4.1}$$

This relation is valid for spectral types M5 – L5, and we find good agreement with this relation for the two stars with spectral type later than M5 V. We also calculate the gravity dependent Na-index described in Allers et al. (2007), which is independent of spectral type for M5–L5. The results are, however, inconclusive for the two stars with spectral types within this range due to the poor quality of the J-band spectra. From the continuum shapes of the H- and K-band spectra we find no evidence of low surface gravity, hence all of our targets are likely stellar.

In the K-band spectra of both components in 2M J221718(BC), emission in the Br γ line at $\lambda = 2.17\,\mu$m is seen (see Fig. 4.4). The equivalent width (EW) of the line was modeled for both stars using IRAF. We find $\mathrm{EW_B} = -3.3$Å for the brighter component, and $\mathrm{EW_C} = -3.2$Å for the fainter one. The relative uncertainties are of the order of $\sim 15\%$ due to the uncertainty of where to place the continuum level, but the strengths are still on the same order as the Hα emission measured by Riaz et al. (2006) for the unresolved binary. As Br γ is in general weaker than Hα, this could be a sign of variability, i.e., the SINFONI spectra might have been taken during a period when the stars had a higher degree of chromospheric activity. This would also be in agreement with the classification of the unresolved binary as a flare star by, e.g., Gershberg et al. (1999). Paβ emission at 1.28μm can also be seen in the J-band spectra. While Paβ, Brγ, Hα could also trace accretion, this is unlikely here given the expected age of the sources.

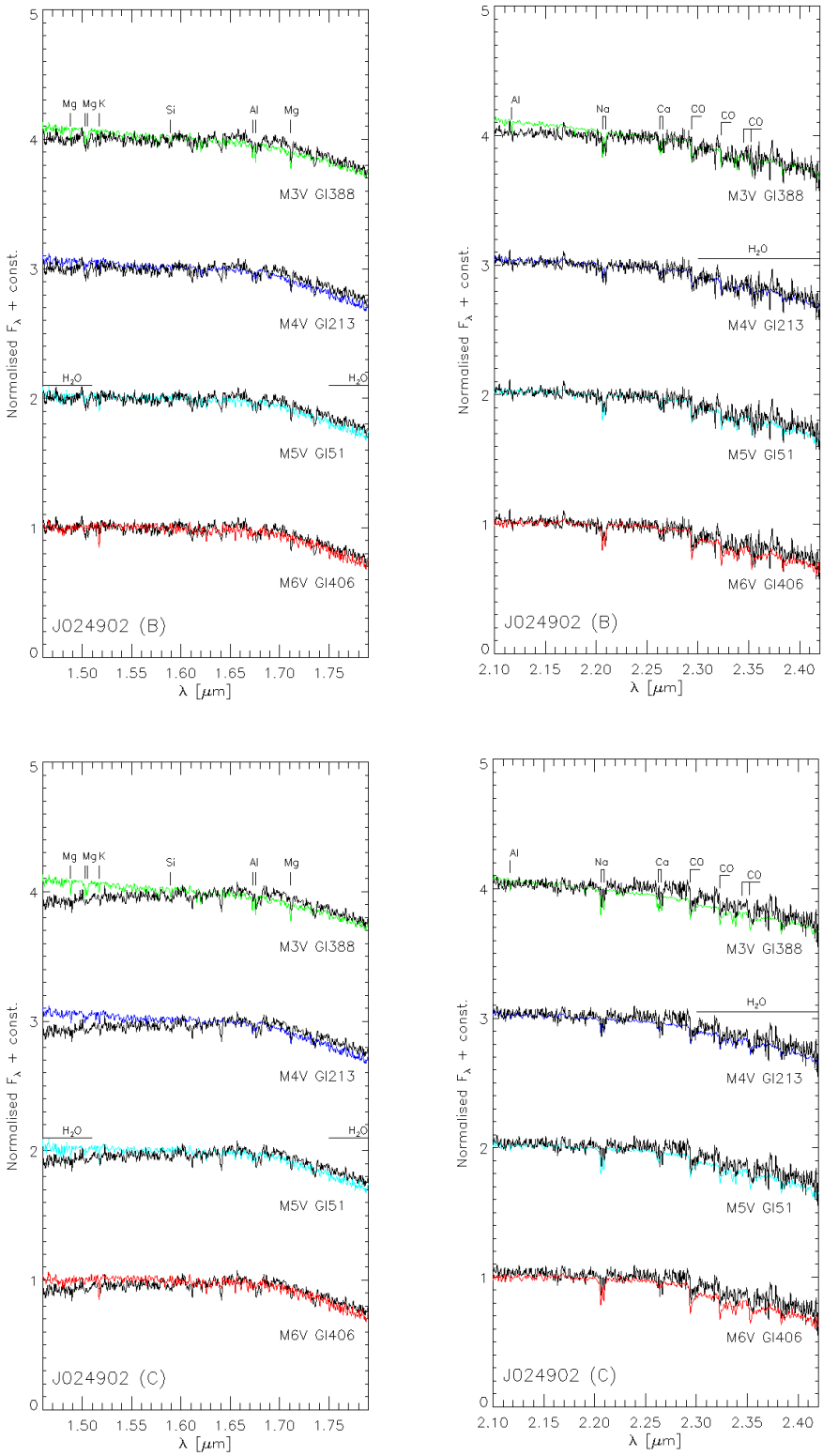

Figure 4.1: H and K spectra of 2M J024902(BC) (black lines) compared to M stars from Cushing et al. (2005); Rayner et al. (2009).

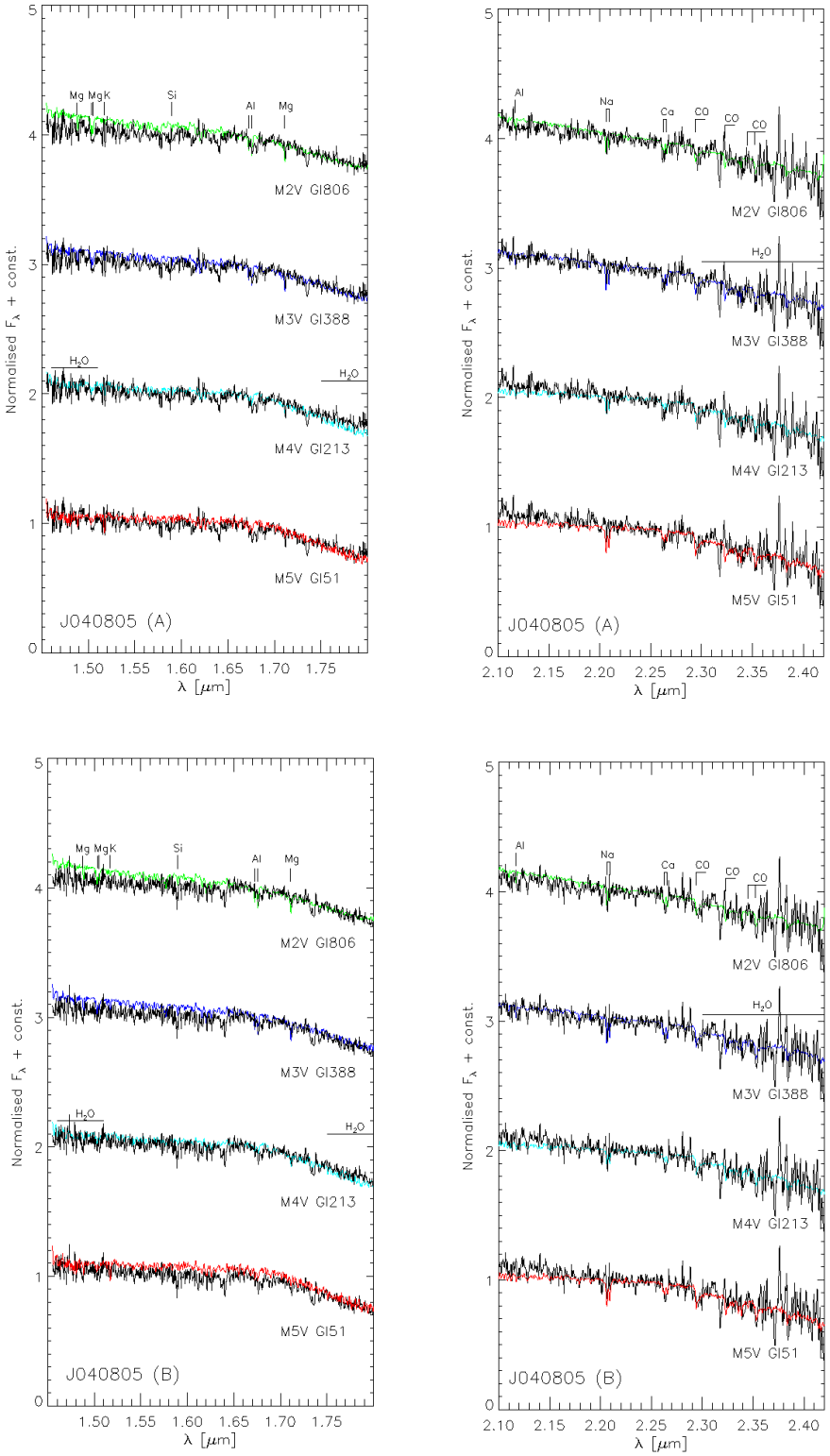

Figure 4.2: H and K spectra of 2M J040805(AB) (black lines) compared to M stars from Cushing et al. (2005); Rayner et al. (2009).

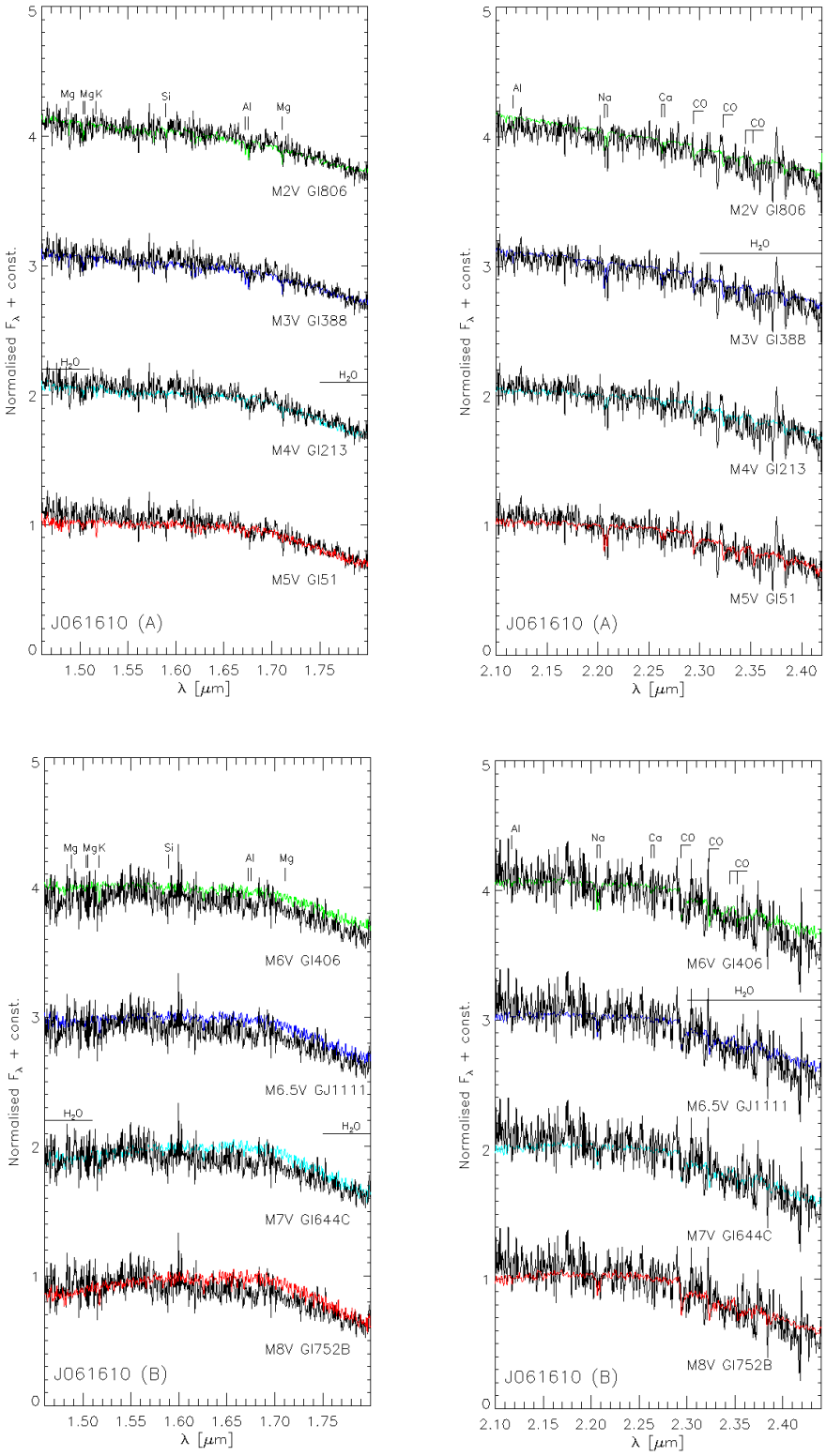

Figure 4.3: H and K spectra of 2M J061610(AB) (black lines) compared to M stars from Cushing et al. (2005); Rayner et al. (2009).

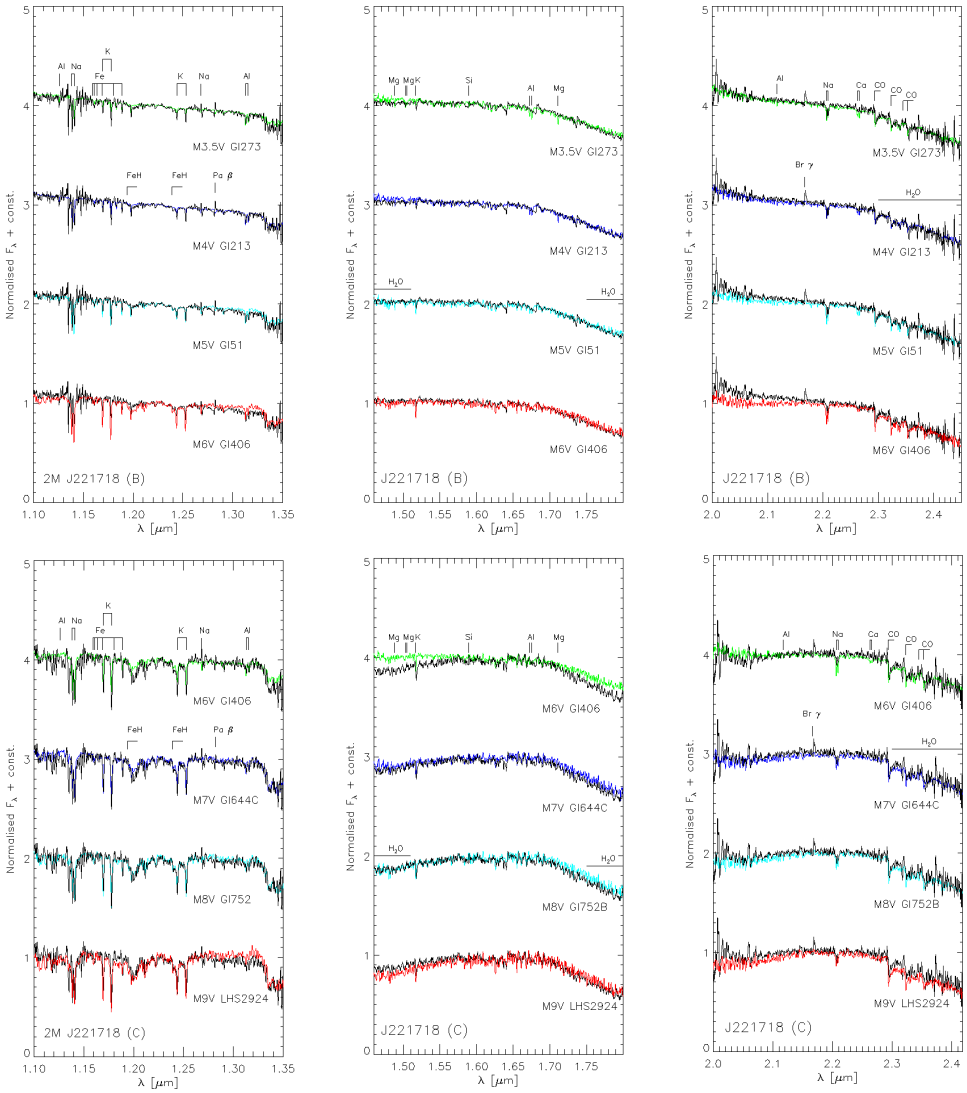

Figure 4.4: J, H and K spectra of 2M J221718(BC) (black lines) compared to M stars from Cushing et al. (2005); Rayner et al. (2009). The J-band spectra have been smoothed using a boxwidth of 5. Br γ emission is seen at $\lambda = 2.17\,\mu$m and Pa β at $\lambda = 1.28\,\mu$m, indicating high chromospheric activity.

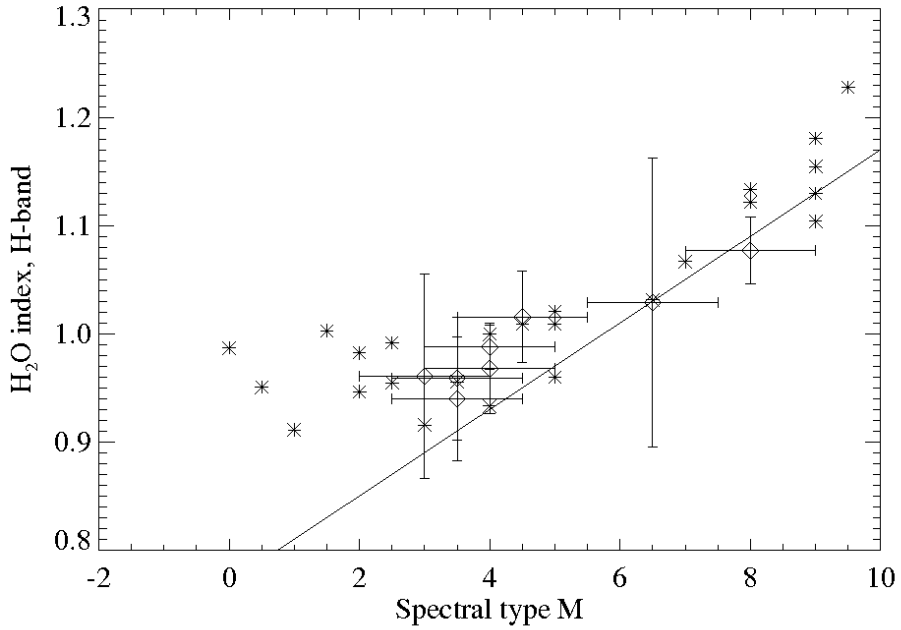

Figure 4.5: H-band H_2O-index as defined by Allers et al. (2007). Asterisks show the H_2O-index calculated for M dwarfs of varying spectral types from the IRTF SpeX catalogue. The stars in our sample are shown as diamonds with errorbars of ±1 in spectral type and rms errors of spectral index. The spectral types are as derived in Sect. 4.3. The solid line depicts the relation calculated by Allers et al. (2007) and is valid for spectral types M5 – L5. Our calculated H_2O-index follow this relation well for later types and the flat part seen among the comparison stars for earlier types.

4.3.1 Derived spectral properties of the individual stars

2M J024902(BC)

(B): The spectral shape in both H- and K-band fit SpeX templates of spectral types ~M4-M5 V well. From this and features such as the weak Al-doublet at 1.67 μm and Mg absorption in H-band, the K absorption at 1.52 μm and the strength of the Na and Ca doublets at 2.21 μm and 2.26 μm and CO absorption bandheads in K-band, we assign to this star a spectral type of M4.0 V.
(C): The over all best fit to the H- and K-band templates is for spectral types M4–M5 V. However, our star shows weaker H_2O absorption at the red end of the K-band, and stronger at the blue end of the H-band than the comparison spectra for these spectral types. From the relative strengths of the features described for the companion, we assign a spectral type of M4.5 V, which is later by one subclass than the spectral type inferred from ($i' - z'$) colours, but is in agreement within errors.

2M J040805

(A): The shapes of the H- and K-band spectra suggests spectral type M3–M4. From visual inspection, the strength of the 1.52 μm K and the Mg lines in H-band, and the Ca doublet at 2.26 μm and Na doublet at 2.21 μm in K-band also indicate spectral type of M3-M4. We assign a spectral type M3.5 to this star, consistent with the photometric $i' - z'$ spectral type. Because of the low S/N obtained, the K-band spectrum was normalized to 2.24 μm for a better comparison to the SpeX spectra.
(B): Also for this companion, the atomic features in H- and K-band as well as the shape of the spectra suggest a spectral type M3–M4. We assign a spectral type of M3.5 to this star, one sub-type earlier than derived from the $i' - z'$ photometry but within the uncertainty estimated to ±1 subclass. Because of the low S/N, the K-band spectrum was normalized to 2.24 μm.

2M J061610

(A): From visual comparison with SpeX M dwarf spectra we infer a spectral type of M3 V. Because of the low S/N we chose to normalize our K-band spectrum to 2.24 μm. The spectral type derived from $i' - z'$ photometry is consistent with this spectral type within errorbars of ±1 subclass.
(B): The shape of the H-band spectrum and the K-band spectrum suggests a spectral type ~M6.5 V. The low S/N only allows visual identification of the strongest features, such as the Na doublet at 2.21 μm and some of the K-band CO bandheads. The K-band spectrum was normalized to 2.24 μm.

2M J221718(BC)

The K-band spectra of both companions show Brγ emission at 2.17 μm and Pa β at 1.28 μm. These stars are known flare stars (Gershberg et al., 1999).
(B): The H and K band spectral shapes both indicate a spectral type of ~M4. The strength of the K line at 1.52 μm and the non-detection of the Mg lines at 1.49, 1.71 μm also indicates spectral type M4 or later (Cushing et al., 2005). The strength of the Na

doublet at 2.21 μm, the Ca doublet at 2.26 μm and K-band ^{12}CO bandheads are also consistent with an M4 V spectral type. The J-band spectrum is a good fit to the M4 V SpeX template in its overall shape as well as characteristic features such as the increasingly strong Na and K doublets at 1.138/1.141 μm, 1.169/1.178 μm,1.244/1.253 μm, the Al absorption at 1.313 μm, and FeH bandheads at 1.194 μm and 1.239 μm (Cushing et al., 2005). We assign a spectral type of M4 V, consistent with the M4.5 V spectral type derived from the ($i' - z'$) colours.
(C): The strong H2O absorption at $\lambda \lesssim 1.51\,\mu$m and $\lambda \gtrsim 1.75\,\mu$m are, together with the strong K line at 1.52μ m, the most prominent features of the H-band spectrum, and consistent with a spectral type of M8 V. In K-band, the non-detection of the Ca lines at 2.26 μm is indicative of a spectral type M7 or later (Cushing et al., 2005). The J-band spectrum fits very well to the M8 V SpeX template both in shape and characteristic features (see 2M J221718(B)). From the combined spectra in J, H and K we infer a spectral type of M8.0. We note that the previously derived photometric spectral type of M8.5 was derived from only SDSS z'-magnitude difference to the close companion, since this star was too faint in i' to be clearly resolved.

4.4 Summary

We presented near-infrared spectra obtained with SINFONI at the VLT for four close M dwarf binaries (or close couples in higher order multiple systems). We derived the spectral types of these eight mid- to late-M type stars from comparison with spectra of stars with known spectral types obtained from the IRTF spectral library. The results agree very well with spectral types determined from photometric observations in SDSS i'– and z'–band, and we can thus confirm that the photometric method provides accurate results over the spectral range of M3–M8 stars. We calculated the H_2O spectral index defined by Allers et al. (2007) from which the spectral type of M5–L5 can be derived independent of surface gravity, and fit our two late-type M dwarfs to their H_2O index – SpT relation. We find no evidence of low surface gravity, which would be expected if the targets were young brown dwarfs, and conclude that the targets are stellar. Br γ and Pa β emission was discovered for the close companion stars 2M J221718(BC). While the chromospheric activity of the unresolved binary was known from previous measurements of Hα emission (Riaz et al., 2006), the strong Br γ and Pa β emission had not been measured.

CHAPTER 5

STELLAR COMPANIONS TO EXOPLANET HOST STARS: LUCKY IMAGING OF TRANSITING PLANET HOSTS

Abstract:

Planetary systems in which the planet host star is part of a binary/multiple system provide clues to the formation of planets from the observed properties of the stars and the planets. In this survey, we search for stellar companions to the hosts of transiting exoplanets. We derive photometric and astrometric properties of the companion candidates and investigate suggested correlations between the planetary properties and binary star separation.

The 21 exoplanet host stars are observed in SDSS i'– and z'–band using the Lucky Imaging technique with the two AstraLux instruments: AstraLux Norte at the 2.2 m telescope at Calar Alto and AstraLux Sur at the 3.5 m NTT, La Silla. Typically, a sensitivity to companions of magnitude difference $\Delta z' = 3.5$ is achieved at angular separation $\rho = 0.5''$ and $\Delta z' \gtrsim 5$ for $\rho = 1''$.

We present observations of two previously unknown binary candidate companions, to the transiting planet hosts HAT-P-8 and WASP-12. We confirm the common proper motion of the planet host TrES-4 and its companion candidate. The distributions of the planetary radii, surface gravities, orbital periods and Safronov numbers are not significantly different for planets in binary systems compared to single-star planets. The mass distribution of transiting exoplanets belonging to single stars compared to that of planets in binary/multiple star systems with separations $a \leq 1\,200$ AU indicate that a secondary star might influence the formation of planets, since on average higher masses for planets belonging to binary/multiple stars are found.

5.1 Introduction

More than half of solar-type stars in our neighbourhood are part of a binary or multiple system (Duquennoy & Mayor, 1991). Understanding how a secondary star affects the formation and evolution of planets in the system is therefore of high importance for an estimate of the overall occurrence of planets in our Galaxy.

The frequency by which giant planets are formed in binary stellar systems seems to be slightly lower than in single stars. Eggenberger et al. (2008, 2011) found that giant planets were more common in single-star systems than for binaries separated by 35-100 AU. Nevertheless, we now know of around 50 binary or multiple systems where one of the stars hosts planets (Duchêne, 2010). System characteristics such as binary separation together with properties of the planets (orbital period, mass, eccentricity, etc.) and any differences compared to the properties of the single-star planetary systems provide important constraints on planet formation and dynamical system evolution. A close stellar companion is expected to affect planet formation in several ways, e.g., by heating and truncating the circumstellar protoplanetary disk (Artymowicz & Lubow, 1994; Armitage et al., 1999; Nelson, 2000), or by increasing the relative velocities of the planetesimals (Heppenheimer, 1974, 1978; Whitmire et al., 1998; Mayer et al., 2005). A secondary star may either stimulate (Boss, 2006) or hinder (Nelson, 2000; Kley & Nelson, 2008) planet formation. The occurrence and properties of planets formed in binary systems may provide a way to discriminate between the two most widely supported planet formation models: core accretion (e.g., Pollack et al., 1996) and gravitational instability (e.g., Boss, 1997; Mayer et al., 2002). For instance, Mayer et al. (2005) find that if formed via gravitational instability, planets should be rare in binaries closer than $\sim 60 - 100$ AU, while on the other hand planets formed by core accretion should be common in these kinds of systems.

A few relations between the stellar and planetary properties in binaries have been suggested, some of which have later been discarded when the statistical samples have grown larger. While, e.g., differences in the planetary period-mass relations between single-star and binary-star systems noticed by Zucker & Mazeh (2002) and Eggenberger et al. (2004) have weakened with increasingly large samples, two correlations still seem significant: The most massive planets in short-period orbits belong to stars in binary systems, and so do the planets with the highest eccentricities (Desidera & Barbieri, 2007; Sozzetti & Desidera, 2010; Tamuz et al., 2008).

Transiting exoplanets (TEPs) are unique in the way that properties such as mass and radius can be measured, and a variety of physical parameters such as mean density and surface gravity can thus be derived. The discovery rate of transiting exoplanets has increased tremendously over the last couple of years, with around 50% of the known transiting planets being discovered in 2010 and during the first few months of 2011 (61/125 planets, `http://exoplanet.eu` 2011-03-31). This is mainly due to the success of ground-based transit searches such as SuperWASP (Pollacco et al., 2006) and HATNet (Bakos et al., 2004), as well as space-based programs such as CoRoT (Baglin et al., 2006) and Kepler (Borucki et al., 2010). Correlations between planetary and stellar properties in single and binary/multiple systems previously found in small samples can now be investigated for a larger number of TEPs and candidate binary systems. In this paper we present observations of 21 TEP host stars and investigate a few plausible relations suggested in the literature for TEPs in single and

binary/multiple systems.

Section 5.2 describes the observations of the 21 TEPs with the two AstraLux instruments at the 2.2 m telescope at Calar Alto and at NTT at La Silla, complementing the sample of TEP hosts presented by Daemgen et al. (2009). The methods for obtaining relative astrometry and photometry are described. In Section 5.3 we derive magnitudes, $(i - z)$ colours, and photometric spectral types and distances to the companion candidates from the photometric observations in SDSS i'- and z'-band and known spectral types of the planet host stars. Evidence of physical companionship between the planet host stars and the companion candidates is investigated, and the results for each individual target is compared with previously published astrometric and photometric data if available. Suggested relations between properties of the planets and the stars in the system are investigated in Section 5.4. Section 5.5 summarizes the results from this survey.

5.2 Observations and data reduction

5.2.1 Observations with AstraLux

The 21 transiting exoplanet host stars were observed within three different observing runs with the two AstraLux Lucky Imaging instruments. Most of the TEP hosts in the survey are located in the northern sky and were therefore observed with AstraLux Norte at the 2.2 m telescope at Calar Alto observatory in October-November 2009. The targets observable from the southern hemisphere were observed in November 2008 and April 2009 with the AstraLux Sur instrument mounted to the ESO 3.5 m New Technology Telescope (NTT) at La Silla (see Hormuth et al., 2008; Hippler et al., 2009, for details on the AstraLux instruments). Lucky Imaging is a way to limit the effects of atmospheric turbulence by taking a large number of very short integrations and then select only the least distorted few percent of the frames. These are shifted and added to produce the final image, yielding almost diffraction-limited resolution. The AstraLux field of view (FoV) in the final resampled frames is $\approx 15.7'' \times 15.7''$ for AstraLux Sur, and $\approx 24'' \times 24''$ for AstraLux Norte. The individual exposure time was either 15 ms or 30 ms, depending on the target brightness and observing conditions. The shorter integrations were achieved by decreasing the FoV and reading out only a subframe of the detector. In order to match a total integration time of 300 s, the number of integrations was set to 20 000 or 10 000 respectively.

Each target was observed in SDSS i'- and z'-filter. Stars in the open cluster NGC 3603 were observed several times during each night for calibration of the field rotation and pixel scale. The plate scale for the observations with AstraLux Norte was 23.431 ± 0.058 mas/px with the detector rotated 0.05^{o} to the east, and for the April 2009 observations with AstraLux Sur 15.296 ± 0.019 mas/px and 1.32^{o} to the west.

5.2.2 Photometry and astrometry

In the sample of 21 TEPs, we found candidate companion stars from visual inspection of the reduced Lucky Imaging frames to 7 stars: the previously known companion can-

didates to WASP-2, TrES-2 and TrES-4 (Daemgen et al., 2009), HAT-P-7 (Narita et al., 2010), and new companion candidates to HAT-P-8, WASP-12 and XO-3. Stars for which no companions were detected within the FoV with AstraLux in these observation runs are listed in Table 5.1. The stars for which a candidate companion was observed are listed in Table 5.2.

Most of the companion candidates reside close to the primary stars, within the psf-wings (HAT-P-7 and XO-3 being the exceptions). For these stars we performed relative photometry and astrometry of the companion candidates using mainly the IRAF *allstar* (Tody, 1986, 1993) task for psf-fitting. The psf was built from the primary star in an image where the secondary star had been removed (see Daemgen et al., 2009, for more details on the procedure). Aperture photometry with IRAF *apphot* was used to determine the properties of the wide companion candidate to XO-3. The astrometric and photometric properties in Table 5.2 are averaged measurements of the final images using the Lucky Imaging combination of the best 5% and 10% of the individual integrations. The separation and position angle error bars are propagated errors from 1σ uncertainties in the positional measurements, and take into account systematic errors (i.e., plate scale and detector orientation). The error bars in magnitude differences are propagated from the photometric errors estimated by IRAF *phot*.

Figure 5.1 shows the typical 5σ detection limit for the observations with AstraLux Norte in October-November 2009 (Figure 3.3 showed the sensitivity of the AstraLux Sur observations). The sensitivity was estimated by subtracting two images of single stars with similar peak flux and FWHM from each other and measuring the noise level in concentric circles at increasing separations from the centre.

Table 5.1: Transiting exoplanet host stars with no observed companions.

Planet Host	Instrument	FoV [arcsec]	JD
HAT-P-2	AstraLux Norte	12.00×12.00	2455137.25
HAT-P-11	AstraLux Norte	12.00×12.00	2455134.35
HAT-P-13	AstraLux Norte	12.00×12.00	2455137.66
HD 149026	AstraLux Norte	12.00×12.00	2455137.26
HD 209458	AstraLux Sur	7.87×7.87	2454751.55
HD 80606[a]	AstraLux Norte	12.00×12.00	2455134.70
WASP-3	AstraLux Norte	12.00×12.00	2455135.29
WASP-4	AstraLux Sur	15.74×15.74	2454749.61
WASP-5	AstraLux Sur	15.74×15.74	2454749.62
WASP-7	AstraLux Sur	7.87×7.87	2454934.90
WASP-13	AstraLux Norte	12.00×12.00	2455134.71
WASP-15	AstraLux Sur	7.83×7.83	2454933.63
XO-4	AstraLux Norte	12.00×12.00	2455136.65
XO-5	AstraLux Norte	12.00×12.00	2455135.65

[a]Visual binary star (e.g., Naef et al., 2001), outside of AstraLux field of view.

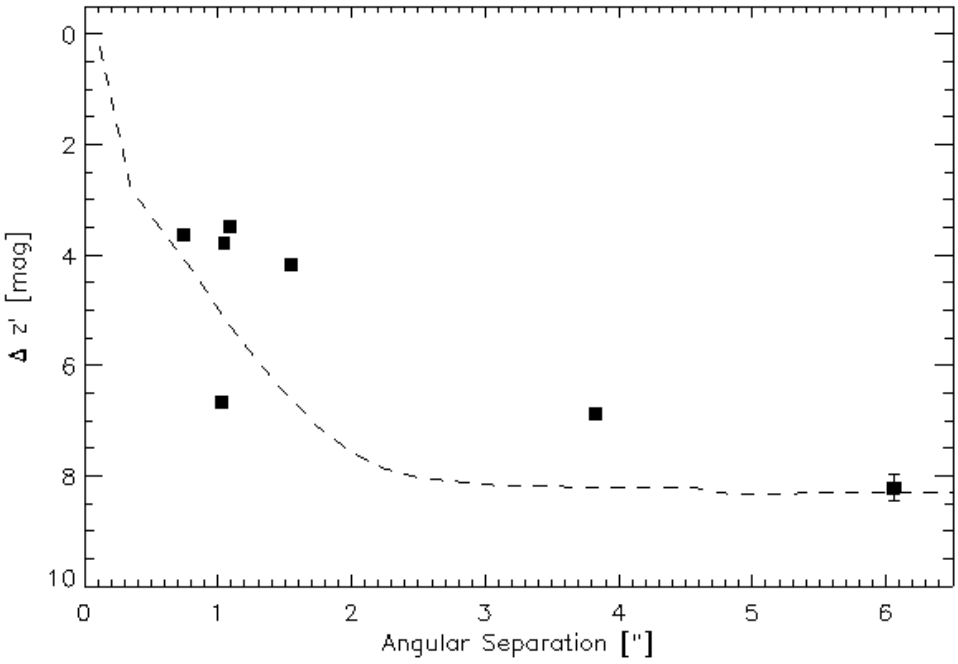

Figure 5.1: Average sensitivity of the AstraLux Norte observations. The squares mark the companion candidates (see Table 5.2). The dashed line represents typical 5σ detection limit for the observations in October-November 2009.

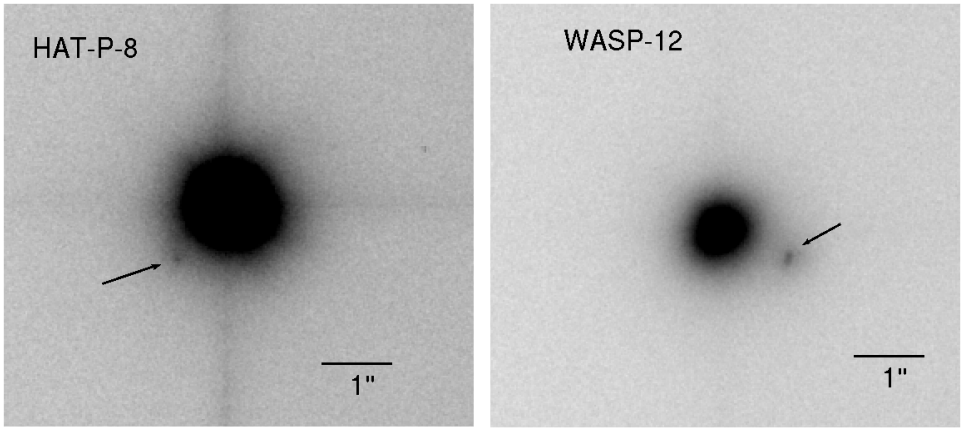

Figure 5.2: AstraLux Norte z'-band observations of the candidate binaries HAT-P-8 and WASP-12. The images are shown in a square root scale with north up and east to the left.

Table 5.2: Relative photometry and astrometry for the companion candidates.

ID	JD	Instrument	FoV [arcsec]	Separation [arcsec]	Position Angle [deg]	$\Delta z'$ [mag]	$\Delta i'$ [mag]
HAT-P-7[a]	2455135.29	AstraLux Norte	12.00×12.00	3.822±0.010	90.4±0.1	6.89±0.07	7.94±0.21
HAT-P-8	2455134.37	AstraLux Norte	12.00×12.00	1.027±0.011	137.3±0.4	6.68±0.07	7.34±0.10
TrES-2[b]	2455134.35	AstraLux Norte	12.00×12.00	1.085±0.006	136.1±0.2	3.48±0.06	3.73±0.03
TrES-4[b]	2455135.27	AstraLux Norte	12.00×12.00	1.550±0.007	359.9±0.2	4.19±0.05	4.57±0.05
WASP-2[c]	2454934.93	AstraLux Sur	15.66×15.66	0.764±0.012	103.6±0.5	3.62±0.05	...[d]
WASP-2[c]	2455134.33	AstraLux Norte	12.00×12.00	0.739±0.024	104.0±1.3	3.64±0.04	4.17±0.03
WASP-12	2455134.60	AstraLux Norte	12.00×12.00	1.047±0.021	249.7±0.8	3.79±0.10	4.03±0.07
XO-3	2455135.53	AstraLux Norte	12.00×12.00	6.059±0.047	296.7±0.3	8.22±0.23	8.57±0.24

[a]These results were first published in Narita et al. (2010)

[b]Companion was discovered by Daemgen et al. (2009)

[c]Companion was discovered by Cameron et al. (2007) and has also been observed by Daemgen et al. (2009)

[d]The companion to WASP-2 could not be resolved in i'-band in these observations.

5.3 Results

5.3.1 Properties of the stellar companion candidates

The apparent magnitudes in SDSS i- and z-band were derived for the primary TEP host stars by combining 2MASS photometry in JHK-band (Cutri et al., 2003) with synthetic colours by Covey et al. (2007). The measured magnitude difference between the primary and secondary stars in i' and z' then provides apparent magnitudes and $(i - z)$ colour for the companion candidate. While we do not explicitly correct for the transformation between SDSS $i'z'$ to iz, the difference, when calculated from the photometric transformation equations (SDSS webpage), is small. The magnitude difference between the two photometric systems is less than $(i - i') = 0.05$ mag for stars bluer than $(r - i) \approx 1.5$, and even less in $(z - z')$. According to the synthetic colours of Covey et al. (2007), this $(r - i)$ colour corresponds to spectral types earlier than M4. None of our derived spectral types are later than M3, and we conservatively assume error bars of ± 0.1 for the derived i, z magnitudes of the primary and secondary stars so as to include the transformation between photometric systems as well as uncertainty in the photometric measurements.

The secondary star spectral types and primary and secondary photometric distances were estimated from the derived $(i - z)$ colour and the synthetic colours of Covey et al. (2007). Interstellar extinction and stellar metallicity were not considered in these estimates but may affect the photometric distances, as well as the colours and spectral types. The components' spectral types, apparent magnitudes, photometric distances and the secondary stars' $(i - z)$ colours are listed in Table 5.3. Note that the photometric distances should only be considered as order-of-magnitude estimates, rather than accurate values for each distance. For instance, if taken at face value, the photometric distances to TrES-4 A and B could seem to imply chance alignment on the sky, but as we discuss in Sect. 5.3.2, the two components share a common proper motion, and hence constitute a real physical binary.

5.3.2 Notes on individual systems

Companion candidates to 7 transiting exoplanet hosts were found from these observations. Of these, the three TEP hosts WASP-2, TrES-2 and TrES-4 and their companion candidates had been observed with AstraLux previously (Daemgen et al., 2009), the candidate companion to HAT-P-7 is discussed in Narita et al. (2010), and the widely separated candidate companion to XO-3 is a physically unrelated background object, judging from the derived magnitudes and colours. The two faint objects at separations of $\rho \sim 1$ arcsec to HAT-P-8 and WASP-12 are previously unknown, plausibly bound stellar companions. Figure 5.2 shows the AstraLux Norte z'–band observations of these two systems obtained in October 2009. All astrometric measurements for the previously observed systems are summarized in Table 5.4.

HAT-P-8

The transiting exoplanet HAT-P-8 b was discovered by Latham et al. (2009). It is a slightly inflated planet with mass $M_p = 1.52^{+0.18}_{-0.16} M_J$ and radius $R_p = 1.50^{+0.08}_{-0.06} R_J$ (Latham

Table 5.3: Derived properties of the primary stars and the companion candidates.

Planet Host	SpT(A)	SpT(B)	m_z(A) [mag]	m_i(A) [mag]	m_z(B) [mag]	m_i(B) [mag]	$(i-z)_B$ [mag]	d(A) [pc]	d(B) [pc]
HAT-P-8[a]	F8 V	M3 V	9.95±0.1	9.98±0.1	16.63±0.1	17.32±0.1	0.69±0.14	176±9	501±23
	F5 V	M3 V (M2/M3)	9.91±0.1	9.89±0.1	16.59±0.1	17.23±0.1	0.64±0.14	207±10	488±27
TrES-2	G0 V	K7 V (K5/K7)	10.90±0.1	10.92±0.1	14.38±0.1	14.65±0.1	0.27±0.14	252±12	330±15
TrES-4	F8 V	M0 V (M0/M1)	11.31±0.1	11.34±0.1	15.50±0.1	15.91±0.1	0.41±0.14	330±15	504±23
WASP-2[b]	K0 V	M2.5 V (M2/M3)	11.03±0.1	11.10±0.1	14.67±0.1	15.27±0.1	0.60±0.14	160±7	243±12
	K2 V	M2.5 V (M2/M3)	11.20±0.1	11.31±0.1	14.84±0.1	15.48±0.1	0.64±0.14	139±7	254±12
WASP-12	G0 V	K7 V (K5/K7)	11.20±0.1	11.22±0.1	14.99±0.1	15.25±0.1	0.26±0.14	290±13	435±20
XO-3	F5 V	K7 V (K7/M0)	9.74±0.1	9.72±0.1	17.96±0.2	18.29±0.2	0.33±0.30	191±9	1700±200

[a] A primary star spectral type of F8 V is suggested by Jones & Sleep (2010), while we find F5 V to better fit the synthetic colours of Covey et al. (2007). We therefore list both alternatives here.

[b] The primary star is of spectral type K1 V. Covey et al. (2007) provides synthetic colours only for K0 V and K2 V, and we choose to present these two alternatives rather than interpolate between spectral types.

Table 5.4: Astrometric measurements.

Planet Host	Date of Obs.	Separation [arcsec]	Pos. Ang. [deg]	Ref.
HAT-P-7	6 Aug 2009	3.88±0.01	89.8±0.3	1
	10 Oct 2009	3.82±0.01	90.4±0.1	1,2
TrES-2	May 2007	1.089±0.008	135.5±0.1	3
	29 Oct 2009	1.085±0.006	136.1±0.2	2
TrES-4	Jun 2008	1.555±0.005	359.8±0.1	3
	30 Oct 2009	1.550±0.007	359.9±0.2	2
WASP-2	Nov 2007	0.757±0.001	104.7±0.3	3
	13 April 2009	0.764±0.012	103.6±0.5	2
	29 Oct 2009	0.739±0.024	104.0±1.3	2

References: (1) Narita et al. (2010); (2) This paper; (3) Daemgen et al. (2009)

et al., 2009). The host star spectral type is only given as F in the discovery paper, but is referred to as F8 V by Jones & Sleep (2010). We find from the 2MASS JHK photometry and colours that a spectral type of F5 V is a better fit to the synthetic colours of Covey et al. (2007), and list both alternatives in the table until a more precise spectral classification can be made. We find for both alternatives of primary spectral type that the stellar candidate companion is likely to be an M3 V or possibly M2 V star from the $(i-z)$-colours.

TrES-2

The companion candidate was first discovered by Daemgen et al. (2009) from AstraLux Norte observations in May 2007. The observations presented here took place in October 2009. We measure a separation of $\rho = 1.085'' \pm 0.006''$ and position angle $\theta = 136.1^{o} \pm 0.2^{o}$, which is consistent with the astrometry of Daemgen et al. (2009) who found $\rho = 1.089'' \pm 0.008''$ and $\theta = 135.5^{o} \pm 0.1^{o}$. The proper motion of TrES-2 is only $\mu_\alpha \cos\delta = 2.34\,\mathrm{mas/yr}, \mu_\delta = -1.55\,\mathrm{mas/yr}$ (PPMX Catalog, Röser et al., 2008), which is within our positional error bars over the time interval of ~ 2 years between observations. We have to await future observations to tell whether the pair is physically bound or not.

TrES-4

The candidate companion star was discovered in AstraLux Norte observations from June 2008 by Daemgen et al. (2009). Our measurement of $\rho = 1.550'' \pm 0.007''$ and $\theta = 359.9^{o} \pm 0.2^{o}$ in October 2009 is consistent with the separation $\rho = 1.555'' \pm 0.005''$ and position angle $\theta = 359.8^{o} \pm 0.1^{o}$ measured by Daemgen et al. (2009). With a proper motion of $\mu_\alpha \cos\delta = -9.94\,\mathrm{mas/yr}, \mu_\delta = -27.80\,\mathrm{mas/yr}$ (Röser et al., 2008), we would expect a relative displacement of $\mu \approx 39$ mas for a physically unrelated stationary background star over the time baseline of ≈ 16 months between the observations of

Daemgen et al. (2009) and our measurements. No such relative motion is measured, and the stars therefore seem to share a common proper motion, by $\sim 2.6\sigma$ confidence (99% certainty if the errors are Gaussian).

WASP-2

WASP-2 b was discovered by Cameron et al. (2007), who also reported the stellar companion candidate to the east of the TEP host star at an angular separation of $\rho = 0.7''$. Although the primary star is a K1 V star, we list in Table 5.3 the derived magnitudes, colours and photometric distances assuming primary spectral type K0 and K2, since colours for K1 is not provided by Covey et al. (2007). In either case, we find that the companion candidate is of spectral type M2.5 (M2/M3). The proper motion of the planet host star is $\mu_\alpha \cos\delta = 3.38\,\mathrm{mas/yr}, \mu_\delta = -52.31\,\mathrm{mas/yr}$, hence the magnitude of proper motion is $\mu = 52.42\,\mathrm{mas/yr}$ corresponding to a total proper motion of $\approx 104\,\mathrm{mas}$ over the $\approx$2 years that passed between the observations of Daemgen et al. (2009) and the October 2009 observations presented in this paper. With the large error bars from the October 2009 observations, additional observations are necessary for confirmation of common proper motion.

WASP-12

The very bloated planet WASP-12 b was discovered by Hebb et al. (2009). It is a highly irradiated planet, and one of the hottest with an equilibrium temperature $T_{eq} = 2516 \pm 36\,\mathrm{K}$ (Hebb et al., 2009).

The stellar companion candidate is not previously known. We derive a spectral type K5/K7 V from the measured $(i-z)$ colour and the synthetic colours of Covey et al. (2007). The measured colour is a slightly closer match to a K7 star of Covey et al. (2007), and the photometric distance has therefore been calculated for this spectral type. The photometric distances for both WASP-12 and the companion candidate are consistent with the distance of $295-465\,\mathrm{pc}$ derived by Fossati et al. (2010). The proper motion of WASP-12 is $\mu_\alpha \cos\delta = -0.36\,\mathrm{mas/yr}, \mu_\delta = -6.38\,\mathrm{mas/yr}$ (Röser et al., 2008), and future observations will be necessary to determine whether or not the stars are physical companions.

XO-3

A very faint companion candidate ($\Delta z \approx 8.2$) was found at large angular separation ($\rho \approx 6''$) from the TEP host star XO-3. The $(i-z)$-colour places the companion candidate at a distance of $\sim 1.7\,\mathrm{kpc}$, if a main sequence star, and it is hence likely a non-related background object.

5.3.3 Probability of chance alignment

The probability of chance alignment is estimated using the statistical approach of Daemgen et al. (2009). The density of detectable background giants, $\rho(m_K)$, is cal-

culated by selecting all stars included in the 2MASS PSC (Cutri et al., 2003) within 30′ of each of the observed targets (Tables 5.1, 5.2) that are brighter than the estimated limiting magnitude of AstraLux, $m_K \approx 14$, and redder than $(J-K) \geq 0.5$. The probability of detecting a background giant is

$$P(\Theta, m_K) = 1 - e^{-\pi\rho(m_K)\Theta^2}, \tag{5.1}$$

where Θ is the maximum angular separation (Brandner et al., 2000). Using the aforementioned cuts in m_K, $(J-K)$ for $\Theta = 2''$ (see Daemgen et al., 2009) the average probability of finding a non-related background star within 2″ to the target star is $P = 0.08\%$. We would then expect to detect unrelated background sources to $E = 21 \times P \approx 0.016$ of our observed targets. This expectation value of chance alignment increases to 0.14 at the separation of 6″ at which we find the probable background object in the observations of XO-3 (see previous section). The close candidate companions in our sample are thus likely to be true companions, although future observations are still necessary for confirmation of common proper motions.

5.4 Discussion

Correlations between properties of the planets (mass, radius, eccentricity, surface gravity, etc.) and the presence of or the distance to a secondary stellar companion might reveal clues to the formation and dynamical evolution of the planetary system. The analysis of chance alignment in Sect. 5.3.3 showed that the probability of non-related background objects is very low. We will assume for the following discussion that:

- The companion candidates observed within the AstraLux Survey (Table 5.2) are, with the exception of XO-3, physical companions.
- The stars for which no companion candidate was found within the AstraLux Survey (Table 5.1 in this paper and Table 1 in Daemgen et al., 2009) are assumed to be single to within 2″ and the detection limits of Fig 1. Companions with wider separations that 2″ should be known from seeing-limited observations (see Daemgen et al., 2009), e.g., HD 80606.
- The TEPs that have not been observed with AstraLux are assumed to be single unless companions are known.

Parameters obtained from literature can be found in Table C.1. We have divided the binaries and candidate binaries into groups depending on their projected separation, which we will assume as their semi-major axis. Theoretical (e.g., Mayer et al., 2005) as well as observational results (e.g., Duchêne, 2010; Bouwman et al., 2006) suggest that only binary companions within a separation of $a \lesssim 100\,\mathrm{AU}$ will affect planet formation. However, Desidera & Barbieri (2007) set a limit of $a < 100 - 300\,\mathrm{AU}$ within which companions may significantly affect planet formation, and observations of disks in the Orion Nebula Cluster by Daemgen et al. (2011, in prep.) supports the notion that a binary companion at wider separations of $100 - 400\,\mathrm{AU}$ may also affect the evolution of the protoplanetary disk. We have, therefore, divided the binary TEP host stars into classes of ”close” binaries with separations $a_{\mathrm{close}} \lesssim 300\,\mathrm{AU}$ and “wide” binaries with larger separations. The adopted separations of all currently known binary/multiple TEP hosts are listed in Table 5.5.

Table 5.5: Binary separations for transiting planet hosts.

Binary/Triple Planet Host	Separation [AU]	Ref.
HAT-P-1	1550	1
HAT-P-20	480	2
HAT-P-22	746	2
HAT-P-7	1200, 1000	3
HAT-P-8	236 (d = 230 pc)[a]	4
HD 189733	216	5
HD 80606	1200	6
TrES-2	239 (d = 220 pc)[a]	4
TrES-4	742 (d = 479 pc)[a]	4
WASP-12	153 (d = 146 pc)[a]	4
WASP-2	106 (d = 144 pc)[a]	4
WASP-22[b]	...	7
WASP-26	3750	8
WASP-31	14 000	9
WASP-34[b]	...	10
WASP-8	420, 12 350	11

[a]Distance to planet host star from `http://exoplanet.eu`.

[b]WASP-22 and WASP-34 show linear RV trends suggesting stellar companions. The properties of these candidates are not yet constrained.

References: (1) Bakos et al. (2007a); (2) Bakos et al. (2010a); (3) Narita et al. (2010); (4) This paper; (5) Bakos et al. (2006); (6) Eggenberger et al. (2003); (7) Maxted et al. (2010c); (8) Smalley et al. (2010); (9) Anderson et al. (2010a); (10) Smalley et al. (2011); (11) Queloz et al. (2010).

5.4.1 Planet mass – radius

Figure 5.3 shows the radius as a function of mass for 114 transiting exoplanets listed at `http://exoplanet.eu` in January 2011. Close binary candidates ($a_{\rm close}$ < 300 AU) are marked with blue open squares. Wider binaries are marked with red diamonds. No obvious trend can be seen in the mass-radius diagram for transiting planets in wide binaries. The TEPs in the close binaries all have masses around one jupiter mass (0.847-1.52 M_J), but the radius, and hence the mean density, varies from the bloated WASP-12 with a radius of R_p = 1.79 R_J (Hebb et al., 2009) to WASP-2 which is only slightly larger than Jupiter (R_p = 1.043 R_J, Southworth, 2010). With only five close binaries, the mass distribution for TEPs in these systems can not be considered to differ much from the masses of single-star TEPs. A Kolmogorov-Smirnov (K-S) test confirms that neither the close-binary TEP mass-distribution nor the wide-binary TEP mass-distributions are significantly different from that of the single-star TEPs.

A K-S test was also performed to make sure that we had observed a representative sample in mass, and showed that the cumulative planetary mass distribution of the TEPs observed with AstraLux is not significantly different to that of TEPs not observed with AstraLux. Figure 5.4 shows the number of exoplanet hosts in each mass bin observed within the AstraLux binary TEP hosts survey (31 targets, see Tables 5.1, 5.2, and Daemgen et al., 2009) compared to the mass distribution of all TEPs.

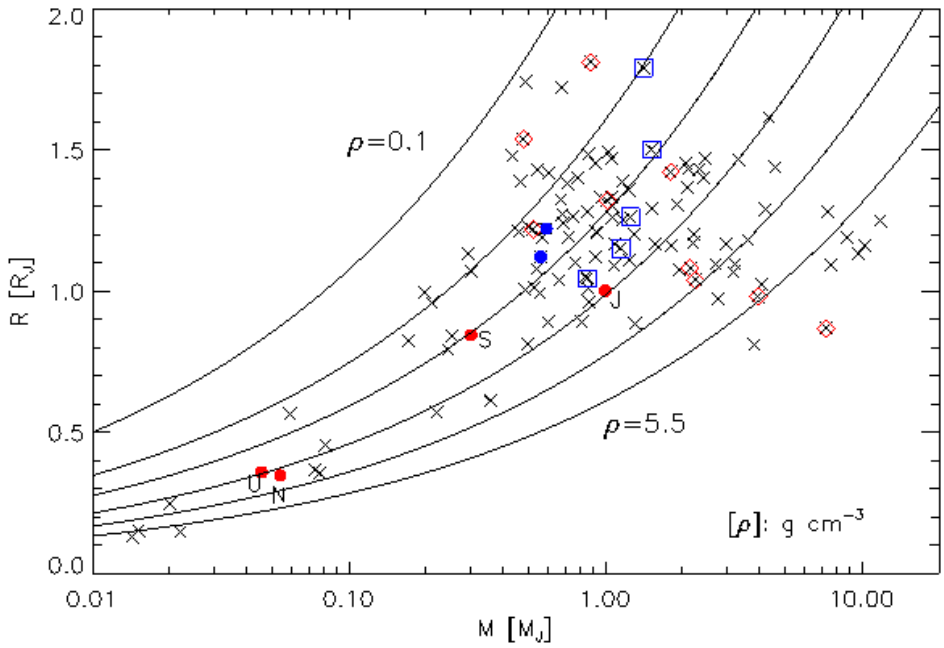

Figure 5.3: Radius and mass for all transiting exoplanets (114). Blue open squares mark the five binary candidates that are separated by $a_{\rm close} < 300$ AU, and red diamonds are the wide binaries, $a_{\rm wide} > 300$ AU. The two blue dots mark the systems WASP-22 and WASP-34, for which the binary companion is inferred only from a linear trend in radial velocity and thus no secondary star properties are known. Lines of constant mean density $\rho = 0.1, 0.3, 0.6, 1.3, 2.7$ and 5.5 are overplotted. The giant planets of our Solar System are marked with red dots for comparison.

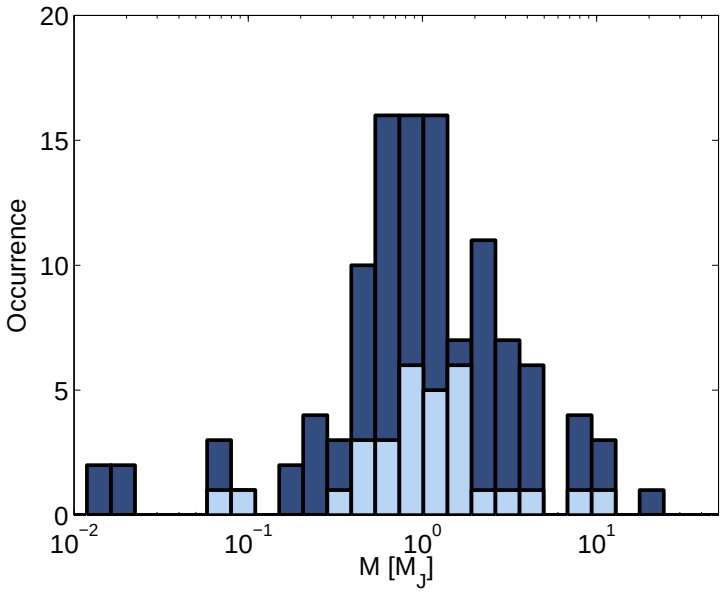

Figure 5.4: Histograms of planetary masses among the 31 observed targets in the AstraLux TEP survey (this Chapter and Daemgen et al., 2009, light blue), and all 114 transiting systems (dark blue). A K-S test shows that a representative sample of planetary mass was observed.

5.4.2 Planet mass – period

Zucker & Mazeh (2002) observed that the mass and period were oppositely correlated for planets in binaries than for planets in single star systems. This correlation was shown to substantially weaken as the sample of exoplanets in both single and binary systems has grown larger (Desidera & Barbieri, 2007). However, two relations between the properties of the planets and the binary characteristics still seem to be significant: The planets with the highest eccentricities all belong to a star in a binary system (Tamuz et al., 2008), and the hosts of the most massive, short-period (P< 40 days) planets are usually part of a close binary (Desidera & Barbieri, 2007).

Figure 5.5 shows the mass-period distribution for 114 transiting exoplanets, with the close binaries ($a < 300$ AU) marked with blue open squares and the wide binaries ($a > 300$ AU) with red diamonds. The transiting planets in the close binaries all have masses in the range $0.8 < M < 1.5\,M_J$ and orbital periods $1.1 < P < 3.1$ days. Hence, from the small sample of close binaries only, we see no clear correlation with TEP mass and binary separation.

We carried out a series of K-S tests to check if the masses of transiting exoplanets in systems with a stellar companion at different separations could have been drawn from the same underlying distributions as the masses of TEPs around single stars. We performed the K-S tests for bins of TEP hosts with increasing maximum binary separation, i.e., the smallest bin consisted of the four closest binary systems, the next smallest bin of the five closest, and so on. The single star sample consists of the hosts to 98 exoplanets. The probability of the masses of single-star TEPs and binary-star

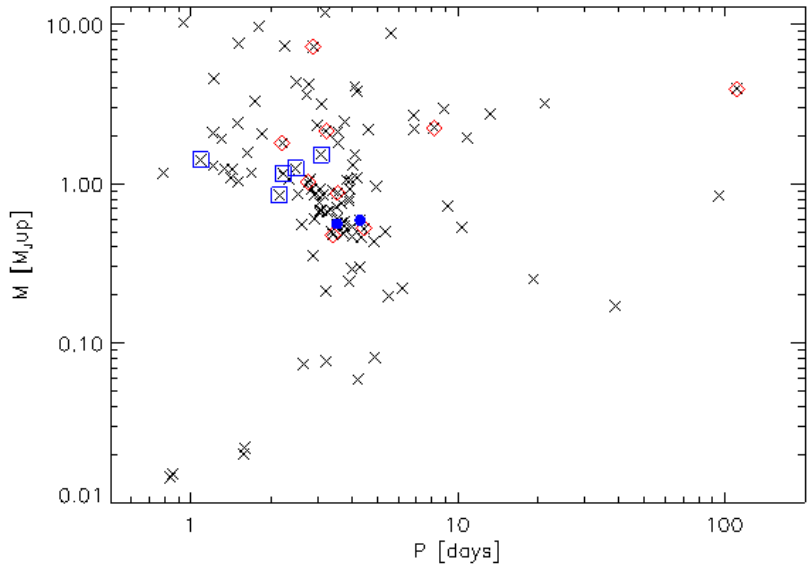

Figure 5.5: Planetary mass as a function of orbital period. The close binaries ($a < 300$ AU) are marked with blue open squares, the wide binaries with red diamonds, and WASP-22 and WASP-34 with blue dots.

TEPs being drawn from the same underlying distribution is lowest for binary separations $a \lesssim 1\,200$ AU, which corresponds to 10 TEPs in binary/multiple star systems. The cumulative planetary mass function for these TEPs is plotted in Figure 5.6. For this sample we can reject the hypothesis that both TEP samples have been drawn from the same distribution at a significance level of ≈96.5%. The transiting planets in these binary systems are on average more massive than their single star counterparts, with 45% of the single-star TEPs having masses below the mass of the lightest binary-star TEP (M = 0.847M_J Wasp-2 b). Thus, the presence of a stellar companion at projected separations $\lesssim$1 200 AU might have an influence on exoplanet properties. On the other hand, our relatively small sample of ten transiting exoplanets in binary systems with separations $\lesssim$1 200 AU might not be fully representative of the overall exoplanet population in binary and multiple stellar systems, and we have for this analysis not considered potential biases in the multiplicity such as chance projection and detection limits in separation. Future surveys for stellar companions to transiting exoplanet hosts expanding the sample will provide an even better view on the influence of stellar companions on the planet formation and migration process.

5.4.3 Planet surface gravity – period

Southworth et al. (2007) suggested a correlation between the planet surface gravity and orbital period for TEPs and found a linear Pearson correlation coefficient of $r = -0.70$, which indicates a significant correlation between these parameters to within the 0.5% level for a sample of 14 transiting exoplanets. When extending the sample to 71 TEPs, Southworth (2010) confirms that there is a 99.80% probability of a real corre-

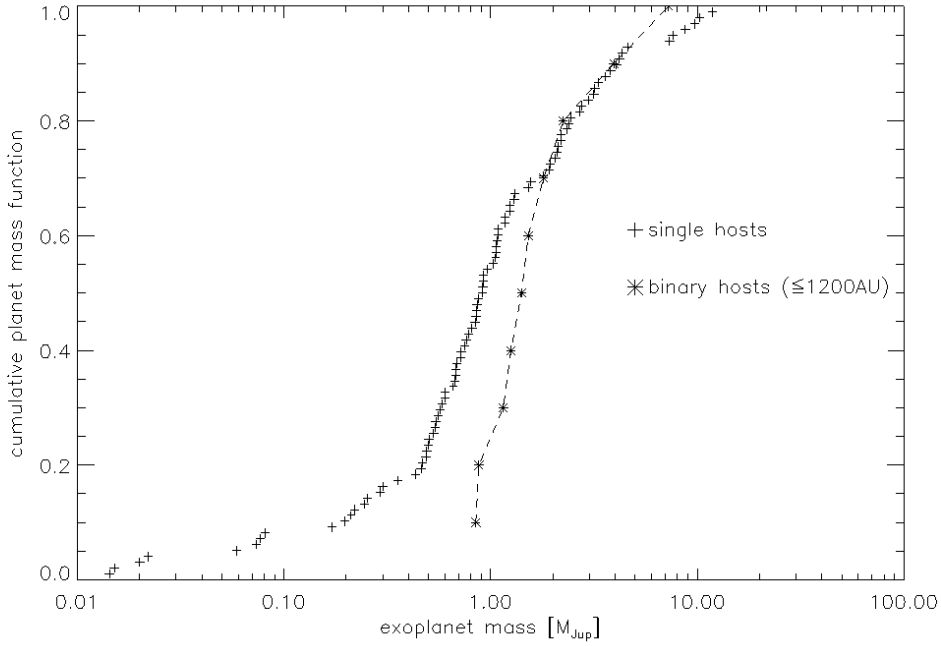

Figure 5.6: Cumulative mass function for planets in single star systems (plus-signs) and binary/multiple star systems closer than 1200 AU (asterisks). Almost half of the planets in single star systems have masses below the lowest-mass planet in the binary/multiple star sample.

lation between surface gravity and orbital period for short period planets ($P < 6$ days).

We plot the surface gravity for the 103 TEPs for which this property could be calculated from published parameters in Fig. 5.7. Southworth (2010) provide surface gravities for 30 transiting planets, and for most of the other TEPs we calculate surface gravity using equation (4) from that same paper:

$$g_p = \frac{2\pi}{P} \frac{\left(1 - e^2\right)^{1/2} K_*}{r_p^2 \sin i}, \tag{5.2}$$

where P is the orbital period, e is the eccentricity, K_* is the stellar velocity amplitude, i is the inclination and the fractional radius $r_p = R_p/a$ is the ratio of the planet radius to the semi-major axis. By using parameters directly inferred from the lightcurve ($k = R_p/R_*$ and a/R_* are often published, which directly gives r_p), the dependence on stellar models of evolution or atmospheres is avoided (see Southworth et al., 2007; Southworth, 2010). For some TEPs these parameters were not found in the literature, and we adopted either derived parameters of R_* and a (for 2 transiting exoplanets) or published values of g_p (20 TEPs). The eccentricity e is often an unknown parameter for TEPs, since it can only be measured from radial velocity observations, which may not allow for precise measurements if the target is faint. If not obviously eccentric, it is in many cases assumed that the orbit is circular and e is set to zero (see Pont et al., 2011, for a discussion on TEP eccentricity).

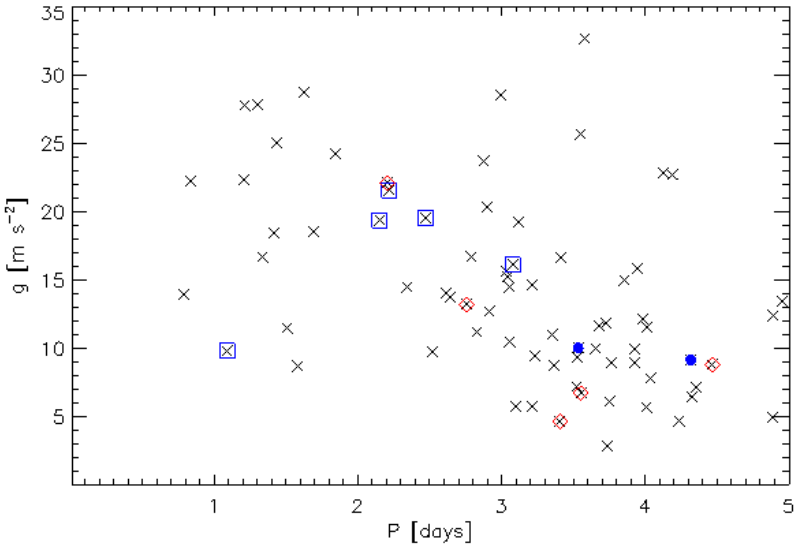

Figure 5.7: Planetary surface gravity as a function of orbital period. Blue open squares mark the close binaries ($\rho < 300$ AU), and red diamonds the wide ones. The two blue dots mark WASP-22 and WASP-34.

Figure 5.7 show the resulting surface gravity – period distribution for orbital periods $P < 5$ days (see Table C.2 for calculated surface gravity g). Taken at face value, no correlation can be seen for this larger sample between surface gravity and orbital period (linear Pearson correlation coefficient $r = 0.05$, taken into account all 103 TEPs).

5.4.4 Safronov number vs. equilibrium temperature

Hansen & Barman (2007) found that the small number of hot jupiters known at the time (19) could be divided into two classes based on their Safronov number and equilibrium temperature. The Safronov number θ is defined as

$$\theta = 0.5\left(\frac{v_{\rm esc}}{v_{\rm orb}}\right)^2 = \frac{a}{R_{\rm p}}\frac{M_{\rm p}}{M_*}, \tag{5.3}$$

where $v_{\rm esc}$ is the planetary escape velocity and $v_{\rm orb}$ the orbital velocity, a is the semi-major axis, $R_{\rm p}$ the planetary radius, $M_{\rm p}$ the planetary mass and M_* is the stellar mass. The Safronov number is a measure of how efficiently the planet scatters or captures nearby bodies, and could if the bimodality seen by Hansen & Barman (2007) persists with a large statistical sample point to different modes of planet migration. The equilibrium temperature, $T_{\rm eq}$, was calculated as

$$T_{\rm eq} = T_{\rm eff}\left(\frac{R_*}{2a}\right)^{1/2}. \tag{5.4}$$

The significance of the division with Class I at $\theta \sim 0.07$ and Class II at $\theta \sim 0.04$ has however been questioned by (e.g., Fressin et al., 2009; Southworth, 2010). In the Figures 5.8 and 5.9 the Safronov number vs. equilibrium temperature is shown

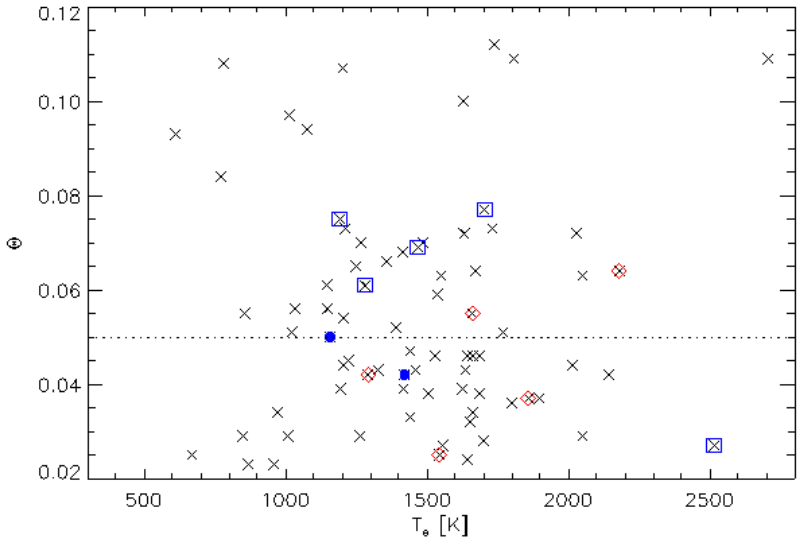

Figure 5.8: Safronov number vs. equilibrium temperature. The two original classes are divided by the dashed line at $\theta \sim 0.5$.

for transiting exoplanets on two different scales. In the literature we could find all the parameters necessary for calculating these properties for 108 TEPs (see Table C.2). In Fig. 5.8 the $\theta - T_{eq}$ plane has the same scale as the original plot by Hansen & Barman (2007), and in Fig. 5.9 a logarithmic scale in θ shows the full range. The division of Hansen & Barman (2007) is marked with a dotted line in Figure 5.8 and 5.9, and with the significantly larger number of known hot jupiters we do not any longer see a clear distinction between the suggested groups.

Daemgen et al. (2009) suggested a correlation between these classes and binary separation, where the "wide binaries" (separation $\gtrsim$ 750 AU) known at the time all belonged to Class II and closer binaries to Class I. In Figures 5.8 and 5.9, the close binary systems or candidate binary systems are marked with blue open squares and the wider systems with red diamonds. We define close binaries as those with projected separation $a < 300$ AU. With the larger sample of TEPs we no longer see any such correlation between binary separation and Safronov number. However, with the exception of WASP-12 which has a $\theta = 0.027$, the close binaries cover a narrow range in θ between ~ 0.061 and ~ 0.077.

5.5 Summary

We observed 21 TEP host stars in our Lucky Imaging survey for binary stellar companions. Two previously unknown companion candidates were discovered, to the TEP hosts HAT-P-8 and WASP-12. Future follow-up observations are necessary to confirm common proper motion and hence physical companionship. Of the three TEP hosts observed previously with AstraLux (Daemgen et al., 2009), TrES-4 could be confirmed as a common proper motion couple from these follow-up observations. Observations

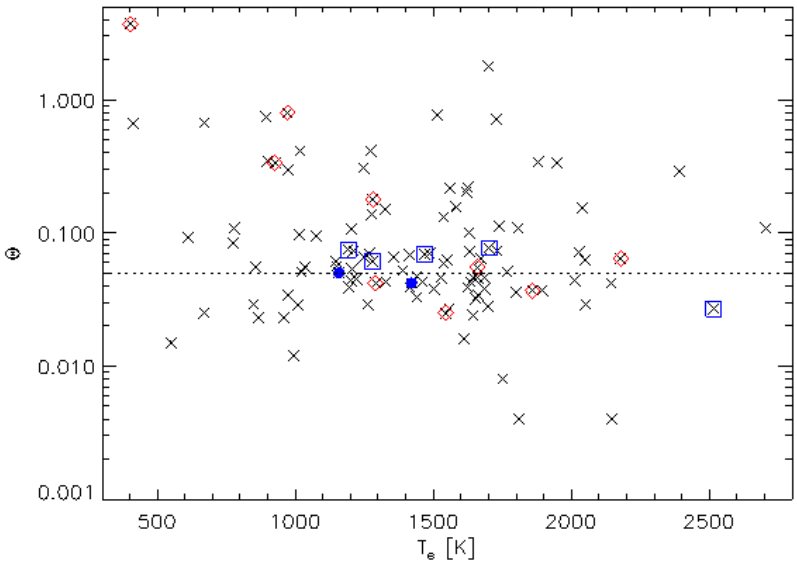

Figure 5.9: Safronov number vs. equilibrium temperature on a linlog scale.

over a longer time baseline are still necessary for companion confirmation for the TrES-2 and WASP-2 systems.

We divided the sample of TEP host stars into singles, close binaries with projected separation $a < 300$ AU, and wide binaries, and tested for possible correlations between planet properties and planet host star binarity. While the sample of close binaries is still very small (5 objects), the distributions of planetary radius, surface gravity, orbital period and Safronov number do not differ significantly from the single-stars TEPs distributions. A Kolmogorov-Smirnov test was applied to the mass distributions of single-star TEPs and planets in binary/multiple systems with binary separations $\leq$1 200 AU, showing that the hypothesis that both samples can be drawn from the same parent distribution can be rejected with 96.5% probability. Almost half of the transiting planets in the single-star sample have masses of less than the smallest-mass TEP in the binary/multiple star sample. Hence, transiting exoplanets in multiples are on average more massive than those hosted by single stars, which indicates that a stellar companion might influence the formation of planets.

CHAPTER 6

VLT/NACO ASTROMETRY OF THE HR8799 PLANETARY SYSTEM: L′-BAND OBSERVATIONS OF THE THREE OUTER PLANETS

Abstract:

HR 8799 is so far the only directly imaged multiple exoplanet system. The orbital configuration would, if better known, provide valuable insight into the formation and dynamical evolution of wide-orbit planetary systems. We present L′-band observations with NACO at VLT, which add to the astrometric monitoring of the planets HR 8799 b, c and d. We investigate how well the two simple cases of (i) a circular orbit and (ii) a face-on orbit fit the astrometric data for HR 8799 d over a total time baseline of ~ 2 years. The results indicate that the orbit of HR 8799 d is inclined with respect to our line of sight, and suggest that the orbit is slightly eccentric or non-coplanar with the outer planets and debris disk.

From Bergfors et al., 2011, A&A 528, A134

6.1 Introduction

As the first and so far only directly imaged multiple exoplanet system, the HR 8799 system carries the promise of providing valuable insight into the structure and characteristics of planetary systems. While more than 500 extrasolar planets have now been discovered, most have been found by radial velocity and transit searches; the sample of known exoplanets is thus heavily biased towards short-period planets. Directly imaged giant extrasolar planets provide a necessary complement to these indirect detection techniques for a full picture of the characteristics of planets, and are crucial for theories of planet formation.

Challenging as it may be to directly image planets, whose relatively faint light is easily lost in the bright stellar glare, several confirmed companions are known. As of November 2010, 7 planetary mass objects belonging to stars, including the quadruple-planet HR 8799 system, have been discovered with direct imaging (Fomalhaut b, Kalas et al. (2008); β Pic b, Lagrange et al. (2009, 2010); 1RXS J160929.1-210524 b, Lafrenière et al. (2008, 2010), and HR 8799 bcde, Marois et al. (2008, 2010)). The HR 8799 system is especially interesting since its multiple planet configuration allows for comparison of the characteristics of planets within the same environment of formation and evolution. The star is a young (30-160 Myr, Marois et al., 2008) A5 V star at at distance of 39.4 pc from the Sun (van Leeuwen, 2007), surrounded by a debris disk (Rhee et al., 2007; Su et al., 2009). Three of the planets in the system, HR 8799 b, c and d, were discovered in 2008 and an additional planet, HR 8799 e, in 2010 (Marois et al., 2008, 2010), adding up to at least four giant planets of masses 7-10 M_J at projected separations 14.5, 24, 38 and 68 AU from the central star.

The astrometric analysis of the three outermost planets at the time of their discovery provided evidence that the planets are co-moving with the star, and suggested that their orbits are almost circular and seen close to face-on. However, dynamical modelling of the HR 8799 system has since shown that this initially presumed configuration of orbits is unlikely for reasons of orbital stability of the system (Fabrycky & Murray-Clay, 2010; Reidemeister et al., 2009; Goździewski & Migaszewski, 2009). Fabrycky & Murray-Clay (2010) found that for the masses derived by Marois et al. (2008) and circular, face-on orbits, the system would become unstable at an age of only $\sim 10^5$ years, i.e. significantly younger than its assumed present age. Stable mean motion resonance configurations were found for the three outer planets known at the time by Fabrycky & Murray-Clay (2010); Goździewski & Migaszewski (2009) and Reidemeister et al. (2009), and Marois et al. (2010) found stable resonant configurations including also the fourth planet.

In this chapter we present astrometric measurements of the three outermost planets in the HR 8799 system. The observations were obtained with NACO at VLT in September 2009 – one year after the discovery of planets b, c and d. We investigate how well two simple models with (i) a circular orbit and (ii) a face-on orbit fit the astrometric data when the new observations are included.

6.2 Observations and data reduction

Acquisition images of HR 8799 in L′-band were obtained with NACO/VLT (Lenzen et al., 2003; Rousset et al., 2003) on the nights of October 5 and 6, 2009, as part of the observation programme 084.C-0072, in which a spectrum of the planet HR 8799 c was obtained (Janson et al., 2010). The observations were acquired in cube-mode and consisted on each night of 2 sets of 10 data cubes, one set taken at the default orientation with north up and one rotated by 33º. The frames were obtained with the purpose of checking the alignment for slit orientation. Each cube contained 749 usable frames on October 5 and 1499 frames on October 6 with individual integration time 20.2 ms, yielding a total integration time of 15 s and 30 s respectively per data cube.

Images of the astrometric binary HD 211742 obtained in September 2009 were retrieved from the ESO (VLT) archive and used for calibration of plate scale and true north orientation of the detector. We derive a field rotation of -0.6º ± 0.2º and plate scale of 27.1 mas/px, consistent with the 27.2 mas/px of the L27 camera described in the NACO User manual, assuming a systematical error of 0.2º and 0.3 mas/px (1% of the pixel scale, see Köhler, 2008).

The data reduction was performed using IRAF and IDL. Skyframes were constructed by averaging the sum frame of 10 data cubes obtained at the approximate same time and airmass with the star in different dither positions, rejecting the 2-3 highest values at each pixel in order to remove the stellar flux. The skyframes were subtracted from each frame in the cubes, and bad pixels were replaced by the mean value of neighbouring pixels. The frames were aligned by fitting a 2-D Gaussian to the star and measuring the centroid position and then co-added to remove residual tip-tilt between individual frames of each data cube and produce one image per rotation angle for each night. Frames of poor quality or with the target too close to the detector edge, hence cutting out the planets, were rejected, resulting in a combination of 4-7 data cubes for each final image (4 images in total, one for each rotation angle on each night). Unsharp masking was used on the co-added frames by smoothing one version of the image using a boxcar average with 15 pixels and subtracting the smoothed image from the original. The positions of the planets and central star were determined using the IRAF *imexamine* task. While the brightest planet, HR 8799 c, was clearly detectable in all four images, the position of the fainter b-planet could only be determined from 3 measurements. Speckle contamination obscured planet d in the 33º rotated images and the position could thus only be determined from 2 frames. The reported position of planet e coincides with the third diffraction ring and is not detected with significant counts. Fig. 6.1 shows rotated and subtracted images from both nights.

When imaging sources with vastly different spectral energy distributions through a broadband filter at an airmass > 1.0, the effect of differential atmospheric refraction on the relative astrometry has to be considered (see, e.g., Hełminiak, 2009). An effective wavelength $\lambda_{\rm eff}$ = 3.777μm for our NACO L′ imaging observation of the star HR 8799 was computed by convolving a spectrum of a star of similar spectral type from the IRTF SpeX spectral library (Cushing et al., 2005; Rayner et al., 2009) with the L′ transmission curve from the NACO Usermanual. For the three exoplanets, an effective wavelength of $3.905 \pm 0.010\,\mu$m was computed using model spectra (Burrows et al., 2006, and priv. comm.) for an effective temperature of 1100 K and log g in the range 3.0 to 5.0.

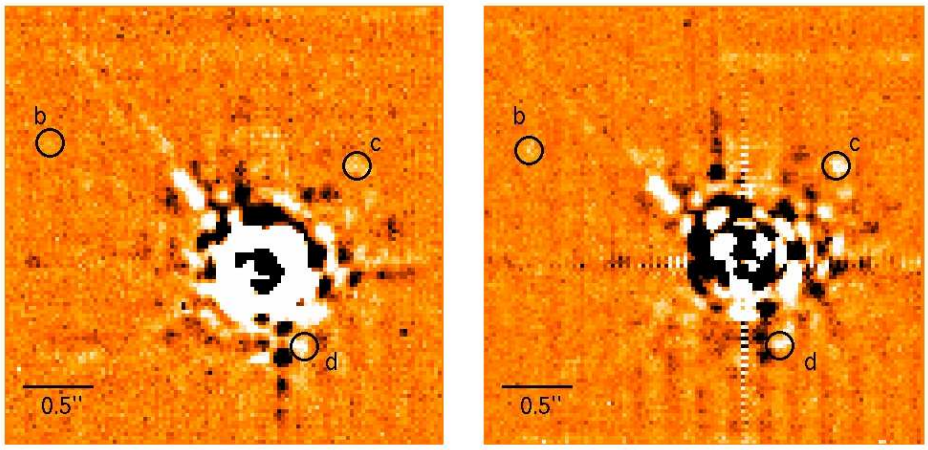

Figure 6.1: Rotated and subtracted 3″ x 3″ images from observations on October 5 (left) and October 6 (right) 2009. North is up and east is to the left. Scaling is linear.

As a consistency check, we also computed the effective wavelength for L′ imaging observations of Jupiter based on the IRTF SpeX library, which resulted in $\lambda_{\rm eff}$ = 3.907 μm. Hence, once effective temperatures in the atmospheres of substellar objects are low enough to allow for the pronounced presence of water, methane and CO molecular absorption bands, the $\lambda_{\rm eff}$ values for L′ observations seem to show little dependence on effective temperature and surface gravity.

Next, we used the model fits for the refractive index of humid air in the infrared as computed by Mathar (2007) to estimate the amplitude of differential atmospheric refraction of HR 8799 and its exoplanets. We found that this effect caused a shift of $\approx 5-6$ mas of the planet positions along the parallactic angle. The positions of the planets relative to the star are presented in Table 6.1, together with all previously published position measurements. The errorbars were estimated by introducing artificial structures in the form of Gaussians with the same approximate peak flux and the same separations from the star as the real planets but at different angles. The deviations from the known positions were measured for a set of 3 different angles per planet and image. The standard deviations of all measurements for each "fake planet" are the estimated errors, mainly due to residual speckles for the two innermost planets.

6.3 Results and discussion

6.3.1 Astrometric measurements of HR 8799 b, c and d

The projected orbital motions of the two outermost planets b and c are slow (the periods are $P_b \sim 460$ and $P_c \sim 190$ years respectively, Marois et al., 2008), and the nominal mostly circular, face-on orbits are still consistent with observations when our data are added to the previously published astrometry. However, observations in 2008

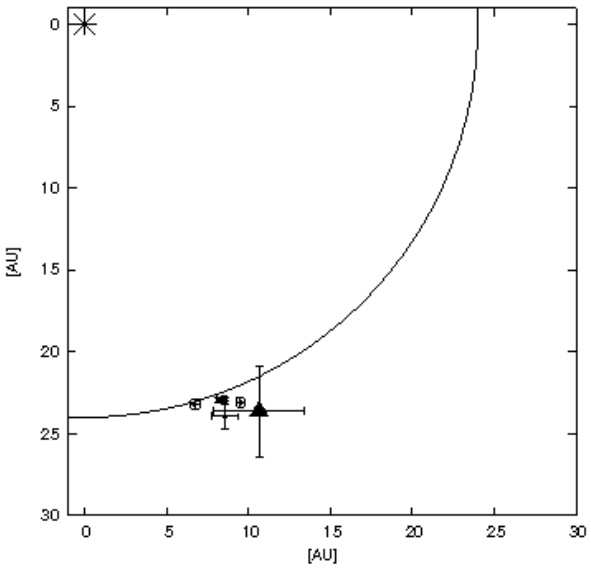

Figure 6.2: Observations of HR 8799 d (see Table 6.1). A distance to the star of 39.4 pc is assumed, and the nominal circular, face-on orbit at 24 AU is overplotted. The star is marked by asterisk at (0,0). The triangle marks our NACO L′ observation.

and 2009 of planet d by Currie et al. (2011) and Hinz et al. (2010)[1] together with our observations suggest that the orbit of this planet might be eccentric and/or inclined. All published astrometric measurements of HR 8799 d are plotted in Fig. 6.2.

6.3.2 Testing the cases of $i = 0$ and $e = 0$ for HR 8799 d

We now want to test if the observed changes in position angle and separation are in agreement with different models. Fabrycky & Murray-Clay (2010) investigated the stability of different possible orbital families for the HR 8799 system. Many of these are for circular ($e = 0$) or face-on ($i = 0$) orbits. We modelled these two simple cases for HR 8799 d from the astrometric observations over a ~ 2 year time baseline. The nominal system mass of 1.5 $M_\odot$ (Marois et al., 2008) was used to compute orbital period from semi-major axis. We did not attempt to fit model orbits that are both inclined and eccentric, since this would add two free parameters and reduce the statistical significance of the result. For the following orbital fits we assumed errors as given in the literature and listed in Table 6.1. We note, however, that while the literature measurements are probably subject to systematic errors of the same order as the ones present in the VLT/NACO set, systematic errors (plate scale, detector orientation) between the different telescopes and instruments used are not necessarily included in these error bars.

[1]The MMT/Clio data by Hinz et al. (2010) were re-reduced by Currie et al. (2011). We have adopted the Currie et al. (2011) astrometry for this analysis.

Table 6.1: Relative positions of the HR 8799 planets.

Epoch	HR 8799b	HR 8799c	HR8799d	HR8799e	Reference
	$\Delta\alpha$, $\Delta\delta$ (arcsec)	$\Delta\alpha$, $\Delta\delta$ (arcsec)	$\Delta\alpha$, $\Delta\delta$ (arcsec)	$\Delta\alpha$, $\Delta\delta$ (arcsec)	
1998.83	1.411±0.009, 0.986±0.009	...	...	...	1
2002.54	1.481±0.023, 0.919±0.017	...	...	...	2
2004.53	1.471±0.005, 0.884±0.005	-0.739±0.005, 0.612±0.005	...	...	3
2007.58	1.522±0.003, 0.815±0.003	-0.672±0.005, 0.674±0.005	-0.170±0.008, -0.589±0.008	...	4
2007.81	1.512±0.005, 0.805±0.005	-0.674±0.005, 0.681±0.005	...	...	3
2008.52	1.527±0.004, 0.799±0.004	-0.658±0.004, 0.701±0.004	-0.208±0.004, -0.582±0.004	...	3
2008.61	1.527±0.002, 0.801±0.002	-0.657±0.002, 0.706±0.002	-0.216±0.002, -0.582±0.002	...	3
2008.71	1.528±0.003, 0.798±0.003	-0.657±0.003, 0.706±0.003	-0.216±0.003, -0.582±0.003	...	3
2008.89	1.532±0.02, 0.796±0.02	-0.654±0.02, 0.700±0.02	-0.217±0.02, -0.608±0.02	...	5
2009.58	...	...	...	-0.299±0.019, -0.217±0.019	6
2009.58	...	...	...	-0.303±0.013, -0.209±0.013	6
2009.62	1.536±0.01, 0.785±0.01	...	...	...	5
2009.70	1.538±0.03, 0.777±0.03	-0.634±0.03, 0.697±0.03	...	...	5
2009.76	1.535±0.02, 0.816±0.02	-0.636±0.04, 0.692±0.04	-0.270±0.07, -0.600±0.07	...	7
2009.77	1.532±0.007, 0.783±0.007	-0.627±0.007, 0.716±0.007	-0.241±0.007, -0.586±0.007	-0.306±0.007, -0.217±0.007	5
2009.83	...	...	...	-0.304±0.010, -0.196±0.010	6
2010.53	...	...	...	-0.325±0.008, -0.173±0.008	6
2010.55	...	...	...	-0.324±0.011, -0.175±0.011	6
2010.83	...	...	...	-0.334±0.010, -0.162±0.010	6

References: (1) Lafrenière et al. (2009); (2) Fukagawa et al. (2009); (3) Marois et al. (2008); (4) Metchev et al. (2009); (5) Currie et al. (2011); (6) Marois et al. (2010); (7) This work. Only statistical errors have been considered in the table.

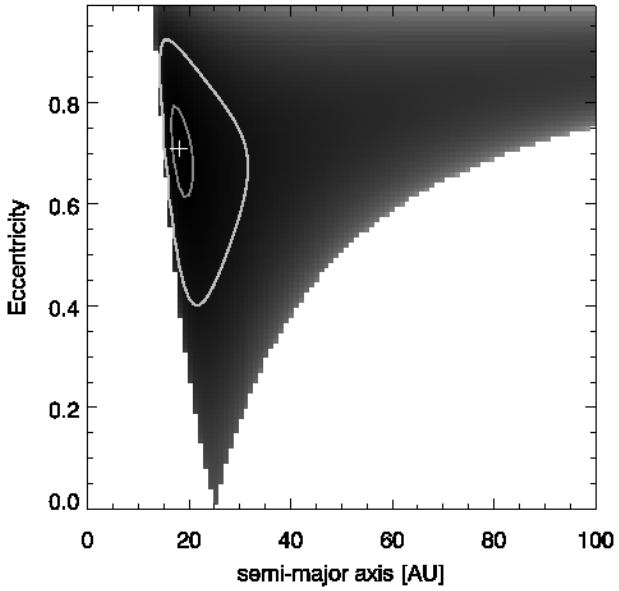

Figure 6.3: χ^2-fit of eccentricity and semi-major axis for the orbit of HR 8799 d assuming $i = 0$ (face-on orbit). The best fit is marked by a cross and the contour lines show the 68.3% and 99.73% confidence regions.

Face-on orbit model for HR 8799 d

Assuming a face-on orbit ($i = 0$) for HR 8799 d, the χ^2 was computed for a grid of 100 semi-major axes and 100 eccentricities and is shown in Fig. 6.3. The cross marks the best fit and the contour lines surround the 68.3% and 99.73% confidence regions. We find that a face-on orbit must have eccentricity $e > 0.4$ to fit the observations with 99.73% confidence. The system should have become dynamically stable at the assumed age of 60 Myr, and one of the stability criteria of Fabrycky & Murray-Clay (2010) is that the orbits of the planets do not cross: $a_d(1 + e_d) < 0.85a_c(1 - e_c)$. Our derived 99.73% confidence minimum eccentricity of $e \approx 0.4$ corresponds to an apastron distance of $r_{ap}(d) \approx 34$ AU for the nominal semi-major axis of planet d at $a_d = 24$ AU, thereby violating the mentioned stability criterion for the nominal orbit of planet c ($a_c = 38$ AU). The stability criterion cannot be fulfilled with respect to both the outer planet c and the inner planet e even if the orbits of both c and e are perfectly circular. A face-on orbit is, with the astrometric data points taken at face value, unstable because of the high eccentricity, and not likely to represent the true orbit of the planet.

Circular orbit model for HR 8799 d

The case of zero eccentricity ($e = 0$) was considered by varying the orbital inclination and semimajor axis in the same way as described above. Figure 4 shows the χ^2 as a function of inclination and semi-major axis for a circular orbit. We find that the inclination is greater than 43° within the 99.73% confidence limits, with a best fit of $i = 63°$ and $a = 36$ AU. This is consistent with the asteroseismic constraints on the stellar rota-

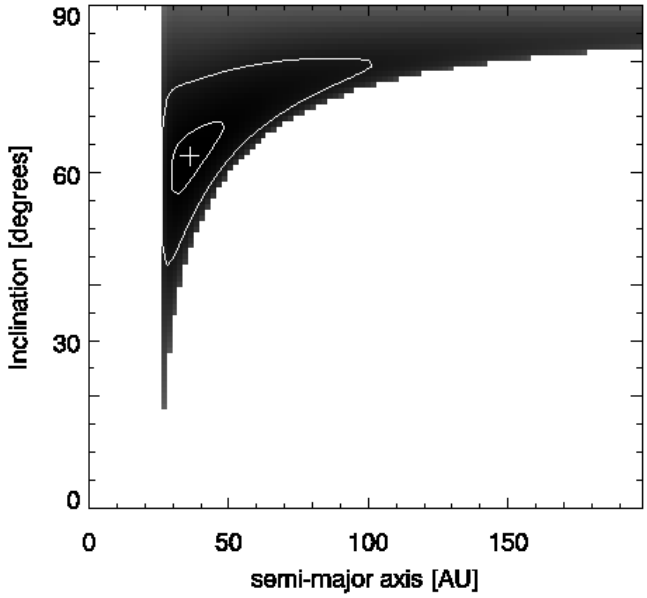

Figure 6.4: χ^2-fit of inclination and semi-major axis for the orbit of HR 8799 d, assuming $e = 0$ (circular orbit). The best fit is marked by a cross, and the contour lines show the 68.3% and 99.73% confidence regions.

tional inclination of $i > 40^o$, with a best fit of $i = 65^o$ derived by Wright et al. (2011). However, this inclination is higher than what has been derived for the orbit of planet b from a 10 year baseline of observations ($i \sim 13 - 23^o$ for a circular orbit, Lafrenière et al., 2009), and also for the debris disk (3σ upper constraint, $i_{disk} < 40^o$, Moro-Martín et al., 2010). The observed configuration with four visible planets around the star at very different position angles supports a low inclination, if the orbits are coplanar. With the astrometric data points taken at face value, the high inclination from the fit with $e = 0$ thus indicates that the orbital eccentricity of HR 8799 d is non-zero, or that the planetary orbits are non-coplanar.

6.4 Conclusions

The initial astrometric analysis performed by Marois et al. (2008) suggested mostly face-on and circular orbits for the three planets of HR 8799 known at the time. The orbital periods of the outermost planets b and c are of the order of hundreds of years, and with our additional astrometric measurements of these planets the orbits are still consistent with the nominal orbits.

Purely circular, face-on and coplanar orbits have been shown to be an unlikely configuration for reasons of dynamical stability (Fabrycky & Murray-Clay, 2010; Goździewski & Migaszewski, 2009; Reidemeister et al., 2009). Our analysis of the orbit of HR 8799 d implies that such a configuration is also inconsistent with the astrometric observations when recent observations by Hinz et al. (2010), Currie et al. (2011) and our NACO

data are included. For a purely face-on orbit, the eccentricity of HR 8799 d is $e > 0.4$ within 99.7% confidence. The system is not stable for such high e and the orbit is hence likely to be inclined with respect to our line of sight. In the case of a purely circular orbit we find that the inclination is $i > 43^{o}$ within the 99.7% confidence limits. While the astrometric data is still limited, this result agrees well with recent constraints on the the stellar rotational inclination (Wright et al., 2011), but not with other measurements of the orbital inclination of planet b and the debris disk. The current astrometric data still allow for different orbital planes for the individual planets and the debris disk (and hence for non-coplanar orbits). Continued astrometric monitoring over a longer time baseline is required in order to put stronger constraints on the orbits of the HR 8799 planets.

CHAPTER 7

SUMMARY AND OUTLOOK

In this thesis, the multiplicity properties of stars and a multiple planet system were investigated with the aim of obtaining a deeper understanding of their physical properties, formation and dynamical evolution. The research includes two high-resolution Lucky Imaging surveys, in which we searched for binary companions to a large number of M dwarfs in the first study, and to the host stars of transiting exoplanets in the other. In addition, a spectroscopic study of four mid- to late-M dwarf binaries from the first survey was presented, and astrometric observations of three directly imaged exoplanets in the HR 8799 system. The efficiency of Lucky Imaging with AstraLux has been demonstrated in the two surveys presented in this thesis. In both surveys, many companion candidates were found within $\approx 1''$ to the target star, thus not detectable in seeing-limited surveys. Some companion candidates were discovered close to the diffraction limit of $\sim 0.1''$.

In the largest M dwarf multiplicity survey to date, we discovered 34 previously unknown companion candidates to M dwarfs, in addition to confirming and providing astrometric and photometric data to 17 known companions. We found that the multiplicity fraction and distributions of mass-ratio and separations are consistent with smaller surveys of the same mass range. However, the large sample allowed for a more detailed look at the distributions, in which we found that these multiplicity properties vary with mass within the M dwarf spectral type. The early type M dwarfs appear more similar to solar-type stars regarding distributions of mass-ratio and separation than the later type M dwarfs, for which these distributions approach the close separations and mass ratios close to unity observed in very low mass- and brown dwarf binaries. The large number of $\sim$ 800 stars observed within the complete AstraLux M dwarf survey will allow for a more detailed look at these trends.

Even though M dwarfs are the most common stars in our neighbourhood[1], many of their physical properties are poorly known, such as the precise mass-luminosity relation. One aim of the AstraLux survey is to find and characterize close, nearby binaries for which astrometric monitoring with AstraLux will provide dynamical masses within a few years time. This will provide a unique opportunity to calibrate the mass-luminosity relation and evolutionary models for very low mass stars and brown dwarfs. We took the first step towards such a calibration by determining the spectral types and looking for signs of chromospheric activity from near-infrared spectra of four close,

[1] 72% of stars within 10 pc from the Sun are M dwarfs,
see `http://www.chara.gsu.edu/RECONS/census.posted.htm`

nearby M dwarf binaries, which are also targets for ongoing astrometric monitoring with AstraLux.

The multiplicity properties of stars that host transiting exoplanets were investigated in another Lucky Imaging survey. We discovered two previously unknown companion candidates to the host stars Wasp-12 and HAT-P-8, and could confirm common proper motion for the previously known binary candidate TrES-4. We found indications that planets belonging to binary/multiple star systems closer than $\sim$ 1200 AU have on average higher mass than planets in single star systems. However, the sample of binary/multiple hosts to transiting exoplanets is still very small, and may not correctly represent the full population of binary/multiple star planets. Future surveys are needed to increase the number of binary/multiple TEP host stars, and to infer how a stellar companion affects formation and migration of exoplanets.

We added to the astrometric measurements of the planets in the HR 8799 system. The multiple-planet configuration allows for putting dynamical constraints on the orbits of the planets. From published astrometry combined with our own observations, and the assumption of dynamically stable orbits, we found that the orbit of HR 8799 d is likely to be inclined with respect to our line of sight, and that the orbit is eccentric and/or non-coplanar with the other planets in the system and the debris disk. This provides observational confirmation to what has been found from models of dynamical system stability. New data obtained with NACO at the VLT in August 2011 will, in addition to L-band spectra of the planets c and d, provide additional astrometric data for these planets.

The AstraLux survey of M dwarf multiplicity has also laid the ground for future work. One may, for instance, also ask the question how the multiplicity properties of low-mass binaries vary with binary separations. In the Lucky Imaging survey, the closest companions were discovered close to the diffraction limit at $\sim 0.1''$, which corresponds to projected separation of $a \approx 3$ AU at the median distance of 30 pc. Hydrodynamical models by Bate (2009) predict a relation between mass-ratio and separation, in which very close systems tend to equal masses, and such a trend has also been observed for early M dwarfs (Delfosse et al., 2004) and solar-type stars (Halbwachs et al., 2003). Ongoing radial velocity spectroscopic observations with FEROS at the ESO/MPG 2.2 m telescope at La Silla aim to investigate multiplicity at closer separations for a subsample of the AstraLux M dwarfs, to, e.g., find closely separated stellar or substellar companions, and investigate the separation dependence of multiplicity fraction and mass-ratio, and how a wide companion affects the properties of a close couple in triple systems.

The low mass of M dwarfs also make them good targets for future astrometric searches for exoplanets. For instance, GRAVITY will be a second generation VLTI instrument, which will combine the light of all four 8 m Unit Telescopes to achieve a positional accuracy of 10μas for targets as faint as $K_s = 16$ mag (Eisenhauer et al., 2008). Nearby M dwarf binaries identified in the AstraLux survey will make good targets for searching for planets of a few Earth-masses to Neptune-masses with GRAVITY (Bergfors et al., 2010b).

Acknowledgements

There are many people who deserve a big Thank You, at the very least, for their contributions and support during these three years. First of all, I am most indebted to my supervisors, Wolfgang Brandner and Thomas Henning, for the great opportunity to come to Heidelberg and MPIA, for their support and for sharing their great knowledge and expertise. A special thanks to Wolfgang for always taking the time to listen and to explain, for teaching me so much and inspiring me to find out more.

I would like to thank Thomas Henning and Ralf Klessen for reviewing my thesis, and Eberhard Grün and Mario Trieloff for kindly agreeing to form part of my examination committee.

I am enormously grateful to my collaborators and many colleagues, for comments and expert advice on observing proposals and papers, for support, and very interesting discussions. A special thank you to Markus Janson, Viki Joergens, Rainer Köhler, Mica Stumpf, Mickaël Bonnefoy and Joe Carson for showing interest and offering to share your expertise.

The many nights of observations would have been much slower without company, so I would like to thank my co-observers. In particular, I want to thank the AstraLux Sur observers Stefan Hippler and Sebastian Daemgen, whose company and expertise have made the observation runs at La Silla into very special occasions.

I cannot thank my loving family enough for the amazing support and for always believing in me. Jessika and Johan, I hope you know you are included here.

For inspiration, for asking difficult questions about the universe, and the constant encouragement: Thank You Ulrik.

Appendix A

The AstraLux Binary M Dwarfs Survey: Tables

Table A.1: Properties of all stars observed 11-16 November 2008.

2MASS ID	Other name	SpT[a]	D [pc][a]	J mag[a]	log [L_x/L_{bol}][a]	Filter	Epoch[b]
J00150240-7250326[c]		M1.0	38	8.62	-3.01	i', z'	2008.86
J00155808-1636578		M4.0	9	8.74	-3.08	z'	2008.87
J00171443-7032021		M0.5	48	9.00	-3.23	i', z'	2008.87
J00213729-4605331	GJ 3029	M3.0	20[d]	8.33	-2.56	z'	2008.87
J00250428-3646176[c]		M2.5	28	8.65	-3.30	i', z'	2008.86
J00275035-3233238[g]		M3.5	28	8.97	-2.75	i', z'	2008.86
J00281434-3227556		M5.0	12	10.12	-2.85	z'	2008.86
J00503319+2449009[c]	GJ 3060A	M3.5	12[d]	7.92	-3.06	i', z'	2008.86
J01025097+1856543		M4.0	13	9.51	-3.24	z'	2008.86
J01071194-1935359[c]		M1.0	30	8.15	-3.13	i', z'	2008.87
J01093874-0710497[c]	HIP 5443	M1.5	38[d]	7.96	-3.70	i', z'	2008.87
J01112343-0525381		M3.5	35	9.47	-2.86	z'	2008.87
J01132817-3821024[c]		M0.5	37	8.49	-3.19	i', z'	2008.88
J01225093-2439505		M3.5	45	10.08	-3.18	z'	2008.88
J01244246-1540454[h]	NLTT 4703	M1.5	27	8.11	-4.01	z'	2008.88
J01365516-0647379[c]	NLTT 5400	M4.0	37	9.70	-2.89	z'	2008.86
J01434512-0602400		M3.5	26	8.77	-3.00	i', z'	2008.86
J01452133-3957204[c]	NLTT 5871	M0.0	32[d]	8.43	-3.81	i', z'	2008.86
J01511997+1324525		M1.5	31	8.56	-3.21	z'	2008.86
J01535076-1459503[c]		M3.0	18	7.94	-3.12	i', z'	2008.86
J02001277-0840516		M2.5	30	8.77	-3.11	i', z'	2008.86
J02002975-0239579[c]		M3.5	48	10.07	-2.95	i', z'	2008.87
J02014384-1017295	NLTT 6782	M4.0	17	10.03	-3.34	z'	2008.87
J02070198-4406444		M5.5	21	11.36	-2.26	z'	2008.87
J02070786-1810077		M4.0	22	10.70	-2.73	z'	2008.87
J02133021-4654505[c]		M4.0	13	9.43	-2.99	i', z'	2008.87
J02155892-0929121[c]		M2.5	26	8.43	-3.11	i', z'	2008.87
J02164119-3059181[i]	GJ 3148 A	M3.5	14[d]	7.99	-3.42	z'	2008.87
J02165488-2322133[c]		M3.5	40	9.79	-2.50	i', z'	2008.87
J02183655+1218579		M2.0	34	8.80	-3.40	z'	2008.87
J02224418-6022476		M4.0	10	8.99	-2.58	z'	2008.87
J02271603-2929263[c]		M3.5	51	10.34	-3.27	i', z'	2008.87
J02303485-1543248	NLTT 8185	M2.5	39	9.29	-3.31	z'	2008.87
J02335984-1811525[c]		M3.0	50	10.09	-2.77	i', z'	2008.87
J02365171-5203036		M2.0	28	8.42	-3.01	z'	2008.87
J02411510-0432177	NLTT 8687	M4.0	11	9.20	-3.64	z'	2008.87
J02411909-5725185[c]		M3.0	45	9.85	-3.15	i', z'	2008.87
J02414730-5259306		M2.5	27	8.48	-2.65	z'	2008.87
J02451431-4344102[c]		M4.0	7	8.06	-3.26	i', z'	2008.88
J02485260-3404246		M4.0	12	9.31	-2.90	z'	2008.88
J02490228-1029220[c]		M2.0	34	8.82	-3.21	i', z'	2008.88
J02492136-4416063		M3.0	45	9.88	-3.30	z'	2008.88
J02543316-5108313		M1.5	34	8.67	-3.33	z'	2008.88
J03033668-2535329[c]	NLTT 9775	M0.0	39[d]	8.00	-3.65	i', z'	2008.88
J03050976-3725058[c]		M2.0	45	9.54	-3.50	i', z'	2008.88
J03100305-2341308	NLTT 10115	M3.5	35	9.41	-3.29	z'	2008.88
J03152341-2821404		M3.5	49	10.25	-2.41	z'	2008.86
J03214689-0640242	GJ 3218	M2.0	16[e]	7.86	-4.74	z'	2008.86
J03244056-3904227		M4.0	40	9.87	-2.27	z'	2008.86
J03271433+2723087	NLTT 10933	M0.5	27[d]	8.64	-3.44	z'	2008.86
J03432333-0819412		M2.5	49	9.86	-3.62	z'	2008.88

Table A.1: continued.

2MASS ID	Other name	SpT[a]	D [pc][a]	J mag[a]	log [L_x/L_{bol}][a]	Filter	Epoch[b]
J03472333-0158195	NLTT 11853	M2.5	16[d]	7.80	-3.14	z'	2008.88
J04071148-2918342[c]		M0.0	51	9.06	-3.16	i', z'	2008.88
J04080543-2731349[c]		M3.5	43	9.89	-3.14	i', z'	2008.88
J04093930-2648489		M1.5	49	9.51	-3.11	z'	2008.88
J04132663-0139211[c]		M4.0	12	9.38	-2.97	i', z'	2008.88
J04141730-0906544		M3.5	37	9.63	-2.70	z'	2008.88
J04175717-3827038		M3.5	36	9.45	-2.91	z'	2008.88
J04213904-7233562		M2.5	50	9.87	-2.97	z'	2008.88
J04240094-5512223		M2.5	48	9.80	-3.26	z'	2008.88
J04241156-2356365		M2.5	24	8.32	-3.70	i', z'	2008.88
J04353618-2527347	NLTT 13598	M3.5	20	8.24	-3.24	i', z'	2008.88
J04365738-1613065		M3.5	30	9.12	-2.63	i', z'	2008.88
J04373746-0229282[c]	GJ 3305	M0.0	23	7.30	-2.71	i', z'	2008.88
J04380252-0556132	NLTT 13666	M4.5	12	9.73	-3.05	z'	2008.88
J04441107-7019247[c]	HD 270712	M1.5	19	7.46	-3.62	i', z'	2008.88
J04522441-1649219	NLTT 14116	M3.0	18	7.74	-3.17	i', z'	2008.88
J05082729-2101444		M5.0	11	9.72	-3.19	i', z'	2008.88
J05241914-1601153[c]		M4.5	8	8.67	-3.14	i', z'	2008.88
J05254166-0909123[c]	NLTT 15049	M3.5	22	8.45	-3.18	i', z'	2008.86
J05332802-4257205		M4.5	6	8.00	-3.13	i', z'	2008.88
J06045215-3433360		M5.0	4	7.74	-2.95	i', z'	2008.88
J06061342-0337082[j]		M2.5	57	10.15	-3.03	i', z'	2008.88
J06161032-1320422[c]		M4.0	31	11.35	-2.32	i', z'	2008.87
J06224133-2737531		M3.5	35	9.43	-3.21	z'	2008.87
J06253604-4815598		M2.5	34	9.10	-3.74	z'	2008.87
J06255610-6003273		M3.5	19	8.09	-2.90	z'	2008.87
J06525392-0524413		M2.5	30	8.71	-3.17	z'	2008.87
J06583980-2021526[c]		M4.0	32	9.40	-3.23	i', z'	2008.87
J07020886-0626206		M2.0	52	9.80	-2.67	z'	2008.87
J07065772-5353463		M0.0	41	8.54	-3.17	z'	2008.87
J07102991-1637350[c]		M2.5	49	9.75	-3.02	i', z'	2008.87
J07105990-5632596[c]		M1.5	52	9.61	-2.43	i', z'	2008.87
J07120447-3048526		M2.5	47	9.71	-3.44	z'	2008.87
J07174710-2558554[c]		M2.0	47	9.53	-3.19	z'	2008.88
J07285137-3014490[c]	GJ 2060	M1.5	16[d]	6.62	-3.04	i', z'	2008.86
J08224744-5726530[c]	LHS 2005	M4.5	8	8.63	-3.14	i', z'	2008.88
J19425324-4406278[c]		M3.5	36	9.43	-3.12	i', z'	2008.87[m]
J19432464-3722108[c]		M3.5	31	9.20	-3.31	i', z'	2008.87
J19513587-3510375		M4.0	8	8.58	-3.23	z'	2008.87
J20100002-2801410[c]		M3.0	26	8.65	-3.16	i', z'	2008.87
J20194981-5816431		M6.0	12	10.66	-2.28	i', z'	2008.87
J20500010-1154092[c]		M3.5	38	9.68	-3.58	i', z'	2008.87
J21010793-4158536		M0.0	52	8.98	-3.46	z'	2008.87
J21073678-1304581		M3.0	27	8.73	-3.16	z'	2008.87
J21103147-2710578[c]		M4.5	16	10.30	-3.00	i', z'	2008.87
J21235271-3908176		M3.5	32	9.33	-3.36	z'	2008.87
J21505366-0553186		M1.0	51	9.38	-3.04	z'	2008.87
J21574119-5100221[k]	GJ 841 A	M2.5	16[d]	6.75	-3.17	i', z'	2008.87
J22114208-2044181		M3.5	39	9.65	-3.18	i', z'	2008.87
J22171899-0848122[c]	GJ 852 A	M4.0	10	9.02	-2.75	i', z'	2008.87
J22174316-1546452		M4.0	22	10.79	-2.83	z'	2008.87

Table A.1: continued.

2MASS ID	Other name	SpT[a]	D [pc][a]	J mag[a]	log $[L_x/L_{bol}]$[a]	Filter	Epoch[b]
J22184009-5326405		M2.5	37	9.24	-3.25	i', z'	2008.87
J22230696-1736250	GJ 4274	M4.0	7[f]	8.24	-3.26	z'	2008.87
J22332264-0936537[c]	GJ 4282	M2.5	26	8.53	-2.96	i', z'	2008.87
J22382974-6522423[c]	GJ 865	M3.5	15[d]	7.27	-3.37	i', z'	2008.87
J22401867-4931045[c]		M5.5	10	9.84	-2.90	i', z'	2008.87
J23115362-4508004[l]	HD 218860B	M3.0	44	9.72	-2.54	i', z'	2008.88
J23131671-4933154		M4.0	15	9.76	-2.68	z'	2008.87
J23261069-7323498		M0.0	46	8.84	-3.09	z'	2008.87
J23285763-6802338		M2.5	38	9.26	-3.07	i', z'	2008.87
J23314492-0244395	GJ 1285	M4.5	11	9.51	-2.76	i', z'	2008.87
J23320018-3917368		M3.0	29	8.90	-2.83	i', z'	2008.88
J23323085-1215513		M0.0	25	7.45	-3.15	z'	2008.87
J23324655-1645081[n]	Gl 897	M2.5	12	6.71	-3.30	z'	2008.87
J23341101-1531012[o]		M0.0	47	8.91	-3.30	z'	2008.87
J23452225-7126505		M3.5	48	10.19	-2.88	z'	2008.87
J23474694-6517249		M1.5	42	9.10	-3.42	z'	2008.87
J23483610-2739385	GJ 4362	M2.5	27	8.58	-3.23	z'	2008.87
J23532520-7056410		M3.5	24	8.68	-3.53	z'	2008.87
J23555512-1321238	NLTT 58441	M2.5	39	9.26	-3.46	z'	2008.87
J23571934-1258406[p]	GJ 4379 B	M3.0	32	9.13	-2.88	z'	2008.87
J23572056-1258487[p]	GJ 4378 A	M4.0	23	8.64	-3.03	z'	2008.87
J23581366-1724338[c]	NLTT 58589	M2.0	28	8.31	-3.14	i', z'	2008.87

[a] Integrated spectral types, J magnitude, and $\log[L_x/L_{bol}]$ from Riaz et al. (2006). Distance is spectroscopic distance from Riaz et al. (2006) if not otherwise indicated. The uncertainty in the spectroscopic distances is 37%.

[b] Epoch of z'-band observations, for which the astrometric properties of the multiple systems are derived.

[c] Binary/multiple system observed with AstraLux, see Tables A.2 and A.3 for properties.

[d] Parallax distance from *Hipparcos* (Perryman & ESA, 1997).

[e] Parallax distance from Reid et al. (2004).

[f] Parallax distance from van Altena et al. (1995).

[g] This is one component of a wide (ρ = 19.9″, epoch 2001) visual double-star system (Mason et al., 2001). The system is therefore not included in the statistical analysis.

[h] This is the secondary component of a wide multiple system with the G-type primary star NLTT 4704. The system is therefore not included in the statistical analysis.

[i] This is the primary component of a *Hipparcos* visual double system, with the secondary component outside our field of view at ρ = 105.0″ (epoch 1991.25, Dommanget & Nys, 2000). The system is not included in the statistical analysis.

[j] The target J06061342-0337082 has spectroscopic distance 57 pc and is therefore not included in the multiplicity analysis.

[k] The star is part of a wide binary system with the white dwarf GJ 841 B (Holberg et al., 2002) and is therefore not included in the statistical analysis.

[l] The star is part of a wide binary system with the primary G8V star HD 218860A (Torres et al., 2006) and is therefore not included in the statistical analysis.

[m] Epoch refers to the i'-band observation, from which astrometric properties were derived.

[n] The star is part of a multiple system in which the K6V star (Torres et al., 2006) Gl 898 is the primary (Dommanget & Nys, 2000). The star is therefore not included in the statistical analysis.

[o]The star is part of a wide binary system (Mason et al., 2001) and is therefore not included in the statistical analysis.

[p]The star is part of a common proper motion system (Mason et al., 2001) and is therefore not included in the statistical analysis.

Table A.2: Photometric and astrometric properties of the observed binary/multiple M dwarfs.

Primary ID (2MASS)	$\Delta z'$	$\Delta i'$	ρ [″]	θ [deg]	New[a] (y/n)	$f_{\rm Mult}$[b]	q[c]
J00150240-7250326	2.13±0.18	1.31±0.14	0.290±0.009	69.1 ± 0.3	y	y	y
J00250428-3646176	2.99±0.21	2.59±0.23	0.605±0.012	242.4 ± 0.3	y	y	y
J00503319+2449009	0.79±0.01	0.94±0.02	1.305±0.002	318.9 ± 0.3	n	y	y
J01071194-1935359	1.16±0.05	0.65±0.03	0.417±0.001	170.0 ± 0.3	y	y	y
J01093874-0710497	1.90±0.01	2.02±0.01	2.554±0.001	74.5 ± 0.3	n	y	y
J01132817-3821024	0.37±0.01	0.22±0.01	1.405±0.003	29.0 ± 0.3	y	y	y
J01365516-0647379	5.07±0.01	...	5.587±0.004	179.9 ± 0.3	y	y	n
J01452133-3957204[d]	2.00±0.10	2.39±0.16	0.943±0.009	130.9 ± 0.3	y	n	n
J01535076-1459503	0.01±0.01	0.13±0.01	2.876±0.001	291.9 ± 0.3	y	y	y
J02002975-0239579	0.75±0.06	0.89±0.05	0.323±0.001	5.9 ± 0.3	y	y	y
J02133021-4654505	0.73±0.27	1.45±0.08	0.135±0.001	124.9 ± 0.3	y	y	y
J02155892-0929121AB	2.62±0.05	2.80±0.05	0.631±0.001	292.2 ± 0.3	y	y	y
J02155892-0929121AC	4.99±0.05	5.52±0.10	3.509±0.002	299.3 ± 0.3	y	y	y
J02165488-2322133	0.91±0.01	0.92±0.01	4.369±0.001	314.1 ± 0.3	n	y	y
J02271603-2929263	1.67±0.02	1.77±0.01	1.939±0.001	236.8 ± 0.3	y	y	y
J02335984-1811525	0.29±0.01	-1.02±0.05	0.854±0.001	48.9 ± 0.3	y	y	y
J02411909-5725185	1.31±0.02	1.47±0.02	1.526±0.001	287.1 ± 0.3	y	y	y
J02451431-4344102	1.12±0.07	0.87±0.03	0.257±0.001	214.6 ± 0.3	y	y	y
J02490228-1029220AB	1.33±0.06	1.42±0.12	0.481±0.006	209.5 ± 0.3	y	y	y
J02490228-1029220AC	1.39±0.06	1.49±0.11	0.622±0.012	210.7 ± 0.3	y	y	y
J03033668-2535329	5.14±0.06	3.69±0.16	0.834±0.005	7.6 ± 0.3	n	y	y
J03050976-3725058	0.93±0.10	0.94±0.07	0.242±0.004	53.7 ± 0.3	y	y	y
J04071148-2918342[d]	0.70±0.05	0.48±0.20	0.295±0.001	44.4 ± 0.3	y	n	n
J04080543-2731349	1.78±0.06	1.00±0.10	0.181±0.005	218.1 ± 0.3	y	y	y
J04132663-0139211	0.95±0.02	-0.45±0.03	0.771±0.001	358.8 ± 0.3	n	y	y
J04373746-0229282[d,f]	1.39±0.16	2.57±0.05	0.221±0.002	20.5 ± 0.3	n	n	n
J04441107-7019247	0.79±0.01	1.09±0.01	2.654±0.001	157.5 ± 0.3	n	y	y
J05241914-1601153	0.36±0.03	0.43±0.01	0.639±0.001	69.1 ± 0.3	y	y	y
J05254166-0909123	0.45±0.07	0.53±0.09	0.616±0.004	58.8 ± 0.3	n	y	y
J06161032-1320422	1.94±0.12	1.40±0.23	0.194±0.008	170.6 ± 0.3	y	y	y
J06583980-2021526AB	0.25±0.01	0.33±0.01	1.420±0.001	199.0 ± 0.3	y	y	y
J06583980-2021526AC[e]	5.89±0.02	...	6.992±0.002	263.3 ± 0.3	y	n	n
J06583980-2021526AD	6.91±0.03	...	5.149±0.001	253.9 ± 0.3	y	y	n
J07102991-1637350AB	0.46±0.09	0.64±0.05	0.568±0.001	354.9 ± 0.3	y	y	y
J07102991-1637350AC	5.26±0.46	...	2.021±0.008	287.6 ± 0.3	y	y	y
J07105990-5632596	1.83±0.07	4.17±0.07	1.120±0.006	309.8 ± 0.3	y	y	y
J07174710-2558554[f]	6.35±0.04	...	5.332±0.002	126.8 ± 0.3	y	n	n
J07285137-3014490	1.29±0.11	1.50±0.18	0.485±0.002	169.9 ± 0.3	n	y	y
J08224744-5726530AB	4.47±0.04	5.32±0.05	0.648±0.002	128.7 ± 0.3	y	y	n
J08224744-5726530AC[e]	1.83±0.04	...	8.429±0.001	26.1 ± 0.3	n	n	n
J19425324-4406278	...	1.39±0.11	0.836±0.002	349.8 ± 0.3	y	y	y
J19432464-3722108	2.84±0.08	2.89±0.07	1.623±0.004	303.7 ± 0.3	y	y	y
J20100002-2801410	0.80±0.04	0.75±0.03	0.615±0.001	280.4 ± 0.3	y	y	y
J20500010-1154092	1.04±0.22	1.17±0.20	0.486±0.046	348.3 ± 0.3	y	y	y
J21103147-2710578[e]	1.07±0.01	1.20±0.01	9.501±0.003	313.2 ± 0.3	n[g]	n	n
J22171899-0848122AB[e]	0.62±0.03	0.74±0.01	7.954±0.001	213.2 ± 0.3	n	n	n
J22171899-0848122AC[e]	3.77±0.03	...	7.794±0.003	220.1 ± 0.3	n	n	n
J22332264-0936537	0.12±0.01	0.65±0.05	1.421±0.028	98.6 ± 0.3	n	y	y
J22382974-6522423	0.23±0.01	0.20±0.02	0.842±0.001	155.8 ± 0.3	n	y	y
J22401867-4931045	0.14±0.01	0.16±0.01	4.039±0.001	41.0 ± 0.3	n	y	y

Table A.2: continued.

Primary ID (2MASS)	$\Delta z'$	$\Delta i'$	ρ [″]	θ [deg]	New[a] (y/n)	f_{Mult}[b]	q[c]
J23581366-1724338	0.01±0.01	0.03±0.01	1.989±0.001	355.7 ± 0.3	n	y	y

[a]Companion discovered in this survey (y) or previously known (n).

[b]Included in multiplicity fraction analysis (y/n).

[c]Included in mass-ratio analysis (y/n).

[d]The primary star spectral type is earlier than M0 (see Table A.3). The system is therefore not included in the statistical analysis.

[e]The survey is not complete for component separations greater than 6″ and these stars are therefore not included in the statistical analysis.

[f]Our primary star is the secondary star in a known binary system in which the primary star is of spectral type F. The system is therefore not included in the statistical analysis.

[g]The companion is the star 2MASS J21103096-2710513. Although the position of the secondary star is previously known, we could find no references to the couple as a common proper motion pair.

Table A.3: Individual spectral types and projected separations.

2MASS ID	Primary SpT	Secondary SpT	Separation [A.U.]
J00150240-7250326	M0.5	M3.5	11.0 ± 4.1
J00250428-3646176	M2.5	M5.0	16.9 ± 6.3
J00503319+2449009	M3.5	M4.5	15.7 ± 1.3
J01071194-1935359	M0.5	M2.5	12.5 ± 4.6
J01093874-0710497	M1.0	M4.0	97.1 ± 13.0
J01132817-3821024	M0.0	M1.0	52.0 ± 19.2
J01365516-0647379	M4.0	>L0	206.7 ± 76.5
J01452133-3957204[a]	K7.5	M3.5	30.2 ± 2.2
J01535076-1459503	M3.0	M3.0	51.8 ± 19.2
J02002975-0239579	M3.5	M4.5	15.5 ± 5.7
J02133021-4654505	M4.0	M5.0	1.8 ± 0.7
J02155892-0929121AB	M2.5	M5.0	16.4 ± 6.1
J02155892-0929121AC	M2.5	M8.0	91.2 ± 33.8
J02165488-2322133	M3.5	M4.5	174.8 ± 64.7
J02271603-2929263	M3.5	M5.0	98.9 ± 36.6
J02335984-1811525	M3.0	M3.5	42.7 ± 15.8
J02411909-5725185	M2.5	M4.0	68.7 ± 25.4
J02451431-4344102	M4.0	M4.5	1.8 ± 0.7
J02490228-1029220AB	M1.5	M3.5	16.4 ± 6.1
J02490228-1029220AC	M1.5	M3.5	21.2 ± 7.8
J03033668-2535329	M0.0	M6.0	32.5 ± 2.8
J03050976-3725058	M1.5	M3.0	10.9 ± 4.0
J04071148-2918342[a]	K7.5	M1.0	15.1 ± 5.6
J04080543-2731349	M3.5	M4.5	7.8 ± 2.9
J04132663-0139211	M4.0	M4.0	9.3 ± 3.4
J04373746-0229282[a,c]	K7.5	M3.0	5.1 ± 1.9
J04441107-7019247	M1.0	M2.5	50.4 ± 18.7
J05241914-1601153	M4.5	M5.0	5.1 ± 1.9
J05254166-0909123	M3.5	M4.0	13.6 ± 5.0
J06161032-1320422	M3.5	M5.0	6.0 ± 2.2
J06583980-2021526AB	M4.0	M4.0	45.4 ± 16.8
J06583980-2021526AC[b]	M4.0	>L0	223.7 ± 82.8
J06583980-2021526AD	M4.0	>L0	164.8 ± 61.0
J07102991-1637350AB	M2.5	M3.0	27.8 ± 10.3
J07102991-1637350AC	M2.5	M9.0	99.0 ± 36.6
J07105990-5632596	M1.5	M4.5	58.2 ± 21.6
J07174710-2558554[c]	M2.0	>L0	250.6 ± 92.7
J07285137-3014490	M1.0	M3.0	7.8 ± 0.3
J08224744-5726530AB	M4.5	>L0	5.2 ± 1.9
J08224744-5726530AC[b]	M4.5	M6.0	67.4 ± 25.0
J19425324-4406278	M3.5	M4.5	30.1 ± 11.1
J19432464-3722108	M3.5	M6.0	50.3 ± 18.6
J20100002-2801410	M2.5	M3.5	16.0 ± 5.9
J20500010-1154092	M3.5	M4.5	18.5 ± 7.1
J21103147-2710578[b]	M4.5	M5.5	152.0 ± 56.3
J22171899-0848122AB[b]	M4.0	M4.5	79.5 ± 29.4
J22171899-0848122AC[b]	M4.0	M8.5	77.9 ± 28.8
J22332264-0936537	M2.5	M3.0	37.0 ± 13.7
J22382974-6522423	M3.5	M3.5	12.6 ± 1.2
J22401867-4931045	M5.5	M5.5	40.4 ± 14.9

Table A.3: continued.

2MASS ID	Primary SpT	Secondary SpT	Separation [A.U.]
J23581366-1724338	M2.0	M2.0	55.7 ± 20.6

[a]The primary star spectral type is earlier than M0. The system is therefore not included in the statistical analysis.

[b]The survey is not complete for component separations greater than 6″ and these stars are therefore not included in the statistical analysis (see Table A.2).

[c]Our primary star is the secondary star in a known binary system in which the primary star is of spectral type F. The system is therefore not included in the statistical analysis.

Table A.4: Separations and position angles for previously known multiple systems.

2MASS ID	ρ [″]	θ [deg]	Epoch	Ref.
J00503319+2449009	1.0	315	1960	1
	2.080	316.0	1991.25	2
	1.648	317.12	2002.64	3
	1.305	318.9	2008.86	4
J01093874-0710497	2.680	77.0	1991.25	2
	2.554	74.5	2008.87	4
J02165488-2322133	4.3	315	1998.67	5
	4.369	314.1	2008.87	4
J04132663-0139211	0.79	217.11	1998.9	6
	0.771	358.8/178.8	2008.88	4
J04373746-0229282	0.225	195	2003.05	7
	0.093	189.5	2004.95	7
	0.221	20.5	2008.88	4
J04441107-7019247	2.3	174	1990	8
	2.654	157.5	2008.88	4
J05254166-0909123	0.537	69.40	2005.78	9
	0.616	58.8	2008.86	4
J07285137-3014490	0.175	143.71	2002.83	9
	0.485	169.9	2008.86	4
J08224744-5726530	8.6	23	1999.99	5
	8.429	26.1	2008.88	4
J21103147-2710578	9.4	313	1998.59	5
	9.501	313.2	2008.87	4
J22171899-0848122AB	7.8	213	1998.79	5
	7.95	213.2	2008.87	4
J22171899-0848122BC	0.978	305.8	2001.60	10
	0.97	316.7	2008.87	4
J22332264-0936537	1.66	272.25	1997.6	6
	1.571	279.73	2005.44	9
	1.421	98.6/278.6	2008.87	4
J22382974-6522423	0.770	16	1991.25	2
	0.842	155.8	2008.87	4
J22401867-4931045	4.2	40	1999.72	5
	4.039	41.0	2008.87	4
J23581366-1724338	1.904	355.3	2005.54	9

Table A.4: continued.

2MASS ID	ρ [″]	θ [deg]	Epoch	Ref.
	1.989	355.7	2008.87	4

References: (1)Dommanget & Nys (2002); (2)Perryman & ESA (1997); (3)Strigachev & Lampens (2004); (4)This work; (5)Cutri et al. (2003); (6)McCarthy et al. (2001); (7)Kasper et al. (2007); (8)Mason et al. (2001); (9)Daemgen et al. (2007); (10)Beuzit et al. (2004).

APPENDIX B

NOTES ON INDIVIDUAL M DWARF BINARIES AND MULTIPLE SYSTEMS

Table A.4 summarizes our measured angular separations and position angles, and published results for previously known components.

J00503319+2449009 This star, also known as GJ 3060A or NLTT 2805, is a flare star (Norton et al., 2007) with a known stellar companion, NLTT 2804. The Catalog of Components of Double & Multiple Stars (CCDM, Dommanget & Nys, 2002) provides the astrometric measurements ρ = 1.0″ and θ = 315° for epoch 1960. *Hipparcos* observations provide positions of the two components of ρ = 2.080″ and θ = 316° (epoch 1991.25, Perryman & ESA, 1997). Strigachev & Lampens (2004) present photometric and astrometric observations of visual double stars and for this binary estimate the angular separation to be ρ = 1.648″ and the position angle θ = 317.12° (epoch 2002.64). Our measured separation is ρ = 1.305″ and position angle θ = 318.9°, indicating orbital motion.

J01093874-0710497 This is a high proper motion star with $\mu_{\rm RA}$=-235.5 mas/yr and $\mu_{\rm DEC}$=-351.6 mas/yr. Also known as HIP 5443, it is a *Hipparcos* double star (Perryman & ESA, 1997) with separation ρ = 2.7″ and position angle θ = 77° (epoch 1991.25). We measure the separation ρ = 2.554″ and position angle θ = 74.5°, hence both components form a common proper motion pair. The small change in separation and position angle in the more than 15 years that have passed between the *Hipparcos* and our measurements can be attributed to orbital motion.

J01365516-0647379 The primary star is a high proper motion star for which Shkolnik et al. (2009) estimated an age between 25 and 300 Myr. Because of its faint magnitude, the secondary star could not be seen at the time of observation but only after additional analysis. The star therefore ended up partly outside the field of view in the i'-band observation and we present only z'-band data in this paper.

J02165488-2322133 In 2MASS PSC (Cutri et al., 2003), we find the star J02165465-2322103 at separation ρ = 4.3″ and position angle θ = 315° from our primary (epoch 1998.67), which corresponds well to our measured separation ρ = 4.369″ and position angle θ = 314.1°.

J02335984-1811525 In this double system, the B component is brighter than the A component in i'-band. Since the i' and z' band observations were performed on different nights, the unusual $i' - z'$ colour might indicate that the star is variable or possibly of T Tauri-type. We tentatively assign spectral types M3±1 + M3.5±1 to the stars, but further investigation of this couple is necessary to determine their characteristics.

J02490228-1029220 The B and C components of this triple star are close, ρ_{BC} = 0.145″ corresponding to 4.93 AU.

J03033668-2535329 The primary star is a high proper motion star also known as NLTT 9775. We measure a separation ρ = 0.834″ between the two companions. A possible candidate for the secondary star is the high proper motion star LTT 1453, which has J2000 coordinates RA=03h 03m 36.6s, Dec= −25°35′33″, at an angular separation of 1.42″ from our primary star. Frankowski et al. (2007) studied the binary content of the *Hipparcos* catalogue, listing the primary star as a candidate proper motion binary.

J04080543-2731349 The images in both i'- and z'-band of this binary are affected by "fake tripling". The real B component and the fake triple are equally bright in z'-band but unequal in i'. This means that, although unlikely, the true position angle might be systematically incorrect by 180°.

J04132663-0139211 This binary system was discovered by McCarthy et al. (2001), with a separation ρ = 0.79″ and position angle θ = 217.11° (epoch 1998.9). We measure ρ = 0.771″ and θ = 358.8°, indicating significant orbital motion between observations. In our observations, the B component is brighter than the A component in i'-band. Since the i' and z' band observations were performed on different nights, the unusual $i' - z'$ colour may indicate that the star is variable or possibly of T Tauri-type. If our secondary star is the primary star of McCarthy et al. (2001), the position angle is instead ρ = 178.8°. We tentatively assign the stars spectral types M4 ± 1 + M4 ± 1, but further investigation of this double system is needed to determine its character.

J04373746-0229282 The primary star is also known as GJ 3305, a member of the young β Pictoris moving group (Zuckerman et al., 2001), which has an estimated age of 12 Myr (Shkolnik et al., 2009). The faint close companion that we see was discovered by Kasper et al. (2007) in their L-band NACO imaging of young, nearby stars in search of substellar companions. Kasper et al. (2007) present NACO K-band data from the ESO/ST-ECF Science Archive with which they determine the separation ρ = 0.225″ and position angle θ = 195° (epoch 2003.05), and their obtained L-band data for which ρ = 0.093″ and position angle θ = 189.5° (epoch 2004.95), and the proper motion combined points to a bound companion in a highly eccentric orbit. Our observations are affected by the stellar companion ghost image at 180° discussed in Sect. 3.2.2, which may cause uncertainty in the true position angle. However, the assumed position at ρ = 0.221″ and θ = 20.5° is consistent with physical companionship, and with the non-detection of the secondary companion by Daemgen et al. (2007) (epoch 2005.74) indicates that the orbit has a high inclination, i.e., is seen close to edge-on.

Feigelson et al. (2006) agree with Zuckerman et al. (2001) and conclude from the proper motion and stellar activity that GJ 3305 is part of a wide binary system (ρ = 66″, or ∼ 2000 AU at 30 pc) with the F0 star 51 Eri. Since the primary star is then of earlier spectral type than M0, the system is not included in our statistical analysis.

J04441107-7019247 This is a previously known visual binary, also known as HD 270712. Mason et al. (2001) provides the astrometric measurements ρ = 2.3″ and θ = 174° for epoch 1990. We measure ρ = 2.654″ and θ = 157.5°, indicating orbital motion.

J05254166-0909123 This high proper motion binary (NLTT 15049) was discovered by Daemgen et al. (2007), at a separation of ρ = 0.537″ and position angle θ = 69.40° (epoch 2005.78). We assign spectral types M3.5+M4 to the couple, consistent with the spectral types of Daemgen et al. (2007). We find a separation ρ = 0.616″ and position angle θ = 58.8°, indicating significant orbital motion. Shkolnik et al.

(2009) estimates the age of the stars to between 35 and 300 Myr.

J06583980-2021526 This possibly quadruple system consists of one close M4+M4 pair and two more distant suspected L dwarfs. The two faintest components (C and D) are separated from the brightest star by 5.15″ and 6.99″, respectively, and had not been discovered at the time of observation. They therefore ended up outside the FoV in i'-band. The separation between components A and B is ρ_{AB} = 1.420″, and the two faint stars C and D are separated by ρ_{CD} = 2.093″ with position angle θ_{CD} = 107.3°. The separation between the primary star and the C component is greater than our completeness limit, and the component is therefore not included in the statistical analysis.

J07102991-1637350 The tertiary companion is too faint in i' for accurate photometry and astrometry. We therefore present only z'-band data in this paper.

J07105990-5632596 We obtain different spectral types for the secondary star in i' and z' ($SpT_{i'} \approx$ M5.5, $SpT_{z'} \approx$ M4). Since we did not observe the stars in both filters on the same night, the brightness of either companion might have changed from one observation to the next if the stars are variable. We tentatively assign the secondary spectral type M4.5±1.

J07174710-2558554 Our primary star is also known as CD-25 4322B, the secondary star in a wide double system with CD-25 4322. Our wide but faint secondary component is not, however, found in any catalogue. The star CD-25 4322 is an F-star (F0/F3V, Dommanget & Nys, 2002; Perryman & ESA, 1997) and not within our field of view (CCDM separation ρ = 12.4″, epoch 1897, Dommanget & Nys, 2002). Because of the faintness of our secondary companion, it was not detected at the time of observation and not observed in i'. Since our primary star is the secondary star in a system with an F-star primary, it is not included in the statistical analysis.

J07285137-3014490 This is a known binary system also known as GJ 2060 (Zuckerman et al., 2004), which was concluded by Allen & Reid (2008) to probably be part of a quadruple system with another close, equal mass M dwarf binary at a separation of ρ = 67.2″. GJ 2060 is a likely member of the ∼50 Myr old AB Dor association (Zuckerman et al., 2004). We obtain spectral types M1+M3, while Daemgen et al. (2007) find spectral types M0.5+M1.5. The primary star is a known variable star (V372 Pup). Daemgen et al. (2007) determine the binary separation and position angle to be ρ = 0.175″ and θ = 143.71° (epoch 2002.83), while we find ρ = 0.485″ and θ = 169.9°, indicating significant orbital motion.

J08224744-5726530 The primary star of this triple system is also known as LHS 2005, a high proper motion star. Our separation and position angle for the tertiary component, which is also known as LHS 2004, is ρ = 8.429″ and θ = 26.1°. This is consistent with data from the 2MASS PSC (Cutri et al., 2003) for the star J08224787-5726451 with a separation 8.6″ and position angle θ = 23° (epoch 1999.99) and is indicative of orbital motion. LHS 2004 and LHS 2005 form a known common proper motion pair. The close secondary was not previously known. The wide companion was noticed at the time of observation and fitted into the field of view by placing the primary star in the corner of the detector for the z'-band observations. The wide companion is outside the field of view in i'-band. Since the C component separation from the primary is greater than 6″, it is not included in the statistical analysis.

J19425324-4406278 The secondary star is previously unknown. Only i'-band images could be used in our analysis since the secondary star was too faint in z'. The position angle, separation, and individual spectral types are therefore obtained from the i'-band observation.

J21103147-2710578 The companion is J21103096-2710513 at a 2MASS PSC dis-

tance of 9.4″ and position angle $\theta = 313^{o}$ (epoch 1998.59, Cutri et al., 2003). We find a separation $\rho = 9.50''$, which is greater than our limits for completeness. The system is therefore not included in the statistical analysis.

J22171899-0848122 This is a known visual binary system where the primary star (also known as V* FG Aqr or GJ 852A) and the secondary star (J22171870-0848186, or GJ 852B) are both flare stars (Gershberg et al., 1999). The tertiary companion, close to our secondary star GJ 852B at $\rho_{BC} = 0.97''$ and $\theta_{BC} = 316.7^{o}$, was discovered by Beuzit et al. (2004) at $\rho = 0.978''$ and $\theta = 305.8^{o}$ (epoch 2001.60), hence the system shows orbital motion. The C component is in our observations too faint to be resolved in i' band. Photometric measurements in i' for the B component therefore include the very faint flux from the close C component. The 2MASS PSC (Cutri et al., 2003) infer a proximity of 7.8″ and position angle of $\theta = 213^{o}$ (epoch 1998.79), relating the positions of GJ 852 A and GJ 852 B. Our measured separation between these stars is $\rho = 7.95''$ and position angle $\theta = 213.2^{o}$.

J22332264-0936537 Also known as GJ 4282, this flare star was discovered to be a binary by McCarthy et al. (2001), who derived a separation of $\rho = 1.66''$ and position angle $\theta = 272.25^{o}$ for epoch 1997.6. Daemgen et al. (2007) observed a separation of $\rho = 1.571''$ and $\theta = 279.73^{o}$ for epoch 2005.44. We find $\rho = 1.421''$ and $\theta = 98.6^{o}$, a separation that agrees with previous observations but at a position angle that is clearly inconsistent with the previous measurements by Daemgen et al. (2007) and McCarthy et al. (2001). With an estimated orbital period of approximately 380 years, we need to assume that our primary star (the eastern component) is actually the secondary star of Daemgen et al. (2007) and McCarthy et al. (2001), and our revised position angle is in that case $\theta = 278.6^{o}$, indicating orbital motion. Since in our observations the eastern star is slightly brighter than the western component, one or both of the stars might be variable, causing the discrepancy in position angle between our observations and the observations by McCarthy et al. (2001) and Daemgen et al. (2007). We assign the stars spectral types M2.5 and M3, respectively, in agreement with Daemgen et al. (2007)(M3+M3) and Shkolnik et al. (2009) (eastern component M2.5, western component M2.6). Shkolnik et al. (2009) estimate the age of the system to be 20-150 Myr.

J22382974-6522423 This flare star, which is also known as GJ 865, was identified by Montes et al. (2001) as a possible member of the $\sim$ 600 Myr Hyades supercluster. The star GJ 865 is part of a known triple system. We observed the two close components, separated by $\rho = 0.842''$, which is in agreement with the separation $\rho = 0.770''$ and position angle $\theta = 16^{o}$ found by Perryman & ESA (1997) for epoch 1991.25. The third companion is outside our field of view, with a separation from our primary star of $\rho = 30.4''$ (epoch 1974, Dommanget & Nys, 2002). While we could not find the spectral type of this companion in literature, the V magnitudes of the three companions differ only slightly ($V_A = 12.0, V_B = 12.1, V_C = 12.3$, Dommanget & Nys, 2002, where the close components are B and C) and we assume that the third component is also an M star. We therefore include this system in the binary statistics as an M dwarf binary/multiple system.

J22401867-4931045 This couple of high proper motion stars (Lépine, 2005) are also known as LSR J22403-4931W (our primary star) and LSR J22403-4931E located at RA = 22h 40m 18.96s, Dec = $-49^{o}31'01.4''$ (J2000). Cutri et al. (2003) found $\rho = 4.2''$ and $\theta = 40^{o}$ for epoch 1999.72. We measure $\rho = 4.039''$ and $\theta = 41.0^{o}$.

J23581366-1724338 The binary character of this high proper motion star, also known as NLTT 58589, was discovered by Daemgen et al. (2007), who derived the same individual spectral types M2+M2, as we do. We find $\rho = 1.989''$, in good agree-

ment with the Daemgen et al. (2007) separation ρ = 1.904″ for epoch 2005.54, although our measured position angle θ = 355.7° disagrees with the Daemgen et al. (2007) result of θ = 265.30° by 90°. Reanalysis of the Gemini data by Daemgen et al. yields a position angle of 355.3°, which is in good agreement with the AstraLux Sur measurement and indicates some orbital motion. Shkolnik et al. (2009) determine individual spectral types M1.9 (north)+M1.9 (south) and an age of 20-150 Myr for the system.

J23534173-6556543: We also observed this star, which is the secondary star in a widely separated G0 V+M1 V system, and its primary. The primary is HIP 117815 and the secondary is CPD-66 3810B. Our separation of ρ = 12.3″ at θ = 112.2° is in good agreement with Eggenberger et al. (2007) (ρ = 12.14″, θ = 112.37°, epoch 2005.70) for this bound system. This system was only observed in z'-band and is not included in any statistical analysis in this paper because the primary star is a G star.

Appendix C

The AstraLux Binary TEP Hosts Survey: Tables

Table C.1: System parameters for transiting exoplanet systems in January 2011. The table lists planet name, planet mass, planet radius, orbital period, semimajor axis, stellar mass, metallicity, effective temperature, stellar velocity amplitude, orbital inclination and eccentricity.

Planet name	m_p [M_J]	r_p [R_J]	P [days]	a [AU]	M_s [$M_\odot$]	R_s [$R_\odot$]	[Fe/H] [dex]	T_{eff} [K]	K_* [ms^{-1}]	i [^{o}]	e	Ref.
CoRoT-1 b	1.030	1.490	1.5089	0.0254	0.950	1.110	-0.30	5950	188.0	85.10	0	1
CoRoT-10 b	2.750	0.970	13.240	0.1055	0.890	0.790	0.26	5075	301.0	88.55	0.530	2
CoRoT-11 b	2.330	1.430	2.9943	0.0436	1.270	1.370	-0.03	6440	280.0	83.17	0	3
CoRoT-12 b	0.916	1.450	2.8280	0.0402	1.078	1.116	0.16	5675	125.5	85.48	0.070	4
CoRoT-13 b	1.308	0.885	4.0351	0.0510	1.090	1.010	0.01	5945	157.8	88.02	0	5
CoRoT-14 b	7.600	1.090	1.5121	0.0270	1.130	1.210	0.05	6035	1230.0	79.60	0	6
CoRoT-16 b	0.500	0.813	5.3534	...	...	0.810	...	...	...	85.82	0	7
CoRoT-17 b	2.450	1.470	3.7681	...	...	2.000	...	...	...	77.47	0	7
CoRoT-2 b	3.310	1.465	1.7429	0.0281	0.970	0.902	...	5625	563.0	87.84	0	8
CoRoT-3 b	21.660	1.010	4.2568	0.0570	1.370	1.560	-0.02	6740	2190.0	85.90	0	9
CoRoT-4 b	0.720	1.190	9.2020	0.0900	1.160	1.170	0.05	6190	63.0	90.00	0	10,11
CoRoT-5 b	0.467	1.388	4.0378	0.0495	1.000	1.186	-0.25	6100	59.1	85.83	0.090	12
CoRoT-6 b	2.960	1.166	8.8865	0.0855	1.055	1.025	-0.20	6090	280.0	89.07	0.100	13
CoRoT-7 b	0.015	0.150	0.8535	0.0172	0.930	0.870	0.03	5275	3.3	80.10	0.070	14,15
CoRoT-8 b	0.220	0.570	6.2122	0.0630	0.880	0.770	0.30	5080	26.0	88.40	0	16
CoRoT-9 b	0.840	1.050	95.273	0.4070	0.990	0.940	-0.01	5625	38.0	89.99	0.110	17
GJ 1214 b	0.020	0.245	1.5804	0.0140	0.153	0.210	0.39	2949	12.2	88.62	0.270	18,19,20
GJ 436 b	0.074	0.365	2.6438	0.0289	0.459	0.454	-0.03	3500	18.3	86.43	0.150	21,22
HAT-P-1 b	0.524	1.217	4.4652	0.0554	1.134	1.112	0.13	5975	59.3	86.25	0	21
HAT-P-11 b	0.081	0.452	4.8878	0.0530	0.810	0.750	0.31	4780	11.6	88.55	0.198	23,24
HAT-P-12 b	0.211	0.959	3.2130	0.0384	0.733	0.701	-0.29	4650	35.8	89.07	0	25
HAT-P-13 b	0.850	1.280	2.9162	0.0426	1.220	1.560	0.43	5638	106.1	83.40	0.021	26,27,28
HAT-P-14 b	2.200	1.200	4.6276	0.0594	1.386	1.468	0.11	6600	222.0	83.50	0.095	29,30
HAT-P-15 b	1.946	1.072	10.863	0.0964	1.013	1.080	0.22	5568	180.6	89.10	0.190	31
HAT-P-16 b	4.193	1.289	2.7759	0.0413	1.218	1.237	0.17	6158	531.1	86.60	0.036	32
HAT-P-17 b	0.530	1.010	10.338	0.0882	0.857	0.837	...	5246	58.4	89.20	0.346	33
HAT-P-18 b	0.197	0.995	5.5080	0.0559	0.770	0.749	0.10	4803	27.1	88.80	0.084	34
HAT-P-19 b	0.292	1.132	4.0087	0.0466	0.842	0.820	0.23	4990	42.0	88.20	0.067	34
HAT-P-2 b	8.740	1.190	5.6334	0.0674	1.279	1.680	0.14	6290	983.9	85.90	0.517	21,35
HAT-P-20 b	7.246	0.867	2.8753	0.0361	0.756	0.694	0.35	4595	1246.0	86.80	0.015	36
HAT-P-21 b	4.063	1.024	4.1244	0.0494	0.947	1.105	0.01	5588	548.3	87.20	0.228	36
HAT-P-22 b	2.147	1.080	3.2122	0.0414	0.916	1.040	0.24	5302	313.3	86.90	0.016	36
HAT-P-23 b	2.090	1.368	1.2128	0.0232	1.130	1.203	0.15	5905	368.5	85.10	0.106	36
HAT-P-24 b	0.685	1.242	3.3552	0.0465	1.191	1.317	-0.16	6373	83.0	88.60	0.067	37
HAT-P-25 b	0.567	1.190	3.6528	0.0466	1.010	0.959	0.31	5500	74.3	87.60	0.032	38
HAT-P-26 b	0.059	0.565	4.2345	0.0479	0.816	0.788	-0.04	5079	8.5	88.60	0.124	39
HAT-P-27 b[1]	0.6600	1.038	3.0395	0.0403	0.945	0.898	0.29	5300	96.1	84.70	0.078	40
HAT-P-3 b	0.599	0.890	2.8997	0.0389	0.936	0.824	0.27	5185	89.1	87.24	0	41
HAT-P-4 b	0.680	1.270	3.0565	0.0446	1.260	1.590	0.24	5860	81.1	89.67	0	42,43
HAT-P-5 b	1.060	1.260	2.7884	0.0408	1.160	1.167	0.24	5960	138.0	86.75	0	44
HAT-P-6 b	1.057	1.330	3.8529	0.0524	1.290	1.460	-0.13	6570	115.5	85.51	0	45
HAT-P-7 b	1.800	1.421	2.2047	0.0379	1.490	1.920	0.26	6350	213.2	84.10	0	46
HAT-P-8 b	1.520	1.500	3.0763	0.0487	1.280	1.580	0.01	6200	153.1	87.50	0	47
HAT-P-9 b	0.780	1.400	3.9228	0.0530	1.280	1.320	0.12	6350	84.7	86.50	0	48
HD 149026 b	0.356	0.610	2.8758	0.0429	1.271	1.290	0.36	6143	43.3	88.00	0	21
HD 17156 b	3.191	1.095	21.216	0.1623	1.275	1.508	0.24	6079	274.2	86.49	0.677	49,50
HD 189733 b	1.150	1.151	2.2185	0.0314	0.840	0.752	-0.03	5050	200.6	85.78	0	21
HD 209458 b	0.714	1.380	3.5247	0.0475	1.148	1.162	0.02	6117	85.1	86.59	0.014	21,51
HD 80606 b	3.940	0.980	111.43	0.4490	0.970	0.978	0.43	5645	474.0	89.32	0.933	52,53
Kepler-10 b	0.014	0.127	0.8374	0.0168	0.895	1.056	-0.15	5627	3.3	84.40	0	54
Kepler-4 b	0.077	0.357	3.2134	0.0456	1.223	1.487	0.17	5857	9.3	89.76	0	55
Kepler-5 b	2.114	1.431	3.5484	0.0506	1.374	1.793	0.04	6297	227.5	86.30	0	56
Kepler-6 b	0.669	1.323	3.2342	0.0457	1.209	1.391	0.34	5647	80.9	86.80	0	57
Kepler-7 b	0.433	1.478	4.8855	0.0622	1.347	1.843	0.11	5933	42.9	86.50	0	58

[1]Also known as WASP-40 b

Table C.1: continued.

Planet name	m_p [M_J]	r_p [R_J]	P [days]	a [AU]	M_s [$M_\odot$]	R_s [$R_\odot$]	[Fe/H] [dex]	T_{eff} [K]	K_* [ms^{-1}]	i [^{o}]	e	Ref.
Kepler-8 b	0.603	1.419	3.5225	0.0483	1.213	1.486	-0.06	6213	68.4	84.07	0	59
Kepler-9 b	0.252	0.842	19.243	0.1400	1.000	1.100	0.17	5722	...	88.55	0	60
Kepler-9 c	0.171	0.823	38.908	0.2250	1.000	1.100	0.17	5722	...	88.12	0	60
Kepler-9 d	0.022	0.147	1.5928	0.0273	1.000	1.100	0.17	5722	...	...	0	60,61
KOI-428 b	2.200	1.170	6.8734	0.0800	1.480	2.130	0.10	6510	179.0	89.70	0	62
Lupus-TR-3 b	0.810	0.890	3.9140	0.0464	0.870	0.820	...	5000	114.0	88.30	0	63
OGLE-TR-10 b	0.680	1.720	3.1012	0.0452	1.277	1.520	0.28	6075	80.9	83.87	0	21
OGLE-TR-111 b	0.540	1.077	4.0144	0.0465	0.833	0.842	0.19	5044	78.0	88.11	0	21
OGLE-TR-113 b	1.240	1.110	1.4324	0.0228	0.768	0.780	0.15	4804	267.0	87.70	0	21
OGLE-TR-132 b	1.170	1.250	1.6898	0.0303	1.297	1.370	0.37	6210	167.0	83.30	0	21
OGLE-TR-182 b	1.060	1.470	3.9791	0.0521	1.187	1.530	0.37	5924	120.0	84.30	0	21
OGLE-TR-211 b	0.750	1.262	3.6772	0.0511	1.312	1.560	0.11	6325	82.0	88.00	0	21
OGLE-TR-56 b	1.300	1.200	1.2119	0.0239	1.233	1.260	0.25	6119	212.0	79.40	0	21
OGLE2-TR-L9 b	4.340	1.614	2.4855	0.0404	1.420	1.503	-0.05	6933	510.0	82.07	0	21
Qatar-1 b	1.090	1.164	1.4200	0.0234	0.850	0.823	0.20	4861	218.0	83.47	0	64
SWEEPS-04	3.800	0.810	4.2000	0.0550	1.240	1.180	...	...	...	...	0	65
SWEEPS-11	9.700	1.130	1.7960	0.0300	1.100	1.450	...	...	...	...	0	65
TrES-1	0.761	1.099	3.0300	0.0395	0.892	0.818	0.06	5226	115.2	88.67	0	21
TrES-2	1.253	1.261	2.4706	0.0364	1.049	1.002	0.06	5795	181.3	83.80	0	21
TrES-3	1.910	1.305	1.3061	0.0228	0.929	0.818	-0.19	5650	369.0	82.07	0	21
TrES-4	0.877	1.810	3.5539	0.0497	1.292	1.920	0.14	6200	97.4	81.53	0	21
WASP-1 b	0.860	1.484	2.5199	0.0390	1.243	1.455	0.23	6110	111.0	88.00	0	21
WASP-10 b	3.160	1.067	3.0927	0.0378	0.752	0.703	0.03	4675	553.1	88.81	0.057	21,66
WASP-11 b[2]	0.4870	1.005	3.7224	0.0435	0.830	0.790	0.13	4980	74.5	88.60	0	67
WASP-12 b	1.410	1.790	1.0914	0.0229	1.350	1.570	0.30	6300	226	83.10	0.049	68
WASP-13 b	0.460	1.210	4.3529	0.0527	1.030	1.340	0.00	5826	55.7	86.90	0	69
WASP-14 b	7.341	1.281	2.2437	0.0360	1.211	1.306	0.00	6475	993.0	84.32	0.091	70
WASP-15 b	0.542	1.428	3.7520	0.0499	1.180	1.477	-0.17	6300	63.4	85.50	0	71
WASP-16 b	0.855	1.008	3.1186	0.0421	1.022	0.946	0.01	5550	116.7	85.22	0	72
WASP-17 b	0.490	1.740	3.7354	0.0510	1.200	1.380	-0.25	6550	56.9	87.80	0.129	73
WASP-18 b	10.29	1.158	0.9414	0.0203	1.256	1.222	0.00	6400	1816.9	85.00	0.009	21,74
WASP-19 b	1.168	1.386	0.7888	0.0166	0.970	0.990	0.02	5500	257.0	79.40	0.005	75,76
WASP-2 b	0.847	1.043	2.1522	0.0303	0.803	0.807	-0.08	5150	153.6	84.81	0	21
WASP-21 b	0.300	1.070	4.3224	0.0520	1.010	1.060	-0.40	5800	37.2	88.75	0	77
WASP-22 b	0.560	1.120	3.5326	0.0468	1.100	1.130	-0.05	6000	70.0	89.20	0.023	78
WASP-23 b	0.870	0.960	2.9400	...	...	...	...	...	...	...	0	79
WASP-24 b	1.071	1.300	2.3412	0.0365	1.184	1.331	0.07	6075	145.2	83.64	0	80
WASP-25 b	0.580	1.220	3.7648	0.0473	1.000	0.920	-0.05	5750	75.5	88.00	0	81
WASP-26 b	1.020	1.320	2.7566	0.0400	1.120	1.340	-0.02	5950	135.5	82.50	0	82
WASP-28 b	0.910	1.120	3.4088	0.0455	1.080	1.050	-0.29	6100	116.2	89.10	0.046	83
WASP-29 b	0.244	0.792	3.9227	0.0457	0.825	0.808	0.11	4800	35.6	88.80	0.030	84
WASP-3 b	2.060	1.454	1.8468	0.0319	1.260	1.377	0.00	6400	290.5	84.10	0	21
WASP-31 b	0.478	1.537	3.4059	0.0466	1.161	1.241	-0.19	6203	58.2	84.54	0	85
WASP-32 b	3.600	1.180	2.7186	0.0394	1.100	1.110	-0.13	6100	487.0	85.30	0.018	86
WASP-33 b	4.590	1.438	1.2198	0.0256	1.501	1.457	0.10	7435	590.0	87.70	0	87,88
WASP-34 b	0.590	1.220	4.3176	0.0524	1.010	0.930	-0.02	5700	72.1	85.2	0.038	89
WASP-36 b	2.400	1.400	1.5000	...	...	...	...	...	...	...	0	7
WASP-37 b	1.800	1.160	3.5774	0.0446	0.925	1.003	-0.40	5800	250.7	88.82	0	90
WASP-38 b	2.691	1.094	6.8718	0.0752	1.203	1.331	-0.12	6150	253.9	89.69	0.0314	91
WASP-4 b	1.237	1.357	1.3382	0.0231	0.914	0.905	-0.03	5500	242.1	89.00	0	21
WASP-41 b	0.920	1.210	3.0523	0.0403	0.940	0.910	-0.08	5450	135.0	87.30	0	92
WASP-5 b	1.565	1.164	1.6284	0.0271	1.004	1.077	0.09	5700	268.7	85.80	0	21
WASP-6 b	0.503	1.224	3.3610	0.0421	0.880	0.870	-0.20	5450	74.3	88.47	0.054	93
WASP-7 b	0.960	1.330	4.9546	0.0617	1.276	1.432	0.00	6400	97.0	87.03	0	94,95
WASP-8 b	2.244	1.038	8.1587	0.0801	1.030	0.945	0.17	5600	222.23	88.55	0.310	96
XO-1 b	0.924	1.206	3.9415	0.0494	1.037	0.942	0.02	5750	116.0	89.06	0	21
XO-2 b	0.555	0.992	2.6158	0.0365	0.946	0.970	0.45	5340	85.0	88.80	0	21

[2]Also known as HAT-P-10 b

Table C.1: continued.

Planet name	m_p [M_J]	r_p [R_J]	P [days]	a [AU]	M_s [$M_\odot$]	R_s [$R_\odot$]	[Fe/H] [dex]	T_{eff} [K]	K_* [ms^{-1}]	i [^{o}]	e	Ref.
XO-3 b	11.83	1.248	3.1915	0.0453	1.206	1.409	-0.18	6429	1488.0	83.89	0.260	21
XO-4 b	1.521	1.290	4.1250	0.0548	1.285	1.530	-0.04	6397	163.0	89.90	0	21
XO-5 b	1.084	1.089	4.1877	0.0494	0.914	1.065	0.05	5370	144.9	87.04	0	21

References: (1) Barge et al. (2008); (2) Bonomo et al. (2010); (3) Gandolfi et al. (2010); (4) Gillon et al. (2010); (5) Cabrera et al. (2010); (6) Tingley et al. (2011); (7) The Extrasolar Planets Encyclopaedia, http://exoplanet.eu; (8) Alonso et al. (2008); (9) Deleuil et al. (2008); (10) Moutou et al. (2008); (11) Aigrain et al. (2008); (12) Rauer et al. (2009); (13) Fridlund et al. (2010); (14) Léger et al. (2009); (15) Queloz et al. (2009); (16) Bordé et al. (2010); (17) Deeg et al. (2010); (18) Charbonneau et al. (2009); (19) Kundurthy et al. (2010); (20) Berta et al. (2010); (21) Southworth (2010) and references therein; (22) Deming et al. (2007); (23) Bakos et al. (2010b); (24) Dittmann et al. (2009); (25) Hartman et al. (2009); (26) Bakos et al. (2009a); (27) Winn et al. (2010); (28) Szabó et al. (2010); (29) Torres et al. (2010); (30) Simpson et al. (2010); (31) Kovács et al. (2010); (32) Buchhave et al. (2010); (33) Howard et al. (2010); (34) Hartman et al. (2011); (35) Pál et al. (2010); (36) Bakos et al. (2010a); (37) Kipping et al. (2010); (38) Quinn et al. (2010); (39) Hartman et al. (2010); (40) Béky et al. (2011); (41) Torres et al. (2007); (42) Kovács et al. (2007); (43) Christiansen et al. (2011); (44) Bakos et al. (2007b); (45) Noyes et al. (2008); (46) Pál (2009); (47) Latham et al. (2009); (48) Shporer et al. (2009); (49) Nutzman et al. (2011); (50) Winn et al. (2009); (51) Kipping (2008); (52) Naef et al. (2001); (53) Pont et al. (2009); (54) Batalha et al. (2011); (55) Borucki et al. (2010); (56) Koch et al. (2010); (57) Dunham et al. (2010); (58) Latham et al. (2010); (59) Jenkins et al. (2010); (60) Holman et al. (2010); (61) Torres et al. (2011); (62) Santerne et al. (2011); (63) Weldrake et al. (2008); (64) Alsubai et al. (2010); (65) Sahu et al. (2006); (66) Christian et al. (2009); (67) Bakos et al. (2009b); (68) Hebb et al. (2009); (69) Skillen et al. (2009); (70) Joshi et al. (2009); (71) West et al. (2009); (72) Lister et al. (2009); (73) Anderson et al. (2010b); (74) Nymeyer et al. (2010); (75) Hellier et al. (2011); (76) Hebb et al. (2010); (77) Bouchy et al. (2010); (78) Maxted et al. (2010c); (79) Hellier et al. (2010a); (80) Street et al. (2010); (81) Enoch et al. (2011); (82) Smalley et al. (2010); (83) The Extrasolar Planets Encyclopaedia, http://exoplanet.eu; (84) Hellier et al. (2010b); (85) Anderson et al. (2010a); (86) Maxted et al. (2010a); (87) Cameron et al. (2010); (88) Smith et al. (2011); (89) Smalley et al. (2011); (90) Simpson et al. (2011); (91) Barros et al. (2011); (92) Maxted et al. (2010b); (93) Gillon et al. (2009); (94) Hellier et al. (2009); (95) Southworth et al. (2011); (96) Queloz et al. (2010).

Table C.2: Calculated system parameters. Surface gravity, Safronov number and equilibrium temperature for all known transiting exoplanet systems in January 2011.

Planet name	log g_p	θ	T_{eq}
CoRoT-1 b	3.06	0.037	1896
CoRoT-10 b	3.86	0.671	670
CoRoT-11 b	3.45	0.112	1740
CoRoT-12 b	3.04	0.047	1441
CoRoT-13 b	3.62	0.138	1276
CoRoT-14 b	4.21	0.333	1948
CoRoT-16 b	...	...	...
CoRoT-17 b	...	...	...
CoRoT-2 b	3.58	0.131	1537
CoRoT-3 b	4.72	1.782	1700
CoRoT-4 b	3.10	0.094	1076
CoRoT-5 b	2.77	0.033	1440
CoRoT-6 b	3.73	0.411	1017
CoRoT-7 b	3.22	0.004	1809
CoRoT-8 b	3.21	0.055	856
CoRoT-9 b	3.28	0.657	412
GJ 1214 b	2.89	0.015	551
GJ 436 b	3.14	0.025	669
HAT-P-1 b	2.94	0.042	1291
HAT-P-11 b	3.01	0.023	867
HAT-P-12 b	2.76	0.023	958
HAT-P-13 b	3.11	0.046	1645
HAT-P-14 b	3.57	0.157	1582
HAT-P-15 b	3.62	0.345	899
HAT-P-16 b	3.80	0.220	1625
HAT-P-17 b	3.11	0.108	779
HAT-P-18 b	2.69	0.029	848
HAT-P-19 b	2.75	0.029	1009
HAT-P-2 b	4.18	0.773	1514
HAT-P-20 b	4.38	0.797	971
HAT-P-21 b	3.98	0.413	1274
HAT-P-22 b	3.66	0.179	1281
HAT-P-23 b	3.44	0.063	2050
HAT-P-24 b	3.04	0.043	1635
HAT-P-25 b	3.00	0.044	1203
HAT-P-26 b	2.66	0.012	993
HAT-P-27/WASP-40 b	3.18	0.054	1206
HAT-P-3 b	3.27	0.056	1150
HAT-P-4 b	3.02	0.038	1687
HAT-P-5 b	3.22	0.059	1538
HAT-P-6 b	3.17	0.064	1673
HAT-P-7 b	3.34	0.064	2179
HAT-P-8 b	3.22	0.077	1703
HAT-P-9 b	2.99	0.046	1528
HD 149026 b	3.37	0.039	1624
HD 17156 b	3.82	0.741	893
HD 189733 b	3.33	0.075	1191
HD 209458 b	2.96	0.043	1459
HD 80606 b	4.01	3.717	402
Kepler-10 b	3.35	0.004	2148
Kepler-4 b	3.18	0.016	1613
Kepler-5 b	3.41	0.109	1807
Kepler-6 b	2.98	0.038	1503
Kepler-7 b	2.70	0.027	1557
Kepler-8 b	2.86	0.034	1662
Kepler-9 b	...	0.084	773
Kepler-9 c	...	0.093	610
Kepler-9 d	...	0.008	1751

Table C.2: continued.

Planet name	log g_p	θ	T_{eq}
KOI-428 b	3.59	0.203	1620
Lupus-TR-3 b	3.40	0.097	1013
OGLE-TR-10 b	2.76	0.028	1699
OGLE-TR-111 b	3.06	0.056	1035
OGLE-TR-113 b	3.40	0.066	1355
OGLE-TR-132 b	3.27	0.044	2014
OGLE-TR-182 b	3.08	0.063	1549
OGLE-TR-211 b	3.07	0.046	1686
OGLE-TR-56 b	3.35	0.042	2144
OGLE2-TR-L9 b	3.62	0.153	2039
Qatar-1 b	3.30	0.052	1389
SWEEPS-04	...	0.416	...
SWEEPS-11	...	0.468	...
TrES-1	3.19	0.061	1147
TrES-2	3.29	0.069	1467
TrES-3	3.44	0.072	1631
TrES-4	2.82	0.037	1859
WASP-1 b	2.99	0.036	1800
WASP-10 b	3.85	0.297	972
WASP-11/HAT-P-10 b	3.08	0.051	1023
WASP-12 b	3.04	0.027	2515
WASP-13 b	2.89	0.039	1416
WASP-14 b	4.05	0.340	1880
WASP-15 b	2.82	0.032	1653
WASP-16 b	3.32	0.070	1268
WASP-17 b	2.62	0.024	1643
WASP-18 b	4.28	0.287	2392
WASP-19 b	3.18	0.029	2051
WASP-2 b	3.29	0.061	1281
WASP-21 b	2.81	0.029	1263
WASP-22 b	3.04	0.042	1421
WASP-23 b	...	...	...
WASP-24 b	3.20	0.051	1768
WASP-25 b	2.98	0.045	1223
WASP-26 b	3.16	0.055	1660
WASP-28 b	3.25	0.068	1413
WASP-29 b	2.98	0.034	973
WASP-3 b	3.38	0.072	2028
WASP-31 b	2.70	0.025	1544
WASP-32 b	3.80	0.218	1561
WASP-33 b	3.69	0.109	2705
WASP-34 b	2.99	0.050	1158
WASP-36 b	...	...	...
WASP-37 b	3.52	0.149	1326
WASP-38 b	3.75	0.307	1247
WASP-4 b	3.22	0.046	1661
WASP-41 b	3.19	0.065	1249
WASP-5 b	3.46	0.073	1731
WASP-6 b	2.92	0.039	1194
WASP-7 b	3.13	0.070	1487
WASP-8 b	3.69	0.336	927
XO-1 b	3.20	0.073	1210
XO-2 b	3.15	0.043	1328
XO-3 b	4.28	0.711	1729
XO-4 b	3.36	0.100	1630
XO-5 b	3.36	0.107	1202

BIBLIOGRAPHY

Abuter, R., Schreiber, J., Eisenhauer, F., et al. 2006, New A Rev, 50, 398

Aigrain, S., Collier Cameron, A., Ollivier, M., et al. 2008, A&A, 488, L43

Alibert, Y., Mordasini, C., Benz, W., & Winisdoerffer, C. 2005, A&A, 434, 343

Allen, P. R. 2007, ApJ, 668, 492

Allen, P. R. & Reid, I. N. 2008, AJ, 135, 2024

Allers, K. N., Jaffe, D. T., Luhman, K. L., et al. 2007, ApJ, 657, 511

Alonso, R., Auvergne, M., Baglin, A., et al. 2008, A&A, 482, L21

Alsubai, K. A., Parley, N. R., Bramich, D. M., et al. 2010, ArXiv e-prints

Anderson, D. R., Collier Cameron, A., Hellier, C., et al. 2010a, ArXiv e-prints

Anderson, D. R., Hellier, C., Gillon, M., et al. 2010b, ApJ, 709, 159

Armitage, P. J., Clarke, C. J., & Tout, C. A. 1999, MNRAS, 304, 425

Artymowicz, P. & Lubow, S. H. 1994, ApJ, 421, 651

Baglin, A., Auvergne, M., Boisnard, L., et al. 2006, in COSPAR, Plenary Meeting, Vol. 36, 36th COSPAR Scientific Assembly, 3749–+

Bakos, G., Noyes, R. W., Kovács, G., et al. 2004, PASP, 116, 266

Bakos, G. Á., Hartman, J., Torres, G., et al. 2010a, ArXiv e-prints

Bakos, G. Á., Howard, A. W., Noyes, R. W., et al. 2009a, ApJ, 707, 446

Bakos, G. Á., Noyes, R. W., Kovács, G., et al. 2007a, ApJ, 656, 552

Bakos, G. Á., Pál, A., Latham, D. W., Noyes, R. W., & Stefanik, R. P. 2006, ApJL, 641, L57

Bakos, G. Á., Pál, A., Torres, G., et al. 2009b, ApJ, 696, 1950

Bakos, G. Á., Shporer, A., Pál, A., et al. 2007b, ApJL, 671, L173

Bakos, G. Á., Torres, G., Pál, A., et al. 2010b, ApJ, 710, 1724

Baraffe, I., Chabrier, G., Barman, T. S., Allard, F., & Hauschildt, P. H. 2003, A&A, 402, 701

Barge, P., Baglin, A., Auvergne, M., et al. 2008, A&A, 482, L17

Barros, S. C. C., Faedi, F., Collier Cameron, A., et al. 2011, A&A, 525, A54+

Batalha, N. M., Borucki, W. J., Bryson, S. T., et al. 2011, ApJ, 729, 27

Bate, M. R. 2009, MNRAS, 392, 590

Bate, M. R., Bonnell, I. A., & Bromm, V. 2002, MNRAS, 332, L65

Béky, B., Bakos, G. Á., Hartman, J., et al. 2011, ArXiv e-prints

Bergfors, C., Brandner, W., Janson, M., et al. 2010a, A&A, 520, A54+

Bergfors, C., Brandner, W., Janson, M., Köhler, R., & Henning, T. 2011, A&A, 528, A134+

Bergfors, C., Brandner, W., Janson, M., et al. 2010b, in Astronomical Society of the Pacific Conference Series, Vol. 430, Pathways Towards Habitable Planets, ed. V. Coudé Du Foresto, D. M. Gelino, & I. Ribas, 405–+

Berta, Z. K., Charbonneau, D., Bean, J., et al. 2010, ArXiv e-prints

Beuzit, J., Ségransan, D., Forveille, T., et al. 2004, A&A, 425, 997

Bodenheimer, P., Burkert, A., Klein, R. I., & Boss, A. P. 2000, Protostars and Planets IV, 675

Bonnefoy, M., Chauvin, G., Dumas, C., et al. 2009, A&A, 506, 799

Bonnell, I. A., Larson, R. B., & Zinnecker, H. 2007, Protostars and Planets V, 149

Bonnet, H., Abuter, R., Baker, A., et al. 2004, The Messenger, 117, 17

Bonomo, A. S., Santerne, A., Alonso, R., et al. 2010, A&A, 520, A65+

Bordé, P., Bouchy, F., Deleuil, M., et al. 2010, A&A, 520, A66+

Borucki, W. J., Koch, D., Basri, G., et al. 2010, Science, 327, 977

Boss, A. P. 1997, Science, 276, 1836

Boss, A. P. 2006, ApJ, 641, 1148

Boss, A. P., Basri, G., Kumar, S. S., et al. 2003, in IAU Symposium, Vol. 211, Brown Dwarfs, ed. E. Martín, 529–+

Bouchy, F., Hebb, L., Skillen, I., et al. 2010, A&A, 519, A98+

Bouwman, J., Lawson, W. A., Dominik, C., et al. 2006, ApJL, 653, L57

Bouy, H., Brandner, W., Martín, E. L., et al. 2003, AJ, 126, 1526

Brandner, W. & Köhler, R. 1998, ApJL, 499, L79+

Brandner, W., Zinnecker, H., Alcalá, J. M., et al. 2000, AJ, 120, 950

Buchhave, L. A., Bakos, G. Á., Hartman, J. D., et al. 2010, ApJ, 720, 1118

Burgasser, A. J., Kirkpatrick, J. D., Reid, I. N., et al. 2003, ApJ, 586, 512

Burgasser, A. J., Reid, I. N., Siegler, N., et al. 2007, in Protostars and Planets V, ed. B. Reipurth, D. Jewitt, & K. Keil, 427–441

Burrows, A., Marley, M., Hubbard, W. B., et al. 1997, ApJ, 491, 856

Burrows, A., Sudarsky, D., & Hubeny, I. 2006, ApJ, 640, 1063

Butler, R. P., Marcy, G. W., Williams, E., Hauser, H., & Shirts, P. 1997, ApJL, 474, L115+

Cabrera, J., Bruntt, H., Ollivier, M., et al. 2010, A&A, 522, A110+

Cameron, A. C., Bouchy, F., Hébrard, G., et al. 2007, MNRAS, 375, 951

Cameron, A. C., Guenther, E., Smalley, B., et al. 2010, MNRAS, 407, 507

Chabrier, G., Baraffe, I., Selsis, F., et al. 2007, Protostars and Planets V, 623

Charbonneau, D., Berta, Z. K., Irwin, J., et al. 2009, Nature, 462, 891

Chatterjee, S., Ford, E. B., Matsumura, S., & Rasio, F. A. 2008, ApJ, 686, 580

Christian, D. J., Gibson, N. P., Simpson, E. K., et al. 2009, MNRAS, 392, 1585

Christiansen, J. L., Ballard, S., Charbonneau, D., et al. 2011, ApJ, 726, 94

Clarke, C. J. 2007, in IAU Symposium, Vol. 240, IAU Symposium, ed. W. I. Hartkopf, E. F. Guinan, & P. Harmanec, 337–346

Close, L. M., Siegler, N., Freed, M., & Biller, B. 2003, ApJ, 587, 407

Cochran, W. D., Hatzes, A. P., Butler, R. P., & Marcy, G. W. 1997, ApJ, 483, 457

Covey, K. R., Ivezić, Ž., Schlegel, D., et al. 2007, AJ, 134, 2398

Currie, T., Burrows, A. S., Itoh, Y., et al. 2011, ArXiv e-prints

Cushing, M. C., Rayner, J. T., & Vacca, W. D. 2005, ApJ, 623, 1115

Cutri, R. M., Skrutskie, M. F., van Dyk, S., et al. 2003, 2MASS All Sky Catalog of point sources., ed. R. M. Cutri, M. F. Skrutskie, S. van Dyk, C. A. Beichman, J. M. Carpenter, T. Chester, L. Cambresy, T. Evans, J. Fowler, J. Gizis, E. Howard, J. Huchra, T. Jarrett, E. L. Kopan, J. D. Kirkpatrick, R. M. Light, K. A. Marsh, H. McCallon, S. Schneider, R. Stiening, M. Sykes, M. Weinberg, W. A. Wheaton, S. Wheelock, & N. Zacarias

Daemgen, S., Hormuth, F., Brandner, W., et al. 2009, A&A, 498, 567

Daemgen, S., Siegler, N., Reid, I. N., & Close, L. M. 2007, ApJ, 654, 558

Deeg, H. J., Moutou, C., Erikson, A., et al. 2010, Nature, 464, 384

Deleuil, M., Deeg, H. J., Alonso, R., et al. 2008, A&A, 491, 889

Delfosse, X., Beuzit, J.-L., Marchal, L., et al. 2004, in Astronomical Society of the Pacific Conference Series, Vol. 318, Spectroscopically and Spatially Resolving the Components of the Close Binary Stars, ed. R. W. Hilditch, H. Hensberge, & K. Pavlovski, 166–174

Deming, D., Harrington, J., Laughlin, G., et al. 2007, ApJL, 667, L199

Desidera, S. & Barbieri, M. 2007, A&A, 462, 345

Dittmann, J. A., Close, L. M., Green, E. M., Scuderi, L. J., & Males, J. R. 2009, ApJL, 699, L48

Dodson-Robinson, S. E., Veras, D., Ford, E. B., & Beichman, C. A. 2009, ApJ, 707, 79

Dommanget, J. & Nys, O. 2000, VizieR Online Data Catalog, 1260, 0

Dommanget, J. & Nys, O. 2002, VizieR Online Data Catalog, 1274, 0

Duchêne, G. 2010, ApJL, 709, L114

Duchêne, G., Delgado-Donate, E., Haisch, Jr., K. E., Loinard, L., & Rodríguez, L. F. 2007, Protostars and Planets V, 379

Dumas, C., Terrile, R. J., Brown, R. H., Schneider, G., & Smith, B. A. 2001, AJ, 121, 1163

Dunham, E. W., Borucki, W. J., Koch, D. G., et al. 2010, ApJL, 713, L136

Dupuy, T. J., Liu, M. C., & Ireland, M. J. 2009, ApJ, 692, 729

Duquennoy, A. & Mayor, M. 1991, A&A, 248, 485

Durisen, R. H., Boss, A. P., Mayer, L., et al. 2007, Protostars and Planets V, 607

Eggenberger, A., Udry, S., Chauvin, G., et al. 2008, in Astronomical Society of the Pacific Conference Series, Vol. 398, Extreme Solar Systems, ed. D. Fischer, F. A. Rasio, S. E. Thorsett, & A. Wolszczan, 179–+

Eggenberger, A., Udry, S., Chauvin, G., et al. 2007, A&A, 474, 273

Eggenberger, A., Udry, S., Chauvin, G., et al. 2011, ArXiv e-prints

Eggenberger, A., Udry, S., & Mayor, M. 2003, in Astronomical Society of the Pacific Conference Series, Vol. 294, Scientific Frontiers in Research on Extrasolar Planets, ed. D. Deming & S. Seager, 43–46

Eggenberger, A., Udry, S., & Mayor, M. 2004, A&A, 417, 353

Eisenhauer, F., Abuter, R., Bickert, K., et al. 2003, in Presented at the Society of Photo-Optical Instrumentation Engineers (SPIE) Conference, Vol. 4841, Society of Photo-Optical Instrumentation Engineers (SPIE) Conference Series, ed. M. Iye & A. F. M. Moorwood, 1548–1561

Eisenhauer, F., Perrin, G., Brandner, W., et al. 2008, in Society of Photo-Optical Instrumentation Engineers (SPIE) Conference Series, Vol. 7013, Society of Photo-Optical Instrumentation Engineers (SPIE) Conference Series

Enoch, B., Cameron, A. C., Anderson, D. R., et al. 2011, MNRAS, 410, 1631

Fabrycky, D. C. & Murray-Clay, R. A. 2010, ApJ, 710, 1408

Feigelson, E. D., Lawson, W. A., Stark, M., Townsley, L., & Garmire, G. P. 2006, AJ, 131, 1730

Femenía, B., Rebolo, R., Pérez-Prieto, J. A., et al. 2011, MNRAS, 413, 1524

Fischer, D. A. & Marcy, G. W. 1992, ApJ, 396, 178

Fossati, L., Bagnulo, S., Elmasli, A., et al. 2010, ApJ, 720, 872

Frankowski, A., Jancart, S., & Jorissen, A. 2007, A&A, 464, 377

Fressin, F., Guillot, T., & Nesta, L. 2009, A&A, 504, 605

Fridlund, M., Hébrard, G., Alonso, R., et al. 2010, A&A, 512, A14+

Fried, D. L. 1978, Journal of the Optical Society of America (1917-1983), 68, 1651

Fruchter, A. S. & Hook, R. N. 2002, PASP, 114, 144

Fukagawa, M., Itoh, Y., Tamura, M., et al. 2009, ApJL, 696, L1

Gammie, C. F. 2001, ApJ, 553, 174

Gandolfi, D., Hébrard, G., Alonso, R., et al. 2010, A&A, 524, A55+

Gershberg, R. E., Katsova, M. M., Lovkaya, M. N., Terebizh, A. V., & Shakhovskaya, N. I. 1999, A&AS, 139, 555

Ghez, A. M., Neugebauer, G., & Matthews, K. 1993, AJ, 106, 2005

Gillon, M., Anderson, D. R., Triaud, A. H. M. J., et al. 2009, A&A, 501, 785

Gillon, M., Hatzes, A., Csizmadia, S., et al. 2010, A&A, 520, A97+

Goldman, B., Bouy, H., Zapatero Osorio, M. R., et al. 2008, A&A, 490, 763

Goodman, J. & Hut, P. 1993, ApJ, 403, 271

Goodwin, S. P., Kroupa, P., Goodman, A., & Burkert, A. 2007, Protostars and Planets V, 133

Goździewski, K. & Migaszewski, C. 2009, MNRAS, 397, L16

Halbwachs, J. L., Mayor, M., Udry, S., & Arenou, F. 2003, A&A, 397, 159

Hansen, B. M. S. & Barman, T. 2007, ApJ, 671, 861

Hartman, J. D., Bakos, G. Á., Kipping, D. M., et al. 2010, ArXiv e-prints

Hartman, J. D., Bakos, G. Á., Sato, B., et al. 2011, ApJ, 726, 52

Hartman, J. D., Bakos, G. Á., Torres, G., et al. 2009, ApJ, 706, 785

Hebb, L., Collier-Cameron, A., Loeillet, B., et al. 2009, ApJ, 693, 1920

Hebb, L., Collier-Cameron, A., Triaud, A. H. M. J., et al. 2010, ApJ, 708, 224

Hellier, C., Anderson, D. R., Collier Cameron, A., et al. 2010a, ArXiv e-prints

Hellier, C., Anderson, D. R., Collier Cameron, A., et al. 2010b, ApJL, 723, L60

Hellier, C., Anderson, D. R., Collier Cameron, A., et al. 2011, ArXiv e-prints

Hellier, C., Anderson, D. R., Gillon, M., et al. 2009, ApJL, 690, L89

Hełminiak, K. G. 2009, New Astron., 14, 521

Heppenheimer, T. A. 1974, Icarus, 22, 436

Heppenheimer, T. A. 1978, A&A, 65, 421

Hillenbrand, L. A. & White, R. J. 2004, ApJ, 604, 741

Hinz, P. M., Rodigas, T. J., Kenworthy, M. A., et al. 2010, ApJ, 716, 417

Hippler, S., Bergfors, C., Brandner Wolfgang, et al. 2009, The Messenger, 137, 14

Holberg, J. B., Oswalt, T. D., & Sion, E. M. 2002, ApJ, 571, 512

Holman, M., Touma, J., & Tremaine, S. 1997, Nature, 386, 254

Holman, M. J., Fabrycky, D. C., Ragozzine, D., et al. 2010, Science, 330, 51

Holman, M. J. & Wiegert, P. A. 1999, AJ, 117, 621

Holmberg, J., Nordström, B., & Andersen, J. 2009, A&A, 501, 941

Hormuth, F., Brandner, W., Janson, M., Hippler, S., & Henning, T. 2009, in American Institute of Physics Conference Series, Vol. 1094, American Institute of Physics Conference Series, ed. E. Stempels, 935–938

Hormuth, F., Hippler, S., Brandner, W., Wagner, K., & Henning, T. 2008, in Society of Photo-Optical Instrumentation Engineers (SPIE) Conference Series, Vol. 7014, Society of Photo-Optical Instrumentation Engineers (SPIE) Conference Series

Howard, A. W., Bakos, G. Á., Hartman, J., et al. 2010, ArXiv e-prints

Janson, M., Bergfors, C., Goto, M., Brandner, W., & Lafrenière, D. 2010, ApJL, 710, L35

Janson, M., Brandner, W., Lenzen, R., et al. 2007, A&A, 462, 615

Jenkins, J. M., Borucki, W. J., Koch, D. G., et al. 2010, ApJ, 724, 1108

Joergens, V. 2008, A&A, 492, 545

Johansen, A., Youdin, A., & Mac Low, M.-M. 2009, ApJL, 704, L75

Jones, B. W. & Sleep, P. N. 2010, MNRAS, 407, 1259

Joshi, Y. C., Pollacco, D., Cameron, A. C., et al. 2009, MNRAS, 392, 1532

Kalas, P., Graham, J. R., Chiang, E., et al. 2008, Science, 322, 1345

Kasper, M., Apai, D., Janson, M., & Brandner, W. 2007, A&A, 472, 321

Kipping, D. M. 2008, MNRAS, 389, 1383

Kipping, D. M., Bakos, G. Á., Hartman, J., et al. 2010, ApJ, 725, 2017

Kley, W. 2000, in IAU Symposium, Vol. 200, IAU Symposium, 211P–+

Kley, W. & Nelson, R. P. 2008, A&A, 486, 617

Koch, D. G., Borucki, W. J., Rowe, J. F., et al. 2010, ApJL, 713, L131

Köhler, R. 2008, Journal of Physics Conference Series, 131, 012028

Köhler, R., Petr-Gotzens, M. G., McCaughrean, M. J., et al. 2006, A&A, 458, 461

Köhler, R., Ratzka, T., Herbst, T. M., & Kasper, M. 2008, A&A, 482, 929

Kovács, G., Bakos, G. Á., Hartman, J. D., et al. 2010, ApJ, 724, 866

Kovács, G., Bakos, G. Á., Torres, G., et al. 2007, ApJL, 670, L41

Kozai, Y. 1962, AJ, 67, 591

Kraus, A. L. & Hillenbrand, L. A. 2007, AJ, 134, 2340

Kundurthy, P., Agol, E., Becker, A. C., et al. 2010, ArXiv e-prints

Lafrenière, D., Jayawardhana, R., & van Kerkwijk, M. H. 2008, ApJL, 689, L153

Lafrenière, D., Jayawardhana, R., & van Kerkwijk, M. H. 2010, ApJ, 719, 497

Lafrenière, D., Marois, C., Doyon, R., & Barman, T. 2009, ApJL, 694, L148

Lagrange, A., Bonnefoy, M., Chauvin, G., et al. 2010, Science, 329, 57

Lagrange, A., Gratadour, D., Chauvin, G., et al. 2009, A&A, 493, L21

Latham, D. W., Bakos, G. Á., Torres, G., et al. 2009, ApJ, 704, 1107

Latham, D. W., Borucki, W. J., Koch, D. G., et al. 2010, ApJL, 713, L140

Latham, D. W., Rowe, J. F., Quinn, S. N., et al. 2011, ApJL, 732, L24+

Law, N. 2006, PhD thesis Institute of Astronomy & Selwyn College, Cambridge University

Law, N. M., Hodgkin, S. T., & Mackay, C. D. 2006, MNRAS, 368, 1917

Law, N. M., Hodgkin, S. T., & Mackay, C. D. 2008, MNRAS, 384, 150

Law, N. M., Hodgkin, S. T., Mackay, C. D., & Baldwin, J. E. 2005, Astronomische Nachrichten, 326, 1024

Law, N. M., Mackay, C. D., Dekany, R. G., et al. 2009, ApJ, 692, 924

Léger, A., Rouan, D., Schneider, J., et al. 2009, A&A, 506, 287

Leinert, C., Zinnecker, H., Weitzel, N., et al. 1993, A&A, 278, 129

Lenzen, R., Hartung, M., Brandner, W., et al. 2003, in Presented at the Society of Photo-Optical Instrumentation Engineers (SPIE) Conference, Vol. 4841, Society of Photo-Optical Instrumentation Engineers (SPIE) Conference Series, ed. M. Iye & A. F. M. Moorwood, 944–952

Lépine, S. 2005, AJ, 130, 1247

Lissauer, J. J. & Stevenson, D. J. 2007, Protostars and Planets V, 591

Lister, T. A., Anderson, D. R., Gillon, M., et al. 2009, ApJ, 703, 752

Machida, M. N. 2011, in IAU Symposium, Vol. 270, IAU Symposium, ed. J. Alves, B. G. Elmegreen, J. M. Girart, & V. Trimble, 65–72

Maíz Apellániz, J. 2010, A&A, 518, A1+

Marois, C., Macintosh, B., Barman, T., et al. 2008, Science, 322, 1348

Marois, C., Zuckerman, B., Konopacky, Q. M., Macintosh, B., & Barman, T. 2010, Nature, 468, 1080

Mason, B. D., Wycoff, G. L., Hartkopf, W. I., Douglass, G. G., & Worley, C. E. 2001, AJ, 122, 3466

Mathar, R. J. 2007, Journal of Optics A: Pure and Applied Optics, 9, 470

Maxted, P. F. L., Anderson, D. R., Collier Cameron, A., et al. 2010a, PASP, 122, 1465

Maxted, P. F. L., Anderson, D. R., Collier Cameron, A., et al. 2010b, ArXiv e-prints

Maxted, P. F. L., Anderson, D. R., Gillon, M., et al. 2010c, AJ, 140, 2007

Mayama, S., Tamura, M., Hanawa, T., et al. 2010, Science, 327, 306

Mayer, L., Quinn, T., Wadsley, J., & Stadel, J. 2002, Science, 298, 1756

Mayer, L., Wadsley, J., Quinn, T., & Stadel, J. 2005, MNRAS, 363, 641

Mayor, M. & Queloz, D. 1995, Nature, 378, 355

McCarthy, C., Zuckerman, B., & Becklin, E. E. 2001, AJ, 121, 3259

Metchev, S., Marois, C., & Zuckerman, B. 2009, ApJL, 705, L204

Montes, D., López-Santiago, J., Gálvez, M. C., et al. 2001, MNRAS, 328, 45

Moro-Martín, A., Rieke, G. H., & Su, K. Y. L. 2010, ApJL, 721, L199

Moutou, C., Bruntt, H., Guillot, T., et al. 2008, A&A, 488, L47

Naef, D., Latham, D. W., Mayor, M., et al. 2001, A&A, 375, L27

Narita, N., Kudo, T., Bergfors, C., et al. 2010, PASJ, 62, 779

Nelson, A. F. 2000, ApJL, 537, L65

Nero, D. & Bjorkman, J. E. 2009, ApJL, 702, L163

Norton, A. J., Wheatley, P. J., West, R. G., et al. 2007, A&A, 467, 785

Noyes, R. W., Bakos, G. Á., Torres, G., et al. 2008, ApJL, 673, L79

Nutzman, P., Gilliland, R. L., McCullough, P. R., et al. 2011, ApJ, 726, 3

Nymeyer, S., Harrington, J., Hardy, R. A., et al. 2010, ArXiv e-prints

Padoan, P. & Nordlund, Å. 2004, ApJ, 617, 559

Pál, A. 2009, PhD thesis, Department of Astronomy, Eötvös Loránd University

Pál, A., Bakos, G. Á., Torres, G., et al. 2010, MNRAS, 401, 2665

Papaloizou, J. C. B., Nelson, R. P., Kley, W., Masset, F. S., & Artymowicz, P. 2007, Protostars and Planets V, 655

Patience, J., Ghez, A. M., Reid, I. N., & Matthews, K. 2002, AJ, 123, 1570

Perryman, M. A. C. & ESA, eds. 1997, ESA Special Publication, Vol. 1200, The HIPPARCOS and TYCHO catalogues. Astrometric and photometric star catalogues derived from the ESA HIPPARCOS Space Astrometry Mission

Pilat-Lohinger, E. & Dvorak, R. 2002, Celestial Mechanics and Dynamical Astronomy, 82, 143

Pollacco, D. L., Skillen, I., Collier Cameron, A., et al. 2006, PASP, 118, 1407

Pollack, J. B., Hubickyj, O., Bodenheimer, P., et al. 1996, Icarus, 124, 62

Pont, F., Hébrard, G., Irwin, J. M., et al. 2009, A&A, 502, 695

Pont, F., Husnoo, N., Mazeh, T., & Fabrycky, D. 2011, MNRAS, 378

Queloz, D., Anderson, D., Collier Cameron, A., et al. 2010, A&A, 517, L1+

Queloz, D., Bouchy, F., Moutou, C., et al. 2009, A&A, 506, 303

Quinn, S. N., Bakos, G. Á., Hartman, J., et al. 2010, ArXiv e-prints

Rasio, F. A. & Ford, E. B. 1996, Science, 274, 954

Rauer, H., Queloz, D., Csizmadia, S., et al. 2009, A&A, 506, 281

Rayner, J. T., Cushing, M. C., & Vacca, W. D. 2009, ApJS, 185, 289

Reid, I. N., Cruz, K. L., Allen, P., et al. 2004, AJ, 128, 463

Reid, I. N., Cruz, K. L., Burgasser, A. J., & Liu, M. C. 2008, AJ, 135, 580

Reid, I. N. & Gizis, J. E. 1997, AJ, 113, 2246

Reidemeister, M., Krivov, A. V., Schmidt, T. O. B., et al. 2009, A&A, 503, 247

Reipurth, B. & Clarke, C. 2001, AJ, 122, 432

Rhee, J. H., Song, I., Zuckerman, B., & McElwain, M. 2007, ApJ, 660, 1556

Riaz, B., Gizis, J. E., & Harvin, J. 2006, AJ, 132, 866

Rice, W. K. M., Armitage, P. J., Bate, M. R., & Bonnell, I. A. 2003, MNRAS, 339, 1025

Röser, S., Schilbach, E., Schwan, H., et al. 2008, A&A, 488, 401

Rousset, G., Lacombe, F., Puget, P., et al. 2003, in Presented at the Society of Photo-Optical Instrumentation Engineers (SPIE) Conference, Vol. 4839, Society of Photo-Optical Instrumentation Engineers (SPIE) Conference Series, ed. P. L. Wizinowich & D. Bonaccini, 140–149

Sahu, K. C., Casertano, S., Bond, H. E., et al. 2006, Nature, 443, 534

Santerne, A., Diaz, R. F., Bouchy, F., et al. 2011, ArXiv e-prints

Scharf, C. & Menou, K. 2009, ApJL, 693, L113

Seabroke, G. M. & Gilmore, G. 2007, MNRAS, 380, 1348

Shkolnik, E., Liu, M. C., & Reid, I. N. 2009, ApJ, 699, 649

Shporer, A., Bakos, G. Á., Bouchy, F., et al. 2009, ApJ, 690, 1393

Siegler, N., Close, L. M., Cruz, K. L., Martín, E. L., & Reid, I. N. 2005, ApJ, 621, 1023

Simpson, E. K., Barros, S. C. C., Brown, D. J. A., et al. 2010, ArXiv e-prints

Simpson, E. K., Faedi, F., Barros, S. C. C., et al. 2011, AJ, 141, 8

Skillen, I., Pollacco, D., Collier Cameron, A., et al. 2009, A&A, 502, 391

Smalley, B., Anderson, D. R., Collier Cameron, A., et al. 2010, A&A, 520, A56+

Smalley, B., Anderson, D. R., Collier Cameron, A., et al. 2011, A&A, 526, A130+

Smith, A. M. S., Anderson, D. R., Skillen, I., Cameron, A. C., & Smalley, B. 2011, ArXiv e-prints

Southworth, J. 2010, MNRAS, 408, 1689

Southworth, J., Dominik, M., Jørgensen, U. G., et al. 2011, A&A, 527, A8+

Southworth, J., Wheatley, P. J., & Sams, G. 2007, MNRAS, 379, L11

Sozzetti, A. & Desidera, S. 2010, A&A, 509, A103+

Stamatellos, D., Hubber, D. A., & Whitworth, A. P. 2007, MNRAS, 382, L30

Stamatellos, D. & Whitworth, A. P. 2009, MNRAS, 392, 413

Stassun, K. G., Mathieu, R. D., & Valenti, J. A. 2006, Nature, 440, 311

Street, R. A., Simpson, E., Barros, S. C. C., et al. 2010, ApJ, 720, 337

Strigachev, A. & Lampens, P. 2004, A&A, 422, 1023

Su, K. Y. L., Rieke, G. H., Stapelfeldt, K. R., et al. 2009, ApJ, 705, 314

Szabó, G. M., Kiss, L. L., Benkő, J. M., et al. 2010, A&A, 523, A84+

Takeda, G. & Rasio, F. A. 2005, ApJ, 627, 1001

Tamuz, O., Ségransan, D., Udry, S., et al. 2008, A&A, 480, L33

Thies, I. & Kroupa, P. 2007, ApJ, 671, 767

Tingley, B., Endl, M., Gazzano, J., et al. 2011, ArXiv e-prints

Tody, D. 1986, in Society of Photo-Optical Instrumentation Engineers (SPIE) Conference Series, Vol. 627, Society of Photo-Optical Instrumentation Engineers (SPIE) Conference Series, ed. D. L. Crawford, 733–+

Tody, D. 1993, in Astronomical Society of the Pacific Conference Series, Vol. 52, Astronomical Data Analysis Software and Systems II, ed. R. J. Hanisch, R. J. V. Brissenden, & J. Barnes, 173–+

Tohline, J. E. 2002, Ann. Rev. Astron. Astrophys., 40, 349

Toomre, A. 1964, ApJ, 139, 1217

Torres, C. A. O., Quast, G. R., da Silva, L., et al. 2006, A&A, 460, 695

Torres, G., Bakos, G. Á., Hartman, J., et al. 2010, ApJ, 715, 458

Torres, G., Bakos, G. Á., Kovács, G., et al. 2007, ApJL, 666, L121

Torres, G., Fressin, F., Batalha, N. M., et al. 2011, ApJ, 727, 24

Udry, S. & Santos, N. C. 2007, Ann. Rev. Astron. Astroph., 45, 397

Umbreit, S., Burkert, A., Henning, T., Mikkola, S., & Spurzem, R. 2005, ApJ, 623, 940

van Altena, W. F., Lee, J. T., & Hoffleit, E. D. 1995, The general catalogue of trigonometric [stellar] parallaxes, ed. van Altena, W. F., Lee, J. T., & Hoffleit, E. D.

van Leeuwen, F. 2007, A&A, 474, 653

Veras, D., Crepp, J. R., & Ford, E. B. 2009, ApJ, 696, 1600

Voges, W., Aschenbach, B., Boller, T., et al. 1999, A&A, 349, 389

Weldrake, D. T. F., Bayliss, D. D. R., Sackett, P. D., et al. 2008, ApJL, 675, L37

West, R. G., Anderson, D. R., Gillon, M., et al. 2009, AJ, 137, 4834

Whitmire, D. P., Matese, J. J., Criswell, L., & Mikkola, S. 1998, Icarus, 132, 196

Whitworth, A. P. & Zinnecker, H. 2004, A&A, 427, 299

Winn, J. N., Holman, M. J., Henry, G. W., et al. 2009, ApJ, 693, 794

Winn, J. N., Johnson, J. A., Howard, A. W., et al. 2010, ApJ, 718, 575

Wright, D. J., Chené, A., De Cat, P., et al. 2011, ApJL, 728, L20+

Zucker, S. & Mazeh, T. 2002, ApJL, 568, L113

Zuckerman, B., Song, I., & Bessell, M. S. 2004, ApJL, 613, L65

Zuckerman, B., Song, I., Bessell, M. S., & Webb, R. A. 2001, ApJL, 562, L87